NASA
TP
2070
c.1

TECH LIBRARY KAFB, NM
0068375

NASA
Technical
Paper
2070

September 1982

Crash Tests of Four Low-Wing Twin-Engine Airplanes With Truss-Reinforced Fuselage Structure

M. Susan Williams
and Edwin L. Fasanella

LOAN COPY: RETURN TO
AFWL TECHNICAL LIBRARY
KIRTLAND AFB, N.M.

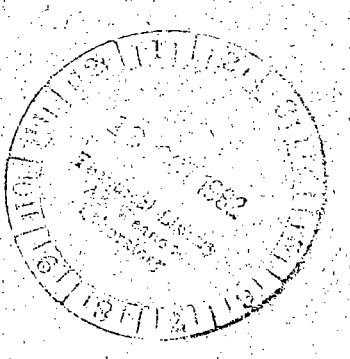

NASA

TECH LIBRARY KAFB, NM
0068375

NASA
Technical
Paper
2070

1982

Crash Tests of Four Low-Wing Twin-Engine Airplanes With Truss-Reinforced Fuselage Structure

M. Susan Williams

Langley Research Center
Hampton, Virginia

Edwin L. Fasanella

Kentron International, Inc.
Hampton, Virginia

NASA
National Aeronautics
and Space Administration

**Scientific and Technical
Information Branch**

CONTENTS

SUMMARY

Four six-place, low-wing, twin-engine, general-aviation airplane test specimens, with tubular-steel truss reinforcement in the cabin area, were crash tested at the Langley Impact Dynamics Research Facility under controlled free-flight conditions. All airplanes were impacted on a concrete test surface at a nominal flight-path velocity of 27 m/sec. Two tests were conducted at a -15° flight-path angle (0° pitch angle and -15° pitch angle), and two were conducted at a -30° flight-path angle (-30° pitch angle).

The average acceleration time histories (crash pulses) in the cabin area for each principal direction were calculated for each crash test. In addition, the peak floor accelerations were calculated for each test as a function of aircraft fuselage longitudinal station number. Typically, the peak crash deceleration decreases from nose to tail of the airplane.

Anthropomorphic-dummy accelerations were analyzed using the dynamic response index (DRI) and severity index (SI) models. A prototype energy-absorbing seat was used in the -15° flight-path, 0° pitch (flat-impact) test. By collapsing in a controlled manner, the seat stroked to increase the duration of the acceleration pulse and lower the average acceleration experienced by the occupant. Parameters affecting the dummy restraint system were studied; these parameters included the effect of no upper-torso restraint, measurement of the amount of inertia-reel strap pullout before locking, measurement of dummy chest forward motion, and loads in the restraints. With the SI model, the dummies with no shoulder harness received head impacts above the concussive threshold.

INTRODUCTION

With the rapid growth of private and commercial air traffic since World War II, increased emphasis has been focused on the causes of passenger injury and death in severe but potentially survivable crashes. The National Advisory Committee for Aeronautics (NACA) conducted a series of full-scale airplane crash tests with instrumented dummies in the 1950's (refs. 1 and 2). These tests were performed by accelerating an airplane along a horizontal guide rail and crashing it into an earthen mound. Later NACA studies on the dynamic response of seat structures to impact loads (ref. 3) resulted in a Civil Aeronautics Administration (CAA) update of static seat-strength requirements. The airplanes tested by NACA, however, were not structurally representative of current general-aviation airplanes.

In 1973, a general-aviation crash-test program was initiated jointly by the National Aeronautics and Space Administration (NASA) and the Federal Aviation Administration (FAA) (ref. 4). As part of this program, NASA Langley Research Center is conducting a series of crash tests to obtain information on general-aviation airplane crashes under controlled free-flight conditions (refs. 5 to 9). The studies at Langley are directed toward those crashes in which the airplane structure retains sufficient cabin volume and integrity for occupant survivability. The objectives of the studies are to determine the dynamic response of the airplane structure, seats, and occupants during a simulated crash; to determine the effect of flight parameters at impact (i.e., flight speed, flight-path angle, pitch angle, roll angle, and ground

condition) on the magnitude and pattern of structural damage; to determine the failure modes of the seats and occupant restraint systems; and to determine the loads imposed upon the occupants. This information is essential for predicting structural collapse and for designing safer seats, occupant restraint systems, and cabin structures with improved crash dynamic characteristics.

The present tests were conducted to obtain a data base of crash information for six-place, low-wing, twin-engine airplanes with an interior-welded tubular-steel truss reinforcing the cabin area. This report describes the results of four airplane crash tests. The gross mass of the airplanes ranged from 1993 kg to 2293 kg, and the test specimens were impacted at a nominal flight-path velocity of 27 m/sec at flight-path angles of -15° and -30° and ground-contact pitch angles of 0°, -15°, and -30°. All test airplanes were crashed on a concrete surface. The crew and passengers were represented by anthropomorphic dummies. Effects of the flight parameters at impact are discussed in terms of structural damage, accelerations of the airplane structure and occupants, and loads in the passenger restraint system. In addition, occupant injury criteria were calculated using the severity index (SI) and dynamic response index (DRI) models (refs. 10 and 11, respectively).

TEST FACILITY AND PROCEDURES

Facility

The crash tests were performed at the Langley Impact Dynamics Research Facility shown in figure 1. The gantry is composed of truss elements arranged with three sets of inclined legs to give vertical and lateral support and another set of inclined legs to provide longitudinal support. The gantry is 73 m high and 122 m long. The supporting legs are spread 81 m apart at the ground and 20 m apart at the 66-m level. An enclosed elevator and a stairway provide access to the overhead work platforms, and catwalks permit a safe traverse of the upper levels of the gantry. A movable bridge spans the gantry at the 66-m level and traverses the length of the gantry. The reinforced concrete impact surface permits tests to be repeated and allows comparison between tests. Detailed information about this facility is reported in reference 12.

Crash-Test Technique

The test technique used to crash the airplane specimens is shown schematically in figure 2. The airplane specimen, suspended by two swing cables attached to the top of the gantry, is drawn back and above the impact surface by a pullback cable to a height of about 49 m. The airplane specimen is then released from the pullback cable by a pyrotechnic separator. The specimen swings pendulum style onto the impact surface. The swing cables are pyrotechnically separated from the airplane specimen when the airplane is about 1 m above the impact surface to free it from restraint during the crash impact. An umbilical cable links the onboard instrumentation to a data acquisition system located in a building adjacent to the gantry. The umbilical cable remains attached to the test specimen during impact for data acquisition and is pyrotechnically separated about 0.5 sec after ground contact.

Airplane specimen attitude at impact can be adjusted prior to testing by changing the length of the cables in the suspension system (fig. 3). The flight-path angle, which can be adjusted up to -60° (see fig. 2), is determined by the length of the swing cables. Adjustments up to about 30° can be made in angle of attack and

roll angle. Only small adjustments can be made in yaw angle because of the small clearance between the pullback harness and empennage of the airplane. Additional yaw can be added by removing the stabilizers and simulating them with concentrated masses.

Test Parameters

Flight-path and attitude angles for the airplanes at impact are identified in figure 4. Positive force directions coincide with the reference axes. The planned and actual test parameters for the four tests reported here, along with photographs illustrating the impact attitude for each airplane test specimen, are presented in figure 5. For consistency and brevity, each test and airplane specimen is hereinafter identified by word description referring to the pitch angle (i.e., flat-impact test, 15° nose-down test, and 30° nose-down tests) for impact positions shown in figures 5(a) through 5(d), respectively. The nominal flight-path velocity was 27 m/sec for all tests.

Detailed descriptions of these impact conditions are given in the appendixes. The appendixes include normal, longitudinal, and transverse acceleration time histories measured on the aircraft structure and in the anthropomorphic dummies for the four airplane tests. Also included are restraint loads and displacement transducer data. Schematics to determine the location of the accelerometers are given in figures 6(a) through 6(d).

Airplane Test Specimen

The airplane specimens used for the tests (fig. 7) were identical six-place, low-wing, twin-engine, general-aviation airplanes with masses of 2237 kg (flat-impact test), 2193 kg (15° nose-down test), 1993 kg (first 30° nose-down test), and 2293 kg (second 30° nose-down test). The airplanes were of aluminum structure with a welded tubular-steel truss inside the cabin. The four airplane specimens were complete except for upholstery and avionics. The fuel tanks were filled with water to simulate the fuel mass. Spoilers were attached to the wings to minimize the aerodynamic lift. The exterior and interior of the airplane specimens were painted to enhance photographic contrast, and black lines were painted over rivet lines to emphasize the underlying structure.

The four airplanes carried the same basic equipment necessary for the tests. Anthropomorphic dummies (all 50th percentile, part 572 (ref. 13)), each with a mass of 75 kg, occupied the seats. All seats except the pilot's seat in the flat-impact test were standard equipment for an airplane of this type. The pilot's seat in the flat-impact test was a prototype energy-absorbing seat supplied by a private organization. The four legs of this seat were attached to slotted seat rails that were supplied by the private organization. The front legs of all other crew seats in this series were connected to "I" cross-section seat rails that are standard for these airplanes. Slotted guides located on the rear of these seats were secured to the main spar. Both front and rear legs of the passengers' seats were attached to seat rails that are standard for these airplanes.

Figure 8 shows the occupants, restraints, and interior camera arrangement for each test. All lap belts were secured to the seats and all shoulder harnesses to the fuselage. The pilot in the flat-impact test was restrained with a lap belt attached

to the seat and a double shoulder harness attached to the fuselage. Both the copilot and passenger had lap belts and single-strap shoulder harnesses with inertia reels. In the 15° nose-down test, all occupants were restrained with lap belts and single-strap shoulder harnesses with inertia reels. In the first 30° nose-down test, the pilot and copilot had lap belts and shoulder harnesses with inertia reels, but the passenger wore a lap belt only. The pilot and second passenger in the second 30° nose-down test had lap belts and shoulder harnesses with inertia reels, but the first passenger (seated behind the pilot) wore only a lap belt. The rated assembly strength of each restraint system was at least 1500 lbf (6672 N) as required by the FAA regulations.

Instrumentation and Data Preparation

Onboard instrumentation for obtaining data pertaining to the dynamic behavior of the airplane structure, seats, and dummies consisted of dc accelerometers (piezo-resistive), high-speed motion-picture cameras, displacement transducers, and load cells. (See fig. 9.) External motion-picture coverage of the crash sequence at various film speeds was provided by tracking and fixed cameras located to the port side, front, back, and overhead of the test specimen. A Doppler radar unit was used to obtain the horizontal velocity of the test specimen at impact.

The locations of the accelerometers onboard the airplanes are shown in figure 6. The accelerometers were oriented along the normal (Z), longitudinal (X), and transverse (Y) axes as shown in figure 4. Each location is designated by its grid coordinates as follows: the first number indicates the longitudinal coordinate; the first letter indicates the normal coordinate (floor to roof); the second number indicates the transverse coordinate; and the second letter indicates the accelerometer orientation with respect to the airplane body-axis system. The normal, longitudinal, and transverse orientations are designated as N, L, and T, respectively. For example, the normal accelerometer location in the center of the ceiling of the cockpit is designated 9J8N. This system applies to the identification of the data traces located in the appendixes.

The physical variables to be measured in the aircraft specimen are converted to electrical signals by the transducers. The transducers are wired to a 90-channel data chassis with a regulated 10-V power supply common to all channels. From the data chassis in the aircraft, the signals are transmitted through an umbilical cable to a junction box on top of the gantry. From there they are transmitted through hard wire to the control room. In the control room, the signals are received through another junction box and sent to a patchboard that has a 150-channel capability. From the patchboard, the signals are fed to the signal-conditioning units, where they are filtered through a 600-Hz low-pass filter and amplified. The signals are multiplexed by a 90-channel multiplex FM system, which incorporates 5 frequencies: 25, 40, 55, 70, and 85 kHz. The signals are then recorded directly onto magnetic tape by a 28-track recorder. The first 18 tracks are dedicated for the 90 data channels (5 channels per track). Tracks 27 and 28 are reserved for voice annotation and time code, respectively. Some data traces have been omitted from this paper because the data were lost as the result of physical and electrical instrumentation failures.

To correlate the recorded data signals with the high-speed motion-picture data, a time code is recorded simultaneously on the magnetic tapes and on the external films. There is also a 100-Hz time-pulse generator onboard the aircraft for use with the onboard cameras that take 400 photographs per second. Two 6-V lamps, in the field

of view of the internal and external cameras, are flashed at cable separation time to synchronize the external time-code generator with the onboard events recorded by the cameras.

The data were filtered through a 600-Hz low-pass filter before being recorded on magnetic tape. The data on the magnetic tapes are digitized at 4000 samples per second. The digitized accelerometer data are passed through a finite impulse response filter $\frac{(\sin x)}{x}$ and filtered as follows:

Dummy head, Hz	600 (unfiltered)
Dummy chest, Hz	180
Dummy pelvis, Hz	180
Restraints, Hz	60
Displacement transducers, Hz	60
Seat, Hz	20
Floor structure, Hz	20

Motion-picture analysis consists of plotting a displacement-time curve from the film data, fitting least-square polynomial functions (up to 10th order) to the measured displacements, and then twice differentiating the displacements to obtain accelerations.

Resultant accelerations a_r are calculated for the dummy's head, chest, and pelvis. The severity index (ref. 10) is calculated from the resultant acceleration by the equation

$$SI = \int_o^t a_r^{2.5}\, dt$$

Another useful index, the DRI (dynamic response index, ref. 11) has been used to help determine the probability of spinal injury for a well-restrained seated occupant subjected to a vertical impact (such as the impulse during ejection from a fighter aircraft). Although the light-aircraft crash pulses reported in this paper are not completely vertical, the DRI was computed for comparison purposes. In the DRI model, a single lump mass is assumed to load the vertebrae, which are modeled in one dimension as a spring with damping. The familiar one-dimensional driven harmonic oscillator equation

$$\frac{d^2\Delta}{dt^2} + 2c\omega_n \frac{d\Delta}{dt} + \omega_n^2 \Delta = \frac{d^2 z}{dt^2}$$

is solved for the maximum spinal compression Δ, and the DRI is computed to be

$$DRI = \frac{\omega_n^2 \Delta_{max}}{g}$$

where

c damping ratio

ω_n natural frequency of model

$\frac{d^2z}{dt^2}$ input acceleration

Δ spine compression

g acceleration due to gravity

A damping ratio of 0.224 and a natural frequency of 52.9 rad/sec were used for calculating DRI values. These values are representative of the U.S. Air Force flying population and would not be representative of the flying population in general. Physically, the DRI represents the peak response acceleration in g units. ($1g = 9.81\ m/sec^2$.)

RESULTS AND DISCUSSION

The crash dynamics, assessments of damage, and acceleration time histories for each crash test are discussed in detail in the appendixes (flat-impact test, appendix A; 15° nose-down test, appendix B; 30° nose-down tests, appendix C). In the following sections, a comparison of the entire crash-test series is made based on the data and the interpretation of the data.

Floor Crash Pulses

A series of four light twin-engine airplanes were crash tested at a 27 m/sec nominal flight-path velocity under the following nominal impact conditions:

1. Flat-impact test (-15° flight-path angle, 0° pitch angle).

2. 15° nose-down test (-15° flight-path angle, -15° pitch angle).

3. 30° nose-down test (-30° flight-path angle, -30° pitch angle).

4. Same as test 3.

In this section the floor acceleration time histories (crash pulses) are analyzed along with each dummy's response to these crash forces.

To obtain a crash pulse, individual acceleration traces in the normal, longitudinal, and transverse directions measured on the floor of the airplane in the cabin area are analyzed for the following values: maximum acceleration g_{max}, total time duration of the main pulse ΔT, and velocity change ΔV obtained from the integrated acceleration trace. (See fig. 10.) These values are then averaged to give a cabin-area floor crash pulse in the normal, longitudinal, and transverse directions. The crash pulses for each test are summarized in table I. The individual acceleration traces used to get the average crash pulses are given in appendixes A, B, and C for

the flat-impact test, 15° nose-down test, and 30° nose-down tests, respectively. Crash pulses from other NASA tests are discussed in reference 14.

For a given flight-path condition, the center-of-gravity (c.g.) impact velocity components in the global (Earth) axes system are the same (independent of pitch attitude). For the -15° flight-path angle, the sink velocity is 7 m/sec and the horizontal component is 26 m/sec; and for the -30° flight-path angle, the sink velocity is 13.5 m/sec and the horizontal component is 23.4 m/sec. The average cabin-area normal floor crash pulse shows a peak acceleration in the flat-impact test nearly twice as high as in the 15° nose-down test. The vertical sink velocity for these two tests was intended to be identical. The change in vertical sink velocity is

$$\Delta V = \int a_i \, dt_i = \bar{a}_i \, \Delta t_i$$

where

$\bar{a}_i$ average acceleration for a given pitch condition

Δt_i time duration of pulse

If the peak accelerations are approximately proportional to the average accelerations, then $a_{peak} \, \Delta t$ for the flat-impact test is approximately equal to $a_{peak} \, \Delta t$ for the 15° nose-down test. That is, the normal peak acceleration and pulse duration for the two tests are inversely related. Consequently, since the time duration of the normal crash pulse for the flat-impact test is about half that of the 15° nose-down test, the peak acceleration is doubled.

The average peak normal accelerations for the 30° nose-down tests and the flat-impact test were about 30g. However, the normal velocity change and pulse duration for the 30° nose-down tests were substantially higher because of the -30° flight-path angle. Consequently, the severity of the crash to human occupants is greatly increased for the 30° nose-down tests. The longitudinal acceleration for the 30° nose-down tests is more than double that for the other two test conditions. Also, initial longitudinal decelerations due to nose crushing slow the aircraft along the flight path. This condition lowers the integrated normal velocity component below that which would be expected from calculations based on components of the flight-path velocity at initial contact with the concrete surface.

Peak floor accelerations were plotted as a function of accelerometer fuselage station number for each crash test for the longitudinal and normal directions (aircraft axes). (See fig. 11.) A linear least-squares fit was placed through the data; and although considerable scatter is evident, basic trends are revealed. An approximate value of the average peak acceleration for each case is found by finding the value of acceleration that corresponds to the main spar (c.g.) location (station 98).

For the flat-impact test, the peak acceleration as a function of station number is relatively constant, but in the 30° nose-down test, the accelerations (normal and longitudinal) show considerable variation and tend to decrease with increasing station numbers. Longitudinal accelerations in the 15° nose-down test fall between those in the flat-impact test and the 30° nose-down tests. For the normal accelerations, the 30° nose-down tests showed the highest peak accelerations in the nose; however, peak accelerations in the flat-impact test were greater for the remainder of the aircraft stations.

The change in velocity obtained by integrating each acceleration time history over the main pulse Δt was also plotted as a function of fuselage station number for the normal direction. The data are presented in figure 12. The figure shows that the normal velocity change for the 30° crash tests is higher than the flat-impact test for all stations.

Dummy Response

To make comparisons of the occupant response to the input crash accelerations, the severity index (SI) and the dynamic response index (DRI) were calculated. Since the human spine is approximately aligned with the normal crash forces, and since in most light airplanes very little underbelly crushable structure is available to attenuate loads transmitted to the occupants, a careful evaluation of the effect of the normal acceleration is in order. The DRI was developed as an approximate model that was useful in the design of military ejection seats. Figure 13 gives the probability of spinal injury as a function of DRI for well-restrained occupants subjected to a vertical acceleration based on cadaver data and actual operational Air Force ejection data. (See ref. 15.) The crash vectors in the 30° nose-down tests do not fall into the "primarily normal" category, and the first passenger in these tests did not have upper-torso restraint. Therefore, the DRI's calculated for these tests should be used with caution. The severity indexes, although used primarily for head impact, were also calculated for the chest and pelvis.

Tables II through V summarize the dummy response behavior for each crash test. By considering the dummy response to each test, the normal crash pulses are ranked with respect to severity in the following descending order: the 30° nose-down tests, the flat-impact test, and the 15° nose-down test. The pilot in the flat-impact test with the energy-absorbing seat experienced one of the mildest responses of all occupants in all tests in terms of the DRI (computed value of 24). From the DRI curve (fig. 13), however, an occupant in such a case would still have approximately a 50-percent chance of spinal injury. All occupants other than the pilot in the flat-impact test and the pilot and copilot in the 15° nose-down test have calculated DRI values greater than 24.

Longitudinal acceleration is more tolerable than normal acceleration, provided the occupant is properly restrained to prevent head injury. Displacement transducer data indicated that inertia reels locked after 1.5 cm of strap pullout for the 15° nose-down test and after 7.8 cm (average) for the 30° nose-down tests. Head injury is the most frequent type of injury and accounts for 75 percent of fatalities in aircraft crashes. (See ref. 16.) The severity index of each occupant is plotted in figure 14 as a function of the floor longitudinal velocity change. The occupants in the first-passenger location in the 30° nose-down tests had no upper-torso restraint; consequently, both occupants struck their heads rather severely. Figure 14 shows that the head severity index was over 1000 for both these occupants and was nearly 1500 for the passenger in the first 30° nose-down test. An SI of approximately 1000 is the concussive threshold for impacts to an unprotected head, and the threshold for helmeted head impacts is approximately 1500. The maximum SI for a dummy head with upper-torso restraint was 689 measured on the second passenger in the second 30° nose-down test. The head of this dummy struck the knees as the legs were rebounding from the floor.

CONCLUDING REMARKS

Four six-place, low-wing, twin-engine general-aviation airplane test specimens, with a tubular-steel truss-reinforced fuselage structure, were crash tested at the Langley Impact Dynamics Research Facility under controlled free-flight conditions. All airplanes were impacted on a concrete test surface at a nominal flight-path velocity of 27 m/sec. The four tests and their nominal flight-path and pitch angles were: (1) flat-impact test, -15° flight-path angle, 0° pitch angle; (2) 15° nose-down test, -15° flight-path angle, -15° pitch angle; (3) and (4) 30° nose-down tests, -30° flight-path angle, -30° pitch angle.

Two tests were conducted at a -15° flight-path angle. These were a flat-impact test (0° pitch angle) and a 15° nose-down test (-15° pitch angle) with the longitudinal aircraft axis aligned along the flight path. The average peak longitudinal acceleration for these two tests was about the same (approximately 6g). However, because of nose crushing and angular rotation of the fuselage in the 15° nose-down test, the duration and velocity change of the longitudinal crash pulse in that test were about double those in the flat-impact test. In the normal direction, the velocity change for both tests was approximately the same. Hence, the peak acceleration and total time duration of the crash pulse for the normal direction are inversely related for these two tests. (The flat-impact test had a peak normal acceleration of approximately 30g and a duration of 0.06 sec, compared with approximately 15g and 0.12 sec for the 15° nose-down test.)

Two tests were conducted at a -30° flight-path angle. Both tests had a -30° pitch angle, so that the longitudinal axis of the plane coincided with the flight path. The longitudinal peak accelerations in these two tests were about 15g for a duration of 0.10 sec with a longitudinal velocity change near 10 m/sec. The vertical sink rate in these tests was about twice that in the flat-impact test and 15° nose-down tests (-15° flight path). However, in the 30° nose-down tests, more vertical stopping distance was available in the form of airplane nose crushing. Since more structural crushing occurred in the 30° nose-down tests, the time duration of the acceleration pulse was double that of the flat-impact test. Peak acceleration for both tests was about 30g.

Ranking the normal crash pulses with respect to severity gives the following descending order: 30° nose-down tests, flat-impact test, 15° nose-down test. Using the dynamic response index (DRI) model, the pilot in the flat-impact test seated in an energy-absorbing seat developed a DRI value of 24 compared with 31 and 35 for the other two occupants in the same test. A value of 24 corresponds to a 50-percent chance of spinal injury, and higher values reflect higher chances of injury. The lowest DRI value was 23 in the 15° nose-down test; the highest DRI calculated was 62 in the second 30° nose-down test.

Two anthropomorphic-dummy passengers in the 30° nose-down tests had no upper-torso restraint, and consequently their heads impacted on the seat in front of them. The head severity index (SI) was calculated to be over 1000 (the concussive threshold) for both of these dummies and was nearly 1500 for the dummy in the first 30° nose-down test. The SI of all occupants with upper-torso restraint remained well below the concussive threshold.

Langley Research Center
National Aeronautics and Space Administration
Hampton, VA 23665
August 16, 1982

TABLE I.- AVERAGE CABIN FLOOR CRASH PULSES

Test	Maximum acceleration, g units	Duration of acceleration pulse, sec	Velocity change, m/sec
Flat-impact:			
Normal	31.0	0.057	9.1
Longitudinal	6.4	.052	1.9
Transverse	2.5	.062	1.0
15° nose-down:			
Normal	16.0	.120	10.6
Longitudinal	5.5	.088	4.0
Transverse	2.0	.060	1.2
First 30° nose-down:			
Normal	27.2	.083	11.3
Longitudinal	15.2	.090	8.2
Transverse	5.0	.068	2.0
Second 30° nose-down:			
Normal	29.9	.096	12.3
Longitudinal	14.0	.112	10.5
Transverse	8.0	.140	7.0

TABLE II.- SUMMARY OF MEASURED DUMMY RESPONSES FOR FLAT-IMPACT TEST

Restraint Loads and Displacements:	
Pilot shoulder harness	700 N
Copilot shoulder harness	1070 N
Passenger lap belt	400 N
Copilot chest forward motion	12.5 cm

Dummy occupant	Normal			Longitudinal			Transverse			Severity index	Dynamic response index
	Maximum acceleration, g units	Duration of acceleration, sec	Velocity change, m/sec	Maximum acceleration, g units	Duration of acceleration, sec	Velocity change, m/sec	Maximum acceleration, g units	Duration of acceleration, sec	Velocity change, m/sec		
Pilot:											
Head				20	0.068	7.6	2	0.072	0.6	>66	
Chest	28	0.104	10.5	11	.052	3.7	2	.048	.6	86	
Pelvis	32	.100	10.5	20	.036	2.0	12	.028	2.0	117	24
Copilot:											
Head	29	.052	8.0				8	.068	3.0	>120	
Chest	32	.076	10.7	7	.080	1.0	6	.056	1.6	118	
Pelvis	31	.076	10.4	15	.068	3.0	8	.056	1.2	126	31
First passenger:											
Head	30	.044	6.7	13	.084	5.5	8	.080	3.3	156	
Chest	35	.060	10.5				13	.048	2.6	>182	
Pelvis	39	.066	11.1								35

TABLE III.- SUMMARY OF MEASURED DUMMY RESPONSES FOR 15° NOSE-DOWN TEST

Restraint Loads and Displacements:	
Pilot shoulder harness	1200 N
Copilot shoulder harness	1100 N
Passenger shoulder harness	1190 N
Pilot chest forward motion	17.5 cm
Pilot inertia-reel pullout	1.5 cm
Copilot inertia-reel pullout	1.4 cm

Dummy occupant	Normal			Longitudinal			Transverse			Severity index	Dynamic response index
	Maximum acceleration, g units	Duration of acceleration, sec	Velocity change, m/sec	Maximum acceleration, g units	Duration of acceleration, sec	Velocity change, m/sec	Maximum acceleration, g units	Duration of acceleration, sec	Velocity change, m/sec		
Pilot:											
Head				31	0.092	11.2	16	0.080	4.0	>139	
Chest	16	0.092	8.8	18	.112	8.3	8	.084	4.0	107	
Pelvis	22	.096	10.8	8	.040	1.0	10	.048	5.0	75	23
Copilot:											
Head	22	.120	11.7	18	.100	9.0	15	.092	9.0	242	
Chest	17	.084	10.6	10	.120	6.2	8	.108	5.0	75	
Pelvis	24	.080	10.3	8	.044	1.1				>77	25
First passenger:											
Head							8	.116	4.1		
Chest	21	.108	10.0	14	.088	5.7	16	.064	5.1	133	
Pelvis	28	.096	11.2	6	.120	2.0				>93	27

TABLE IV.- SUMMARY OF MEASURED DUMMY RESPONSES FOR FIRST 30° NOSE-DOWN TEST

Restraint Loads and Displacements:	
Pilot shoulder harness	2700 N
Pilot lap belt	2000 N
Copilot shoulder harness	4780 N
Copilot lap belt	2080 N
Passenger lap belt	3300 N
Copilot chest forward motion	32.0 cm
Pilot inertia-reel pullout	9.5 cm
Copilot inertia-reel pullout	6.5 cm

Dummy occupant	Normal			Longitudinal			Transverse			Severity index	Dynamic response index
	Maximum acceleration, g units	Duration of acceleration, sec	Velocity change, m/sec	Maximum acceleration, g units	Duration of acceleration, sec	Velocity change, m/sec	Maximum acceleration, g units	Duration of acceleration, sec	Velocity change, m/sec		
Pilot:											
Head	19	0.130	16.5	39	0.090	22.6	22	0.055	6.2	493	
Chest				24	.090	10.6	23	.070	8.9	>148	
Pelvis	47	.090	19.8	12	.100	2.9	36	.020	4.0	479	47
Copilot:											
Head	14		7.0				19	.130	10.2	>72	
Chest	36	.075	11.2	22	.090	10.2	11	.180	8.3	263	
Pelvis	46	.085	15.8	11	.092	2.9	32	.036	6.0	389	41
First passenger:											
Head	55	.100		43	.040	4.0	120	.036	16.0	1493	
Chest	26	.130	7.0	55	.070	16.5	15	.048	3.8	474	
Pelvis	52	.090	17.0				16	.046	4.0	>357	47

TABLE V.- SUMMARY OF MEASURED DUMMY RESPONSES FOR SECOND 30° NOSE-DOWN TEST

Restraint Loads and Displacements:	
First passenger lap belt	1630 N
Second passenger lap belt	2900 N
Pilot chest forward motion	38.0 cm
Second passenger chest forward motion	17.5 cm
Pilot inertia-reel pullout	7.5 cm
First passenger chest forward motion	67.5 cm

Dummy occupant	Normal			Longitudinal			Transverse			Severity index	Dynamic response index
	Maximum acceleration, g units	Duration of acceleration, sec	Velocity change, m/sec	Maximum acceleration, g units	Duration of acceleration, sec	Velocity change, m/sec	Maximum acceleration, g units	Duration of acceleration, sec	Velocity change, m/sec		
Pilot:											
Head	38	0.056	11.2	30	0.160	25.0	24	0.084	6.5	576	
Chest	36	.084	12.2	33	.092	11.1	10	.016	1.9	289	
Pelvis	58	.068	13.9	19	.032	5.3	18	.016	1.8	332	42
First passenger:											
Head	45	.088	21.7	72	.044	12.7	16	.016	2.4	1041	
Chest				96	.040	12.8	10	.056	4.5	>743	
Pelvis	65	.060	12.0	13	.080	6.5	23	.024		500	41
Second passenger:											
Head	70	.180	30.1	20	.132	11.9	7	.020	1.0	689	
Chest	38	.060	10.0	28	.108	13.0	16	.020	2.9	344	
Pelvis	73	.068	17.5	30	.036	3.0	18	.056		1040	62

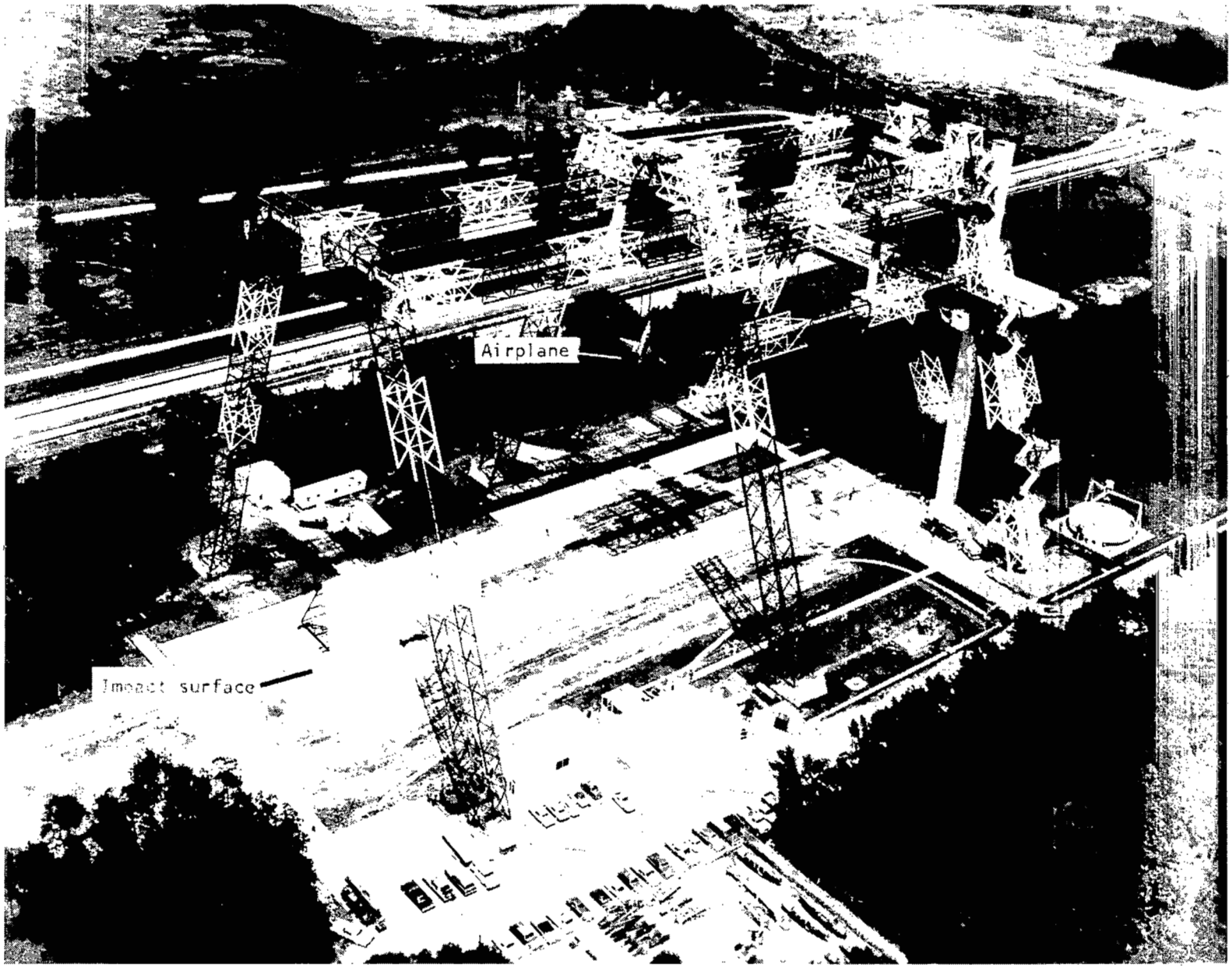

L-74-2505.5

Figure 1.- Langley Impact Dynamics Research Facility.

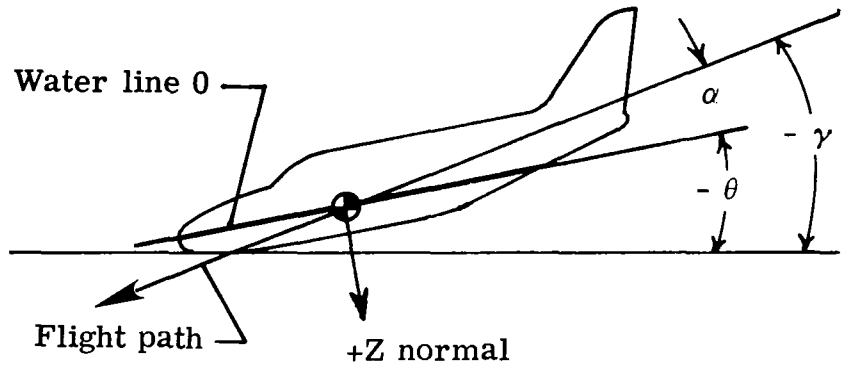

γ Flight-path angle
α Angle of attack
θ Pitch angle,
$\theta = \gamma + \alpha$

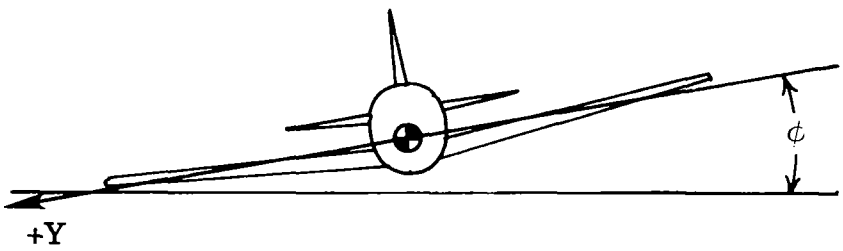

ϕ Roll angle

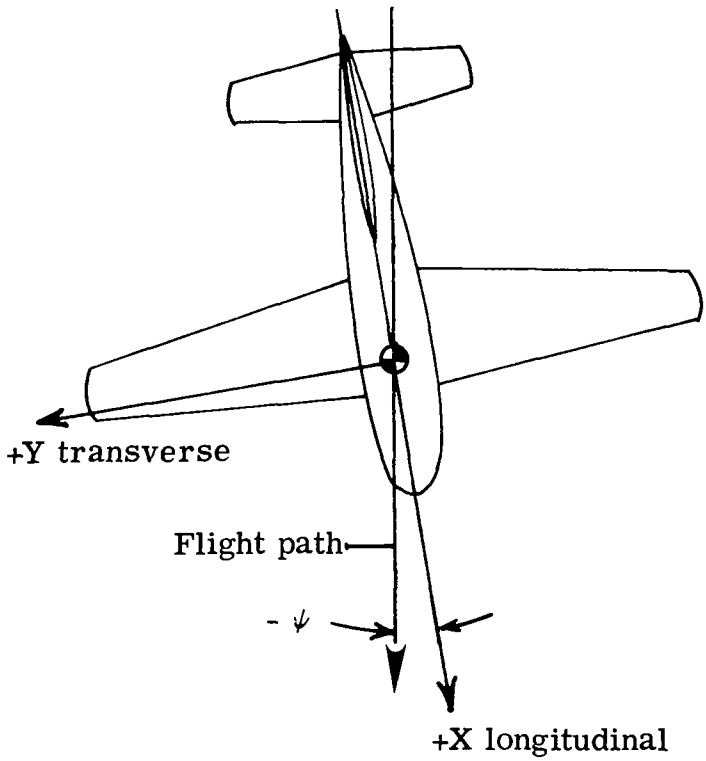

ψ Yaw angle

Figure 4.- Definition of flight path, crash attitudes, and axes.

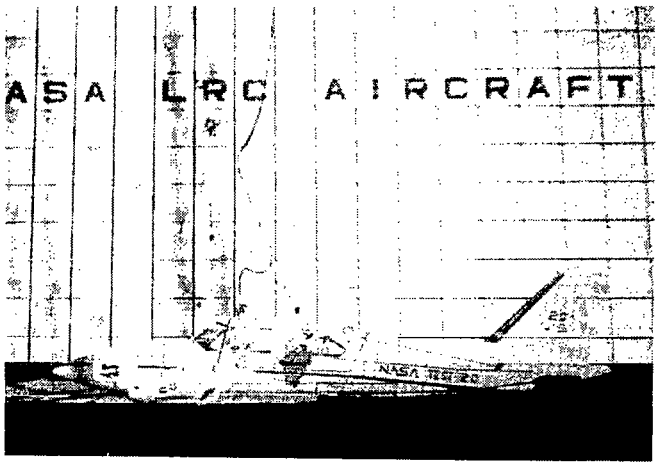

	Planned	Actual
Flight-path angle, γ	-15.0^{o}	-15.4^{o}
Angle of attack, α	15.0^{o}	17.4^{o}
Pitch angle, θ	0.0^{o}	2.0^{o}
Roll angle, ϕ	0.0^{o}	-7.2^{o}
Yaw angle, ψ	0.0^{o}	-3.0^{o}
Flight-path velocity	26.8 m/sec	26.6 m/sec

(a) Flat-impact test.

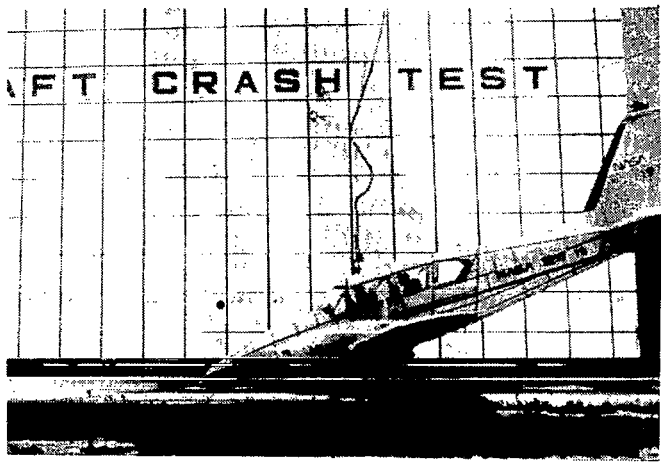

	Planned	Actual
Flight-path angle, γ	-15.0^{o}	-15.0^{o}
Angle of attack, α	0.0^{o}	-2.7^{o}
Pitch angle, θ	-15.0^{o}	-17.7^{o}
Roll angle, ϕ	0.0^{o}	-2.5^{o}
Yaw angle, ψ	0.0^{o}	-1.5^{o}
Flight-path velocity	26.8 m/sec	27.0 m/sec

(b) 15° nose-down test.

L-82-167

Figure 5.- Airplane crash-test parameters.

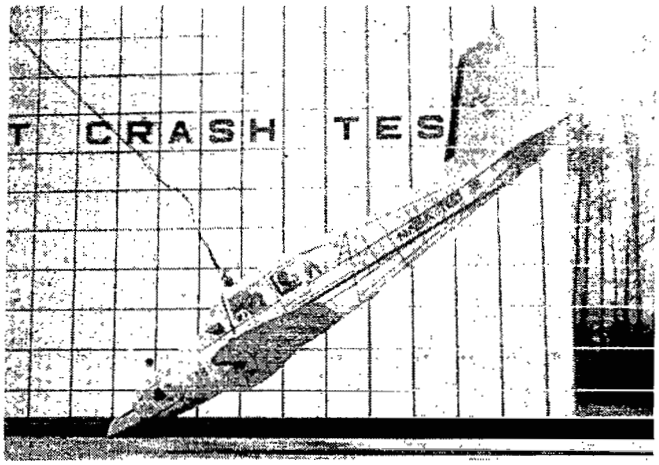

	Planned	Actual
Flight-path angle, γ	-30.0^{o}	-32.0^{o}
Angle of attack, α	0.0^{o}	1.0^{o}
Pitch angle, θ	-30.0^{o}	-31.0^{o}
Roll angle, ϕ	0.0^{o}	5.5^{o}
Yaw angle, ψ	0.0^{o}	6.7^{o}
Flight-path velocity	26.8 m/sec	27.9 m/sec

(c) First 30° nose-down test.

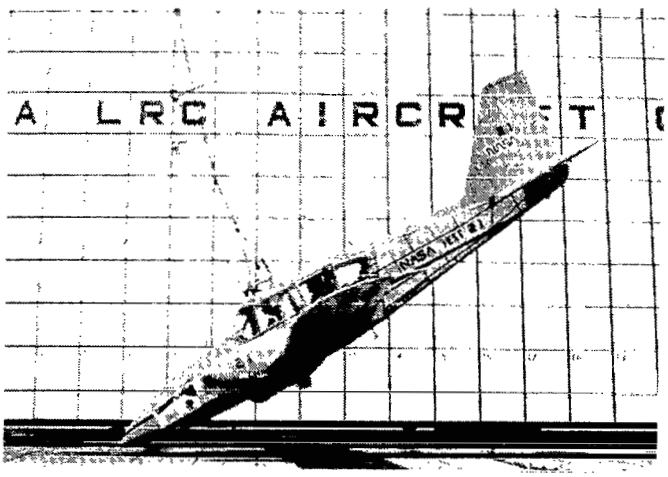

	Planned	Actual
Flight-path angle, γ	-30.0^{o}	-30.0^{o}
Angle of attack, α	0.0^{o}	0.5^{o}
Pitch angle, θ	-30.0^{o}	-29.5^{o}
Roll angle, ϕ	0.0^{o}	2.2^{o}
Yaw angle, ψ	0.0^{o}	4.0^{o}
Flight-path velocity	26.8 m/sec	27.1 m/sec

(d) Second 30° nose-down test.

L-82-168

Figure 5.- Concluded.

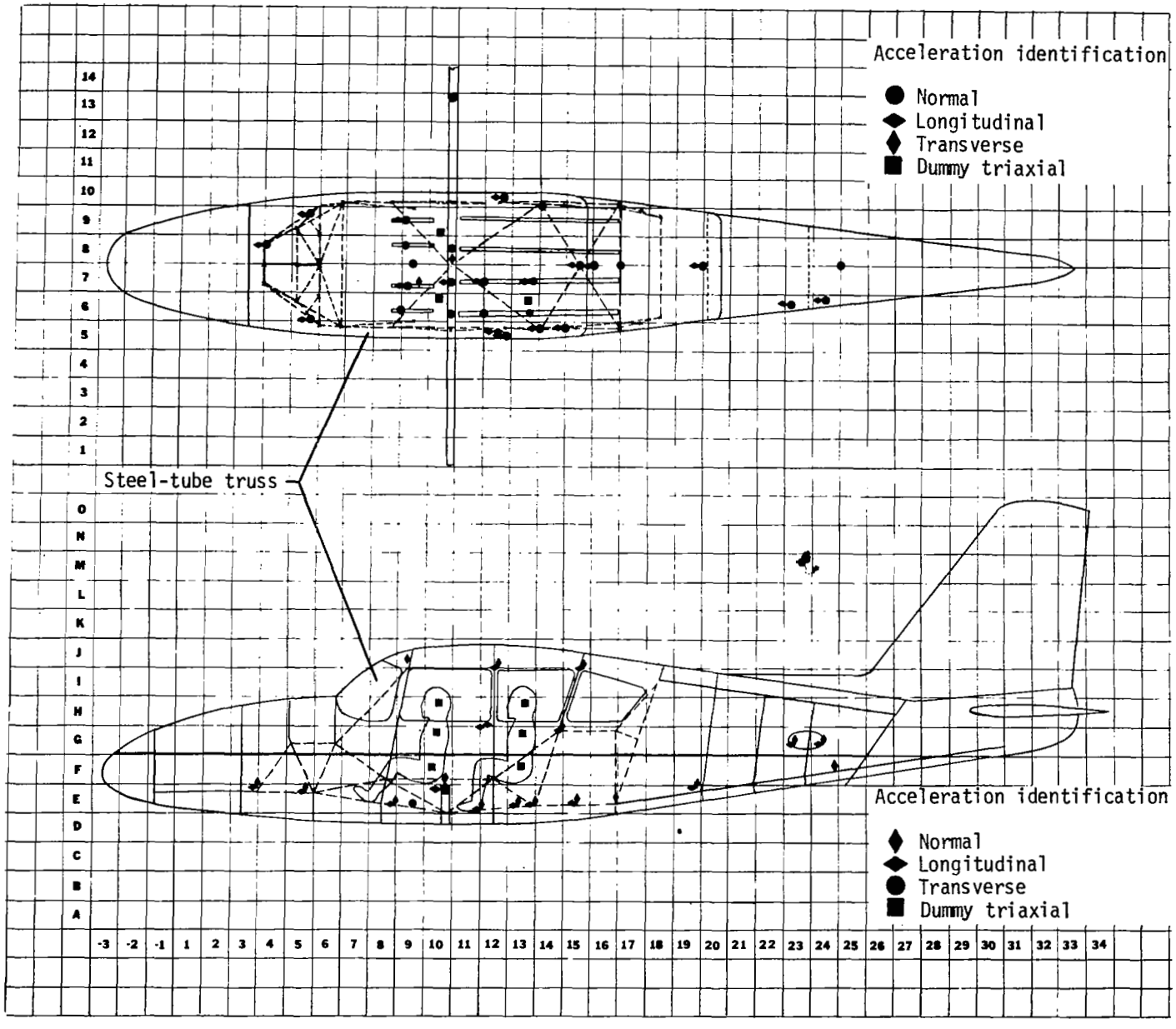

(a) Flat-impact test.

Figure 6.- Diagram of accelerometer locations.

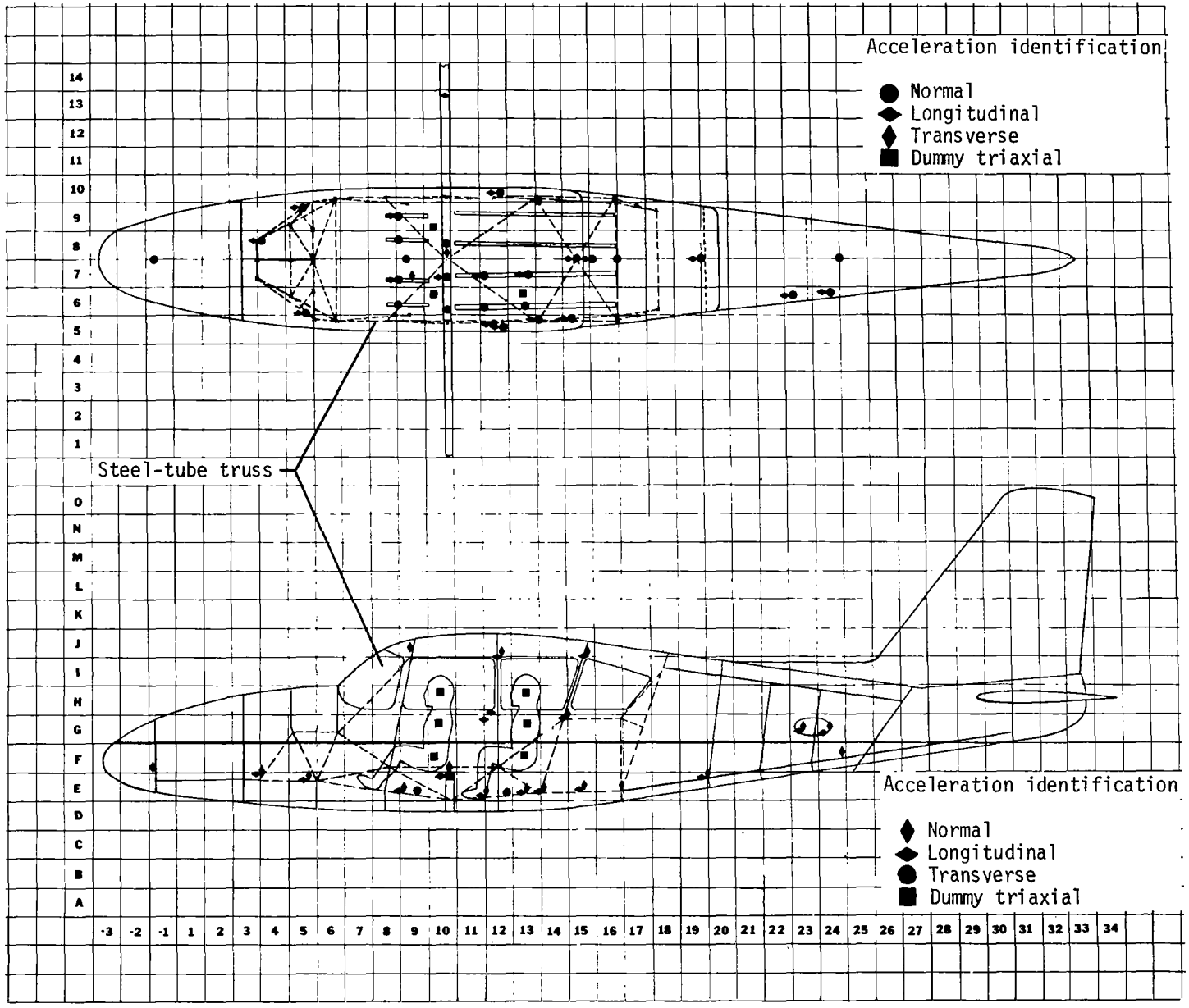

(b) 15° nose-down test.

Figure 6.- Continued.

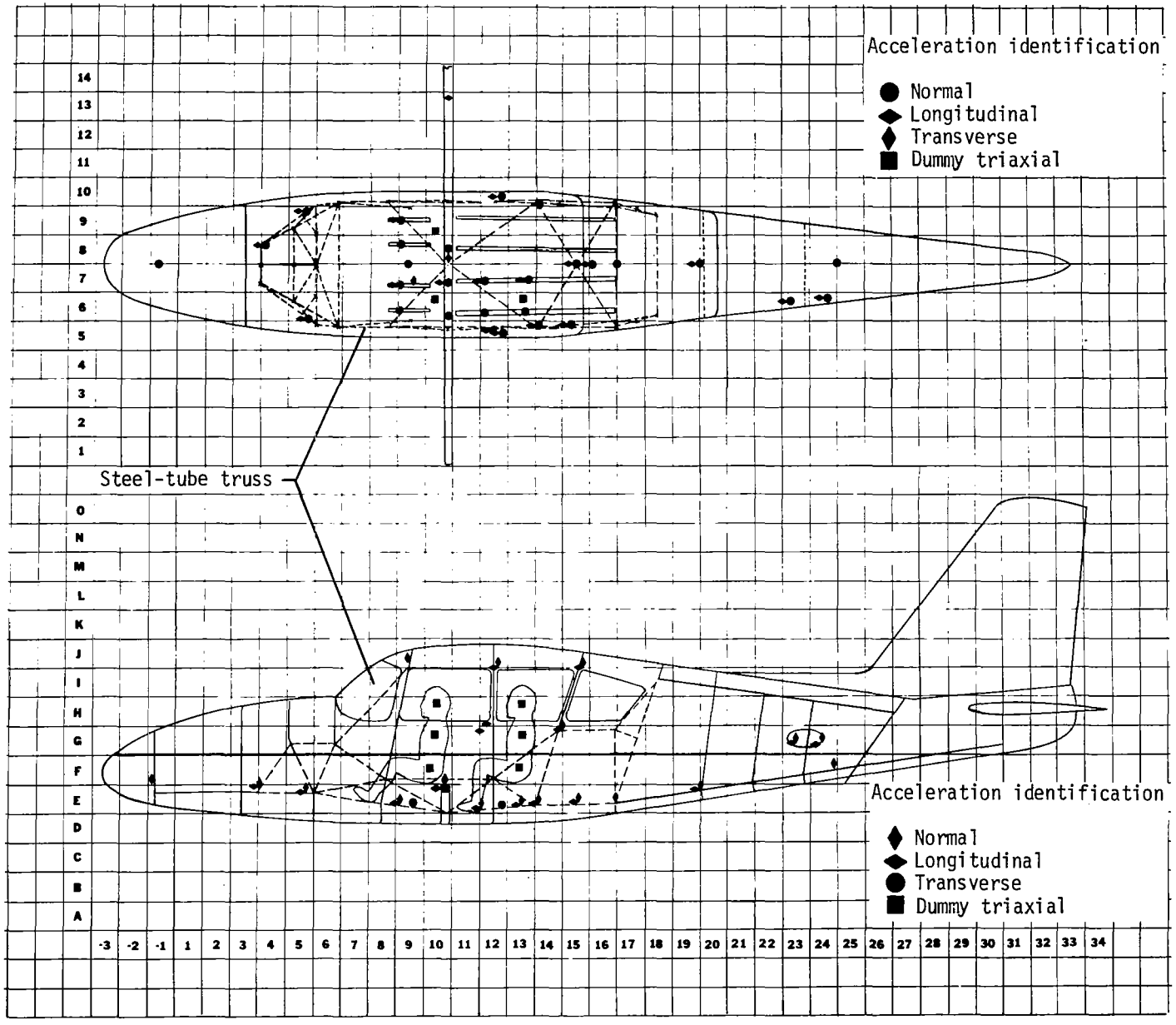

(c) First 30° nose-down test.

Figure 6.- Continued.

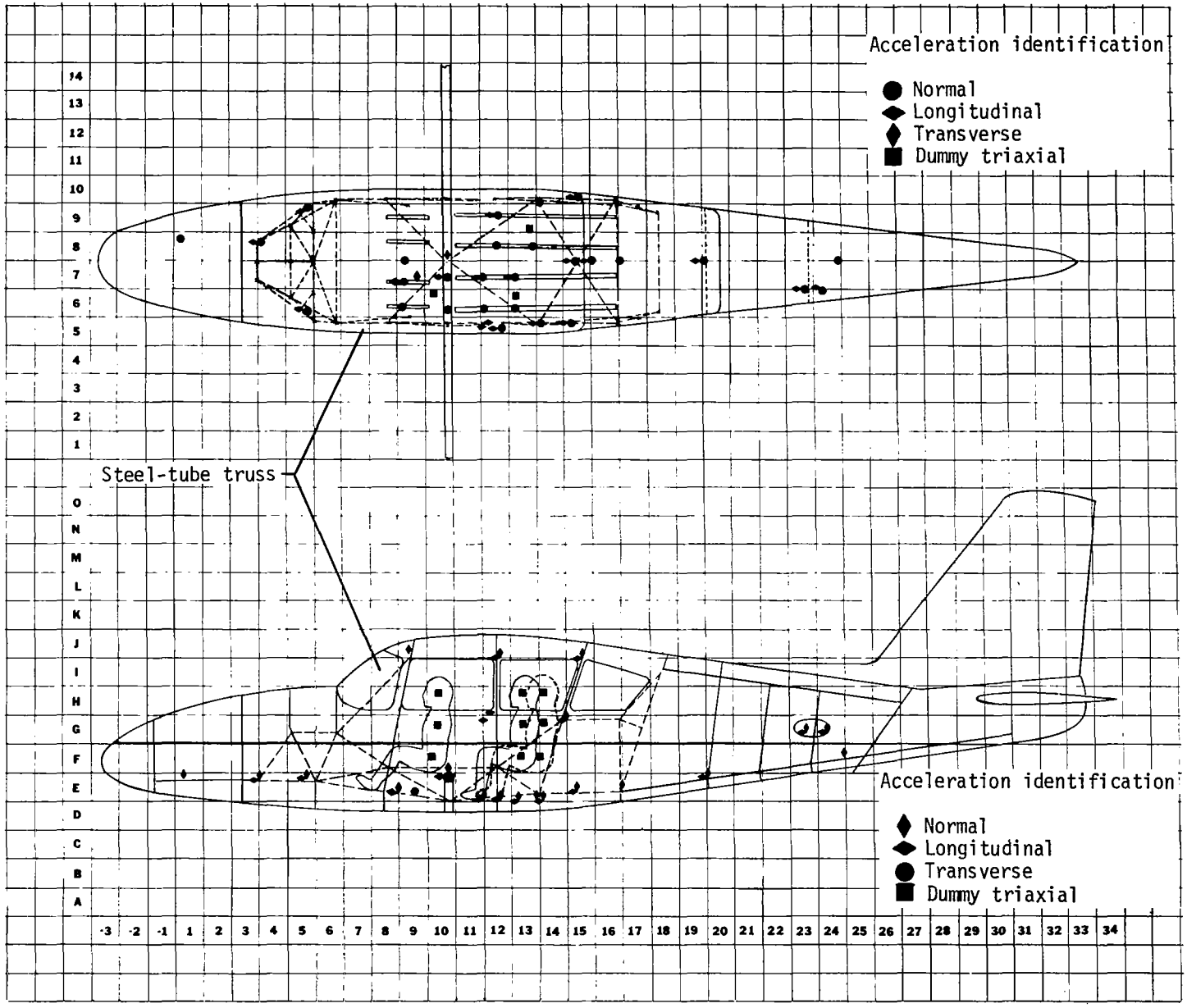

(d) Second 30° nose-down test.

Figure 6.- Concluded.

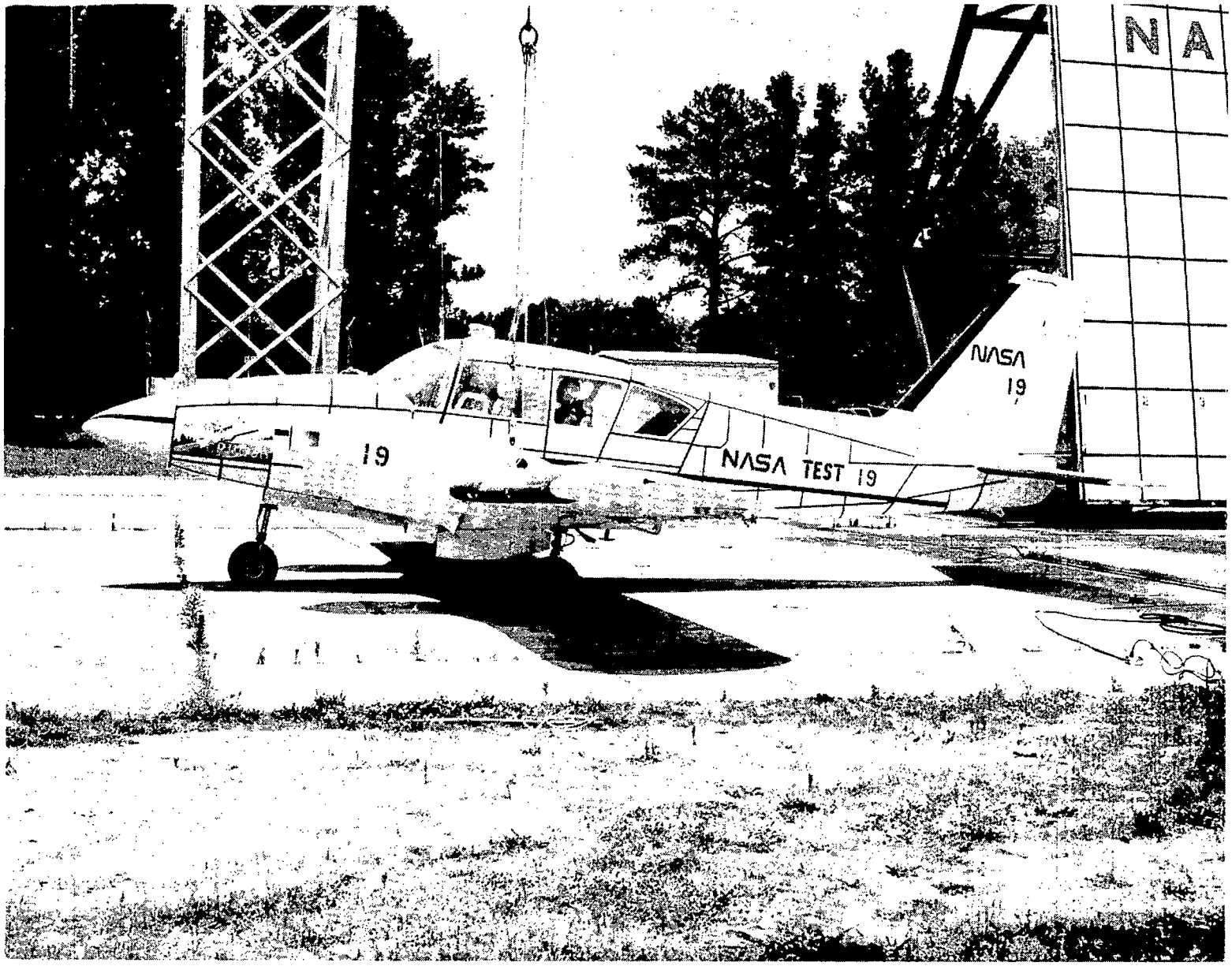

L-80-4823

Figure 7.- Typical airplane test specimen.

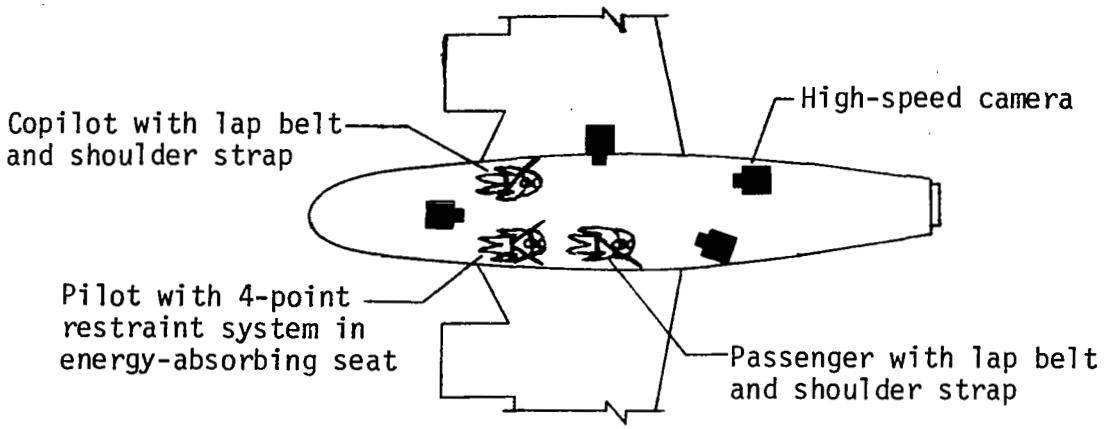

(a) Flat-impact test.

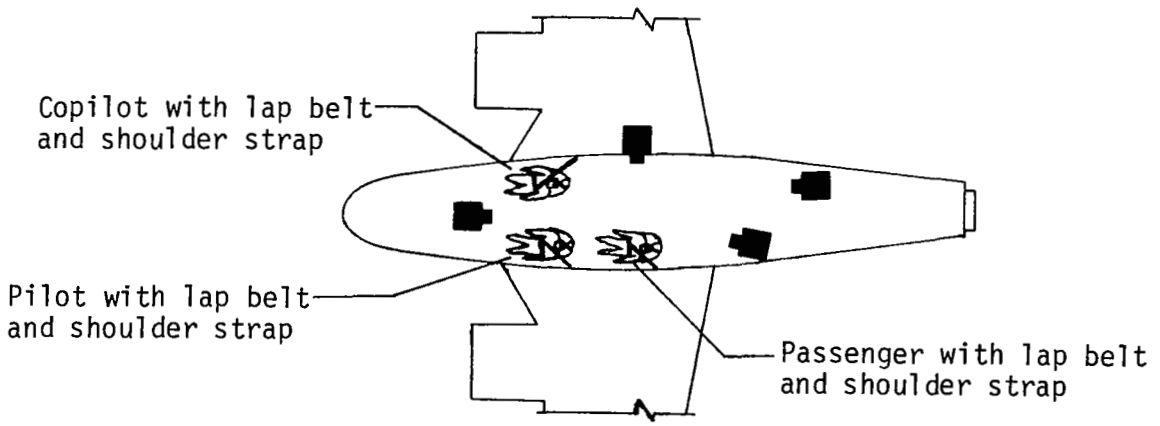

(b) 15° nose-down test.

Figure 8.- Occupants, restraints, and interior camera arrangements.

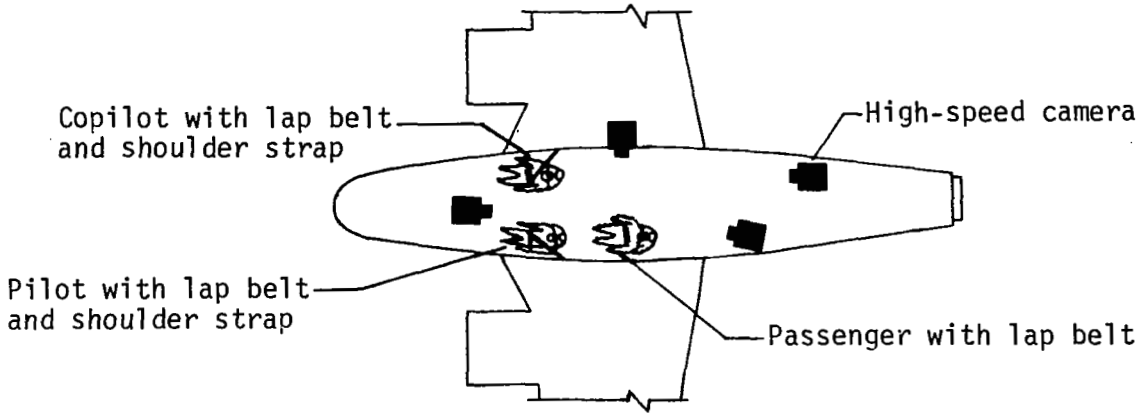

(c) First 30° nose-down test.

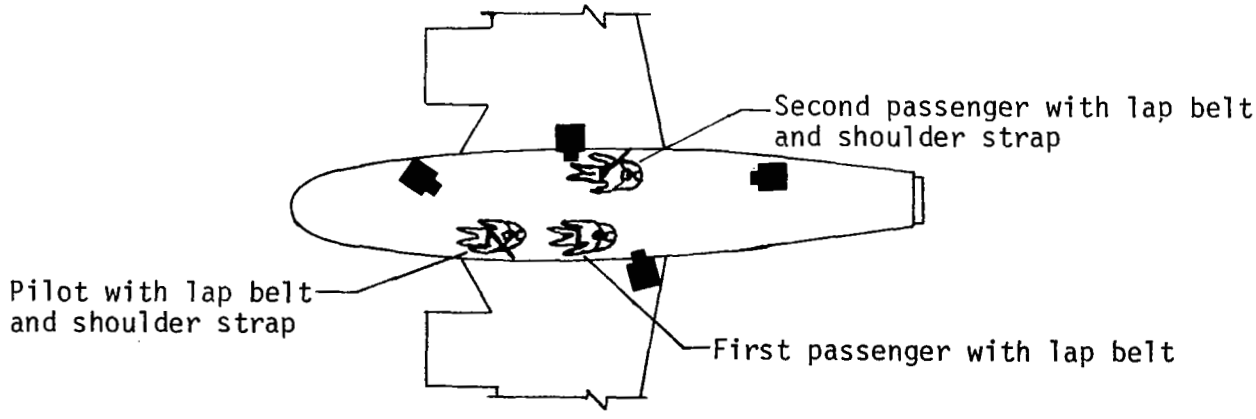

(d) Second 30° nose-down test.

Figure 8.- Concluded.

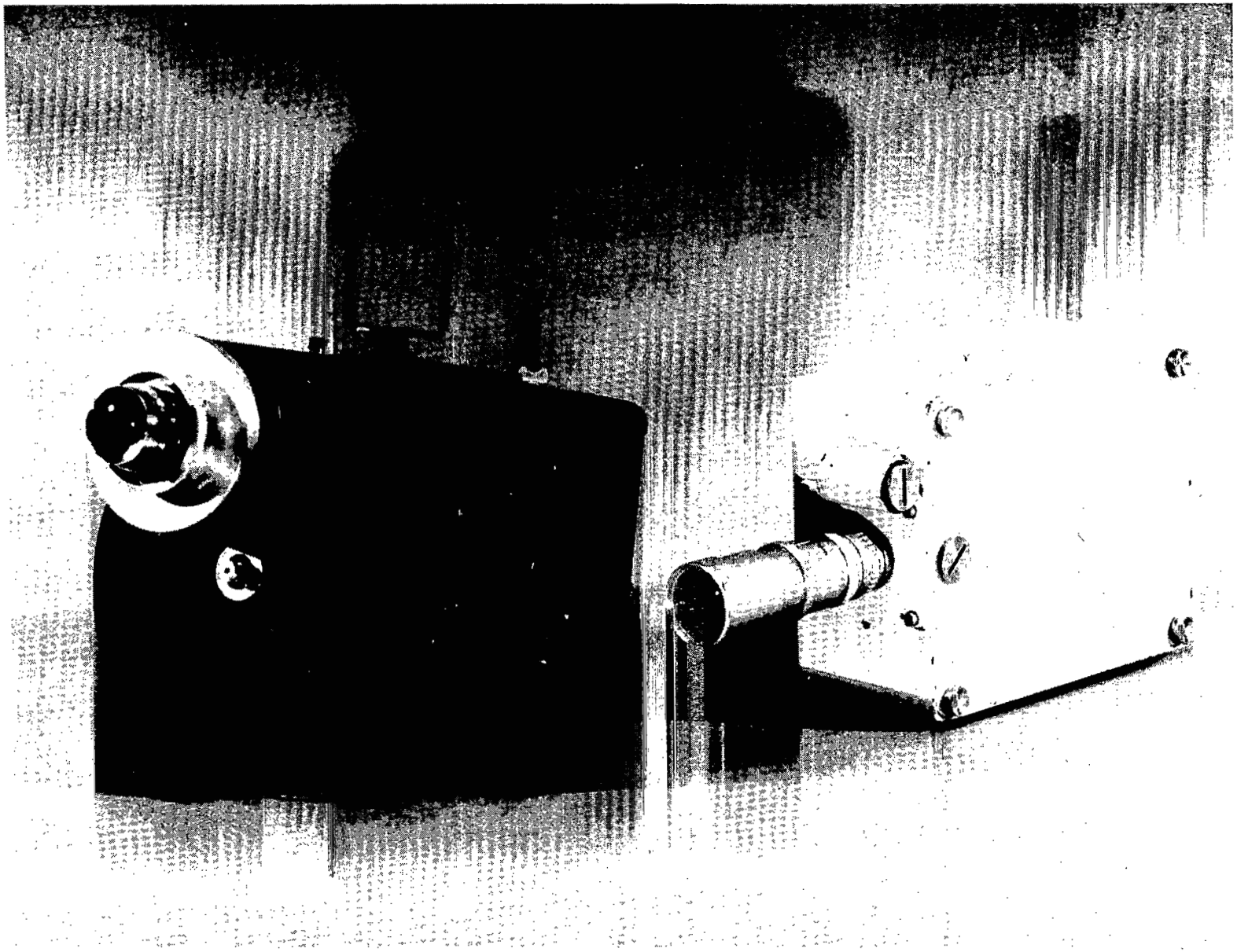

L-82-169

(a) High-speed motion-picture cameras.

Figure 9.- Cameras and onboard transducers.

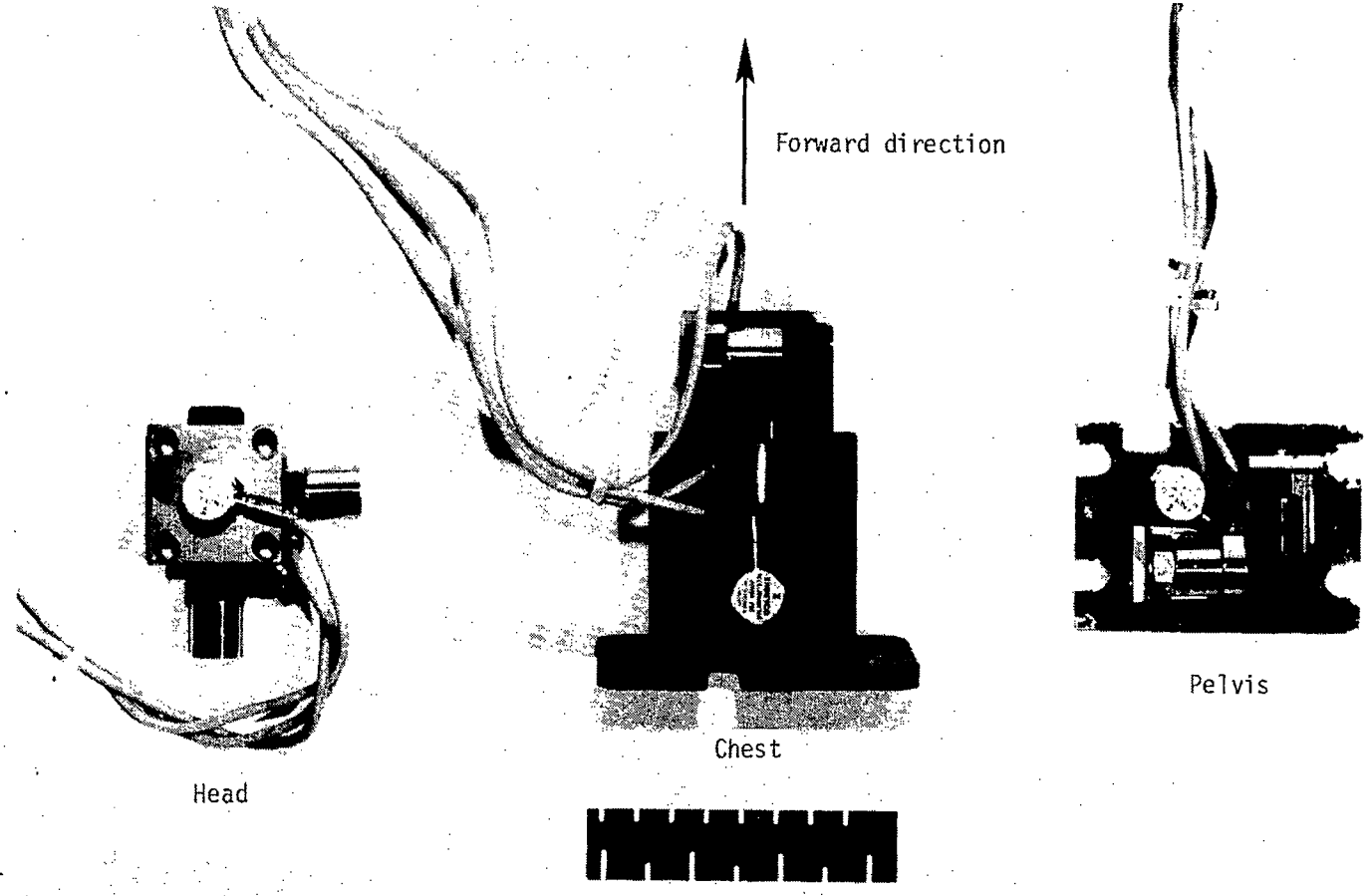

L-82-801.1

(b) Triaxial accelerometer setup in anthropomorphic dummy.

Figure 9.- Continued.

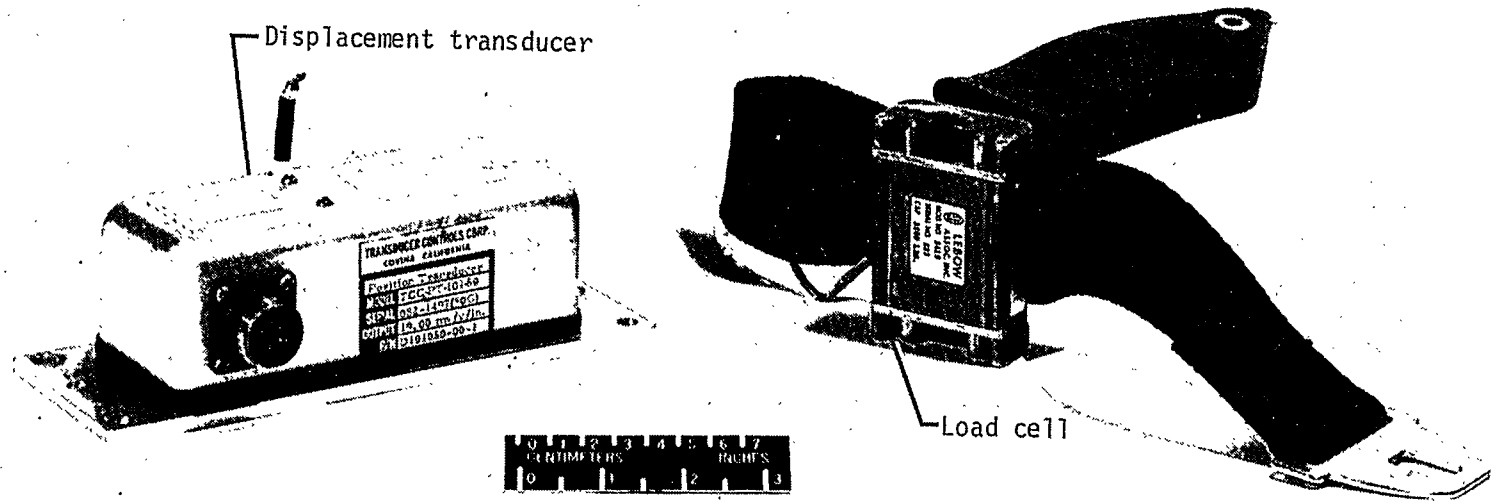

L-82-800.1

(c) Displacement transducer and lap-belt load cell.

Figure 9.- Concluded.

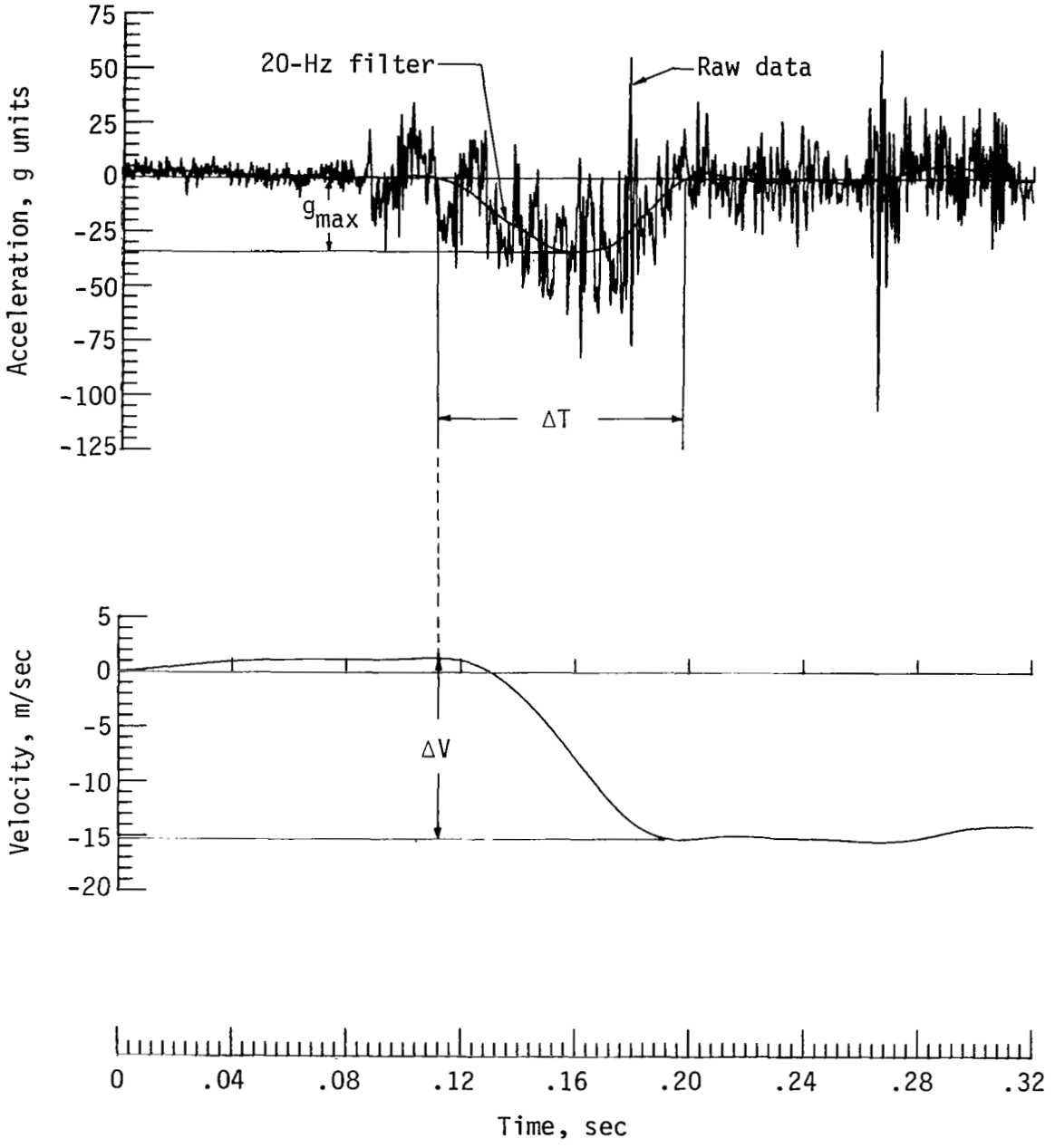

Figure 10.- Method of determining maximum acceleration g_{max}, total time duration of main acceleration pulse ΔT, and integrated velocity change ΔV.

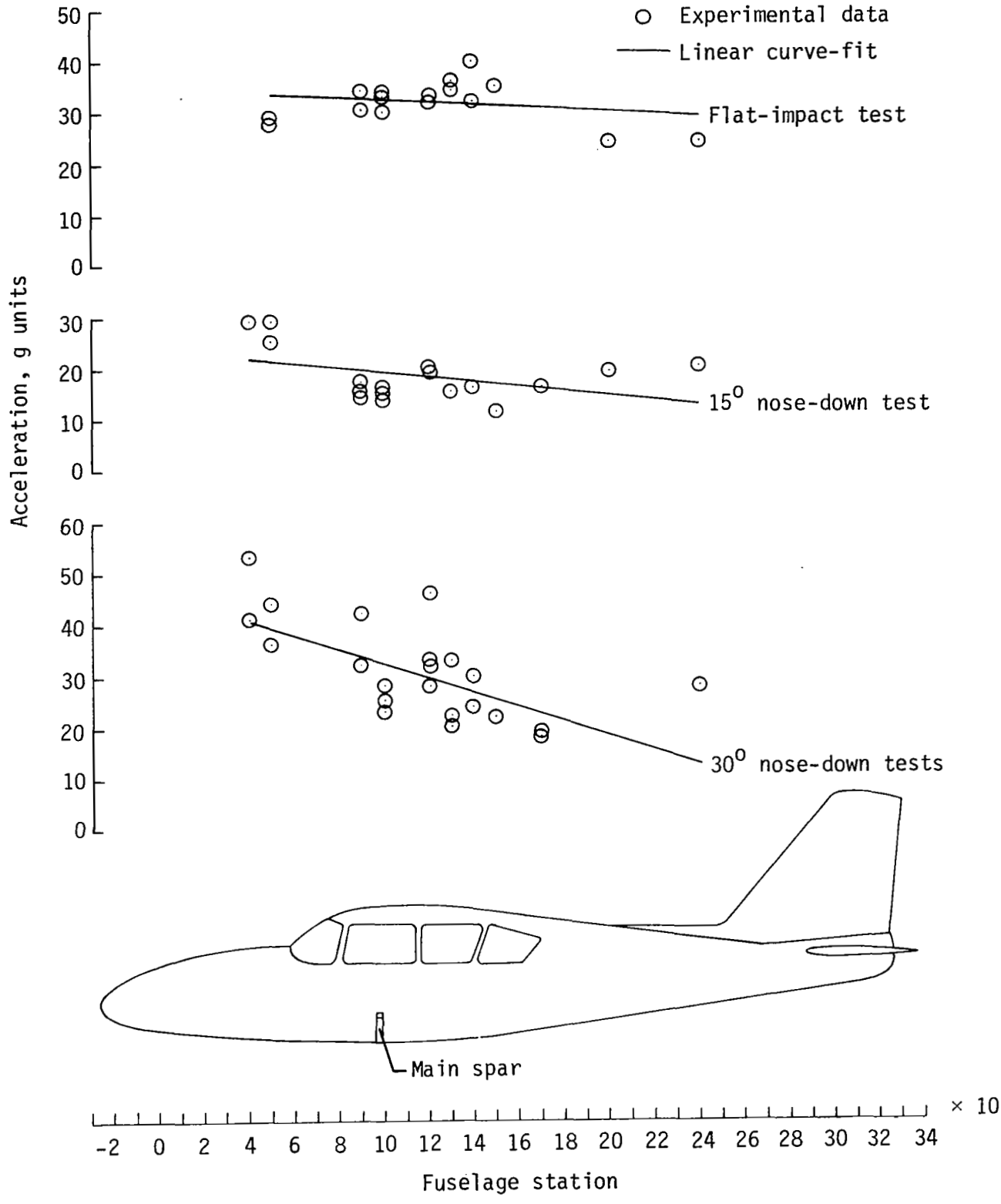

(a) Normal floor accelerations.

Figure 11.- Floor acceleration as a function of fuselage station.

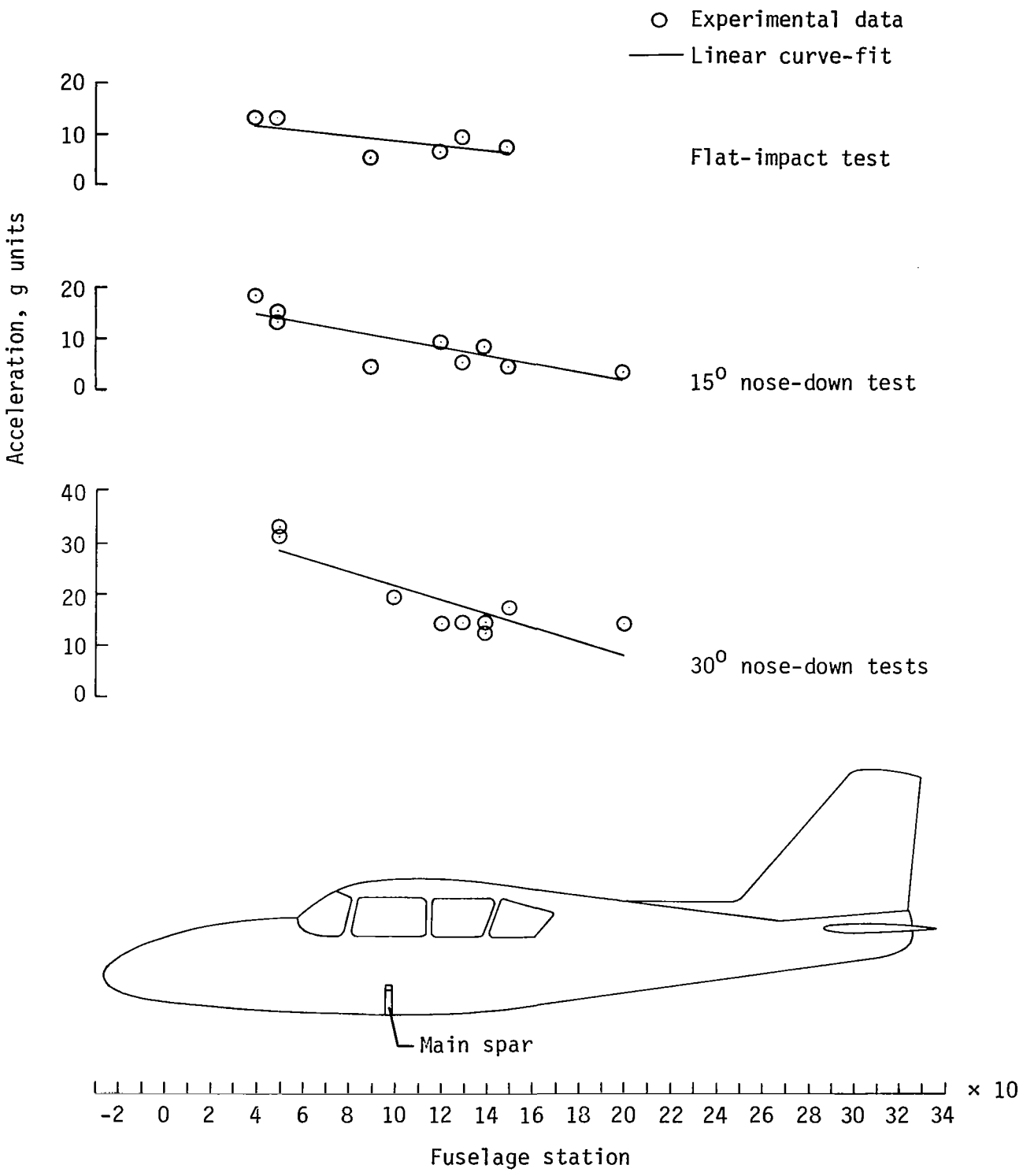

(b) Longitudinal floor accelerations.

Figure 11.- Continued.

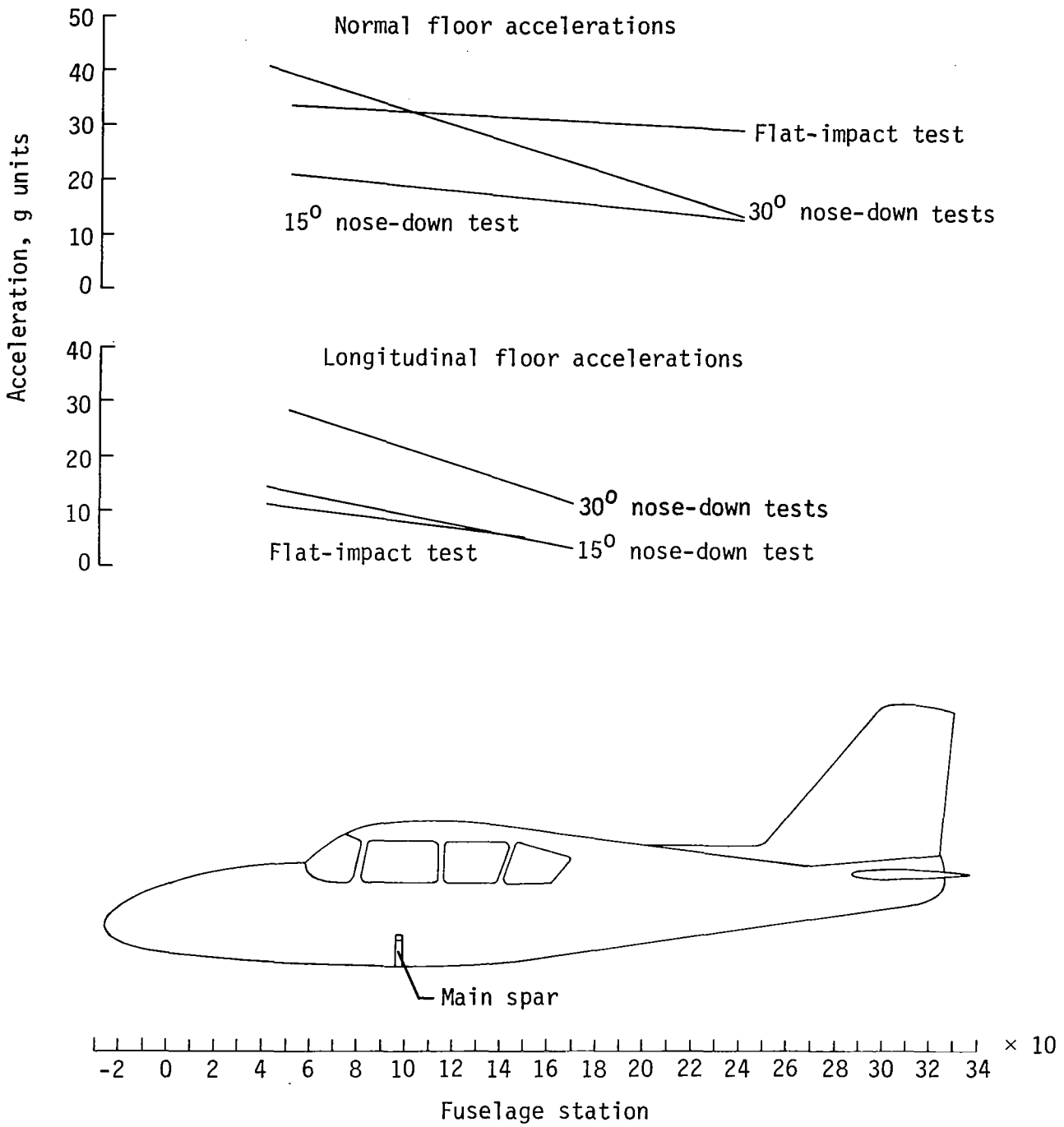

(c) Normal and longitudinal floor accelerations.

Figure 11.- Concluded.

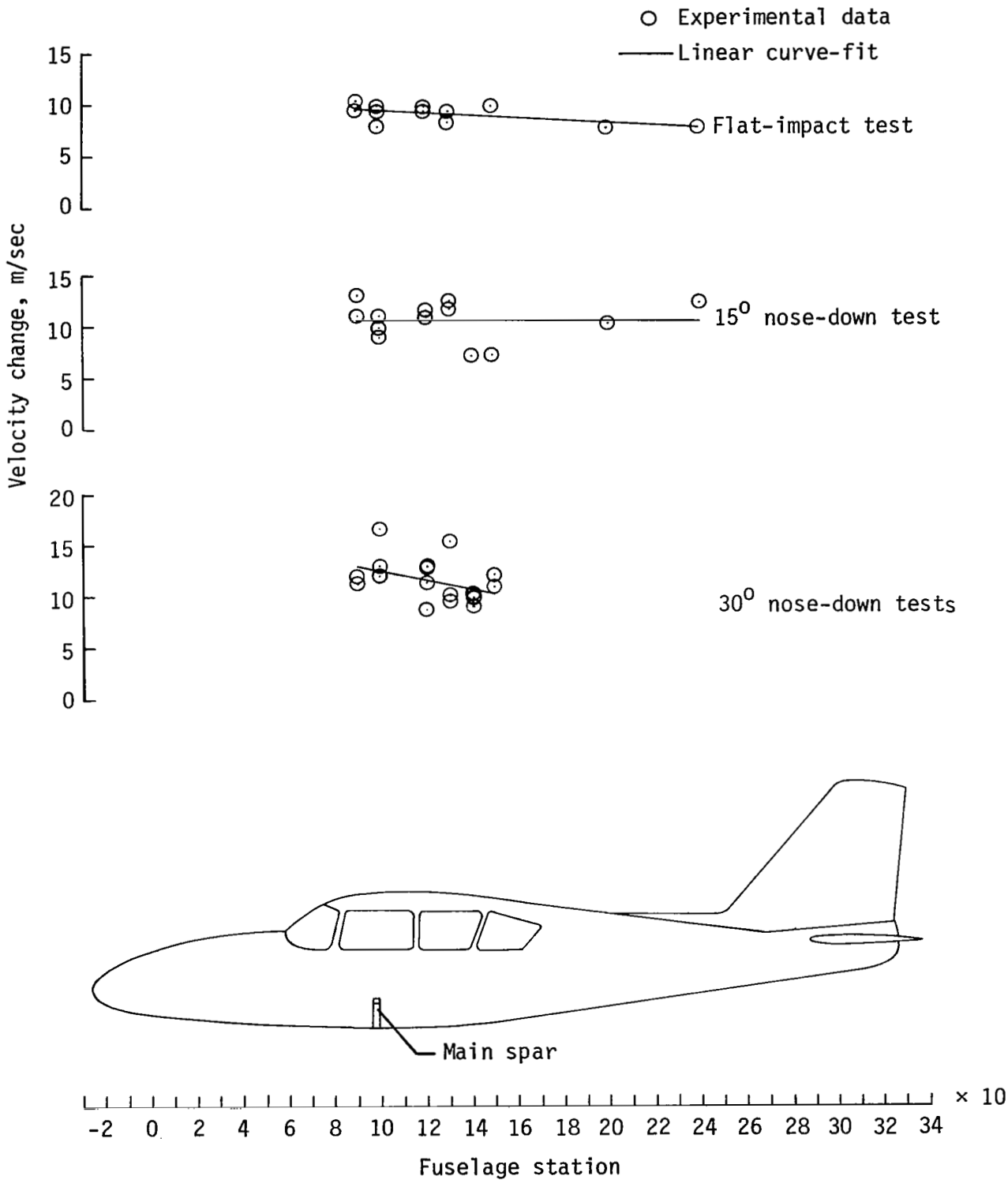

Figure 12.- Normal velocity change ΔV during impact as a function of fuselage station.

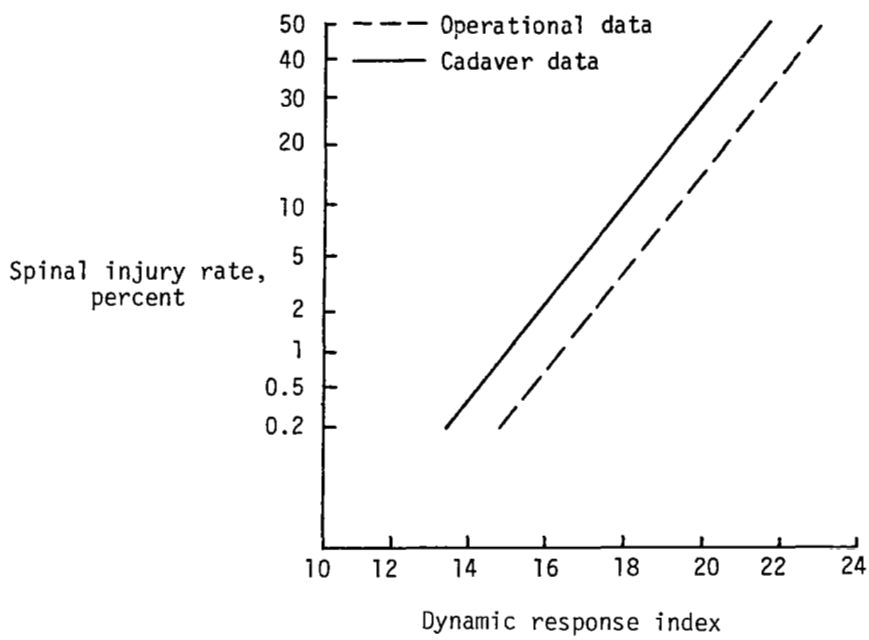

Figure 13.- Probability of spinal injury estimated from cadaver data compared with operational experience.

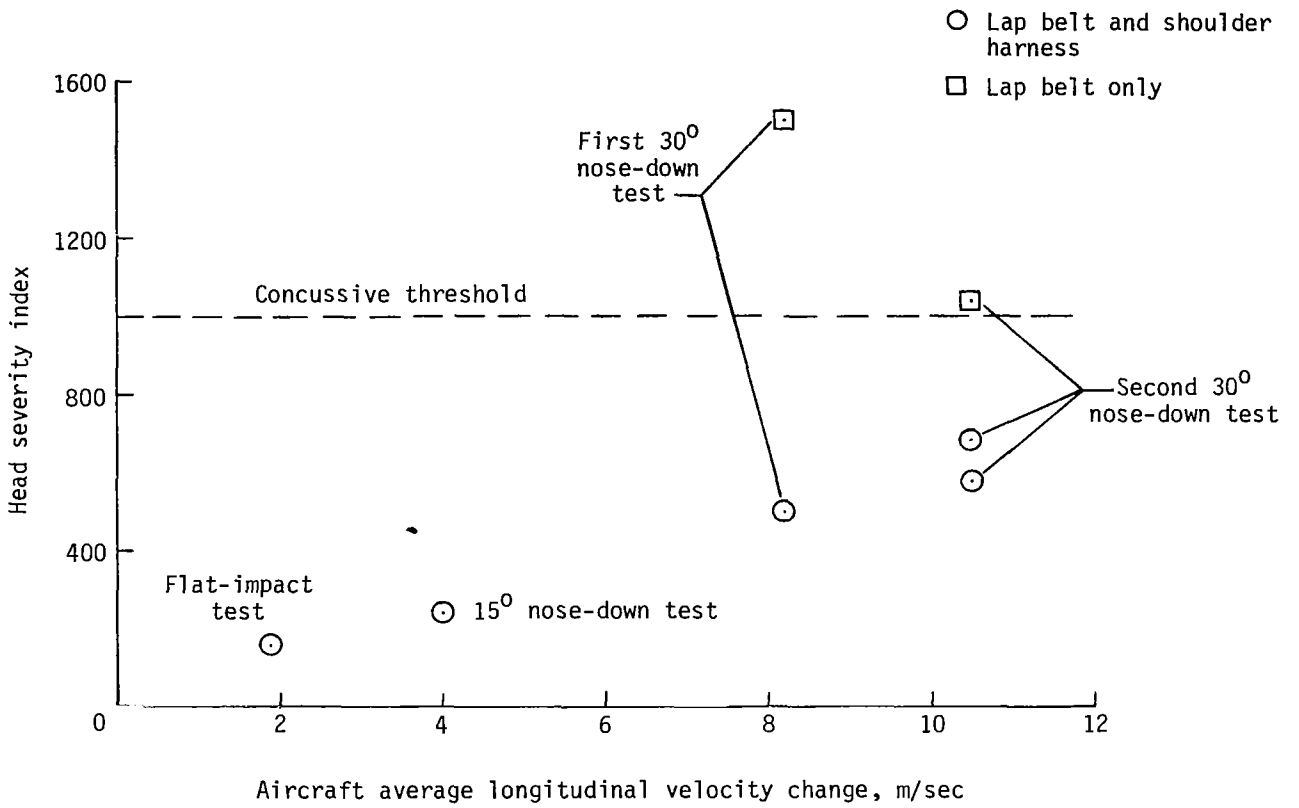

Figure 14.- Occupant head severity index as a function of aircraft floor longitudinal velocity change.

APPENDIX A

FLAT-IMPACT TEST

Crash Dynamics

The crash sequence for the flat-impact test on a concrete test surface is illustrated in figure A1 with nine photographs taken by a scanning camera. The velocity and attitude at impact are given in figure 5(a).

At 0.10 sec the escape hatch has begun to detach from the fuselage. The upper-body forward rotation of the crew and passenger has reached a maximum by this time. At 0.15 sec the fuselage has separated just aft of the welded tubular-steel truss, which surrounds the interior of the cabin. The bottom of the fuselage is now horizontal and flattened as the aircraft slides along the concrete. By 0.20 sec the crew and passenger have begun to rebound to an upright position in their seats. The remaining photographs in figure A1 show the airplane during slide-out.

Assessment of Damage

Precrash and postcrash photographs of the damage sustained by the airplane from the flat-impact test are presented in figure A2. Figures A2(a) and A2(b) show the overall interior arrangement of the anthropomorphic dummies, seats, and instrumentation prior to the test. The livable cabin volume (i.e., a volume sufficient in size to maintain space between the occupants and the structure) was maintained in the crew and passenger positions during the crash impact. The copilot's seat was not damaged except for the rubber-membrane seat pan, which failed at several of the attachment points. However, the seat rail for the front left leg of the copilot's seat was broken by the impact. (See fig. A2(c).)

The final position of the experimental pilot's seat, which stroked approximately 3 in. during the impact, is also shown in figure A2(c). The final position of the passenger seat is shown in figure A2(d). The tubular-steel seat legs were not deformed. The seat cushion and pan ruptured, and the seat rails were slightly depressed in the front.

The final position of the airplane and the overall damage to the structure as viewed from the port side is shown in figure A2(e). Separation of the fuselage just aft of the internal tubular truss is attributed to rivet shear, and the floor is the only structure holding the fuselage together. (See fig. A2(f).) Compression loading of the bottom of the fuselage and nacelles is shown in figure A2(g).

Acceleration Time Histories

Accelerations, loads, and displacements measured on the airplane structure and in the dummies for the flat-impact test are shown in figure A3. Normal, longitudinal, and transverse accelerations measured on the floor of the airplane are given in figures A3(a) and A3(b) as a function of time. The data are grouped according to accelerometer location and orientation. The accelerometers were oriented along the normal (Z), longitudinal (X), and transverse (Y) axes as shown in figure 4. Each location is designated by its grid coordinate corresponding to figure 6. The first number indicates the longitudinal coordinate; the first letter indicates the normal

coordinate (floor to roof); the second number indicates the transverse coordinate; and the second letter indicates the accelerometer orientation with respect to the airplane body-axis system.

The maximum normal accelerations varied from 34g in the crew area to 24g in the aft baggage compartment. The average normal crash pulse for the cabin area was 31g peak, 0.057 sec total pulse duration, and 9.1 m/sec velocity change obtained from the integrated acceleration traces. The maximum longitudinal accelerations ranged from 5g to 9g, with an average of 6g, a 0.052-sec duration, and an integrated velocity change of the main (first) pulse of 1.9 m/sec. The remaining 23.7 m/sec horizontal velocity was dissipated primarily by sliding friction in 76 m with an average deceleration calculated to be 0.38g. The average transverse acceleration was measured to be less than 3g. The total velocity change from the integrated transverse accelerations over 0.32 sec was approximately zero.

The pilot was seated in an energy-absorbing seat that stroked approximately 3 in. Accelerations for all dummies were measured relative to either the dummy head, chest, or pelvis. The pilot's head, chest, and pelvis accelerations are given in figure A3(c). The peak normal pelvis acceleration (fig. A3(c)) reached 32g before leveling off at approximately 15g. The acceleration was greater than 20g for only 0.006 sec. The total time duration of the pulse was approximately 0.10 sec, and there was an integrated velocity change of 10.5 m/sec. The normal chest pulse was similar to the pelvis, but the maximum g level was slightly attenuated. The peak longitudinal accelerations were 20g in the pelvis and 11g in the chest.

The copilot was seated in a standard seat for an airplane of this type. The head, chest, and pelvis accelerations for the copilot are given in figure A3(d). The peak normal pelvis acceleration (fig. A3(d)) was 31g, which is about the same maximum pelvis acceleration as that of the pilot. However, the acceleration for the copilot was greater than 20g for approximately 0.026 sec, compared with 0.006 sec for the pilot. The pilot's stroking energy-absorbing seat spread the acceleration pulse over a longer time duration with an average pelvis acceleration (velocity change during major impact/pulse duration) of 10.7g. The copilot's average pelvis acceleration was 14.0g. These normal pelvis accelerations would probably fall in the area of moderate injury (ref. 17). The longitudinal accelerations were all in the noninjurious range for a well-restrained occupant (ref. 17).

The passenger was also seated in a standard general-aviation seat for this type airplane. The head, chest, and pelvis accelerations for the passenger are given in figure A3(e). The peak normal pelvis acceleration was 39g, with the acceleration being greater than 20g for 0.028 sec. The average normal pelvis acceleration was 17.2g.

Maximum load in the pilot's shoulder harness was 700 N (fig. A3(f)). The maximum load in the copilot's shoulder harness was 1070 N, and the maximum chest forward motion was 12.5 cm (fig. A3(f)). The maximum load in the passenger's lap belt (fig. A3(f)) was approximately 400 N.

Figures A3(g) and A3(h) contain miscellaneous acceleration traces presented for completeness.

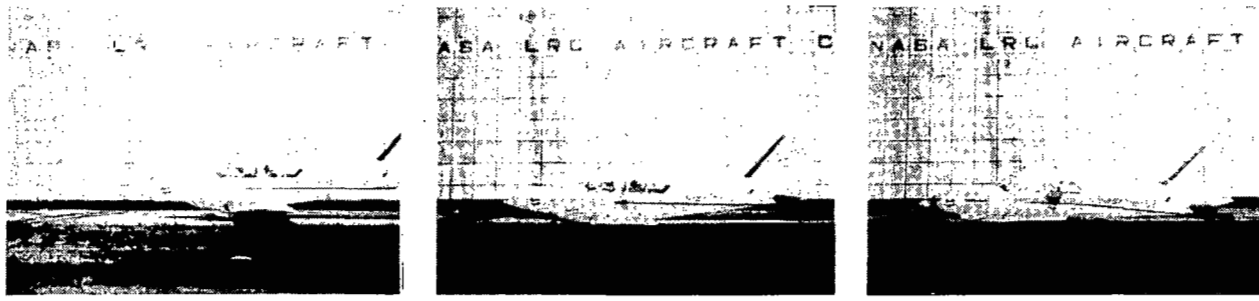

Time = 0.0 sec | Time = 0.05 sec | Time = 0.10 sec

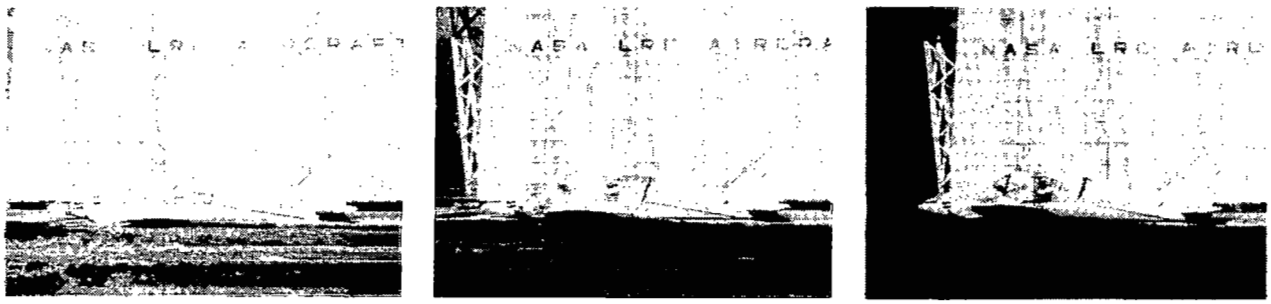

Time = 0.15 sec | Time = 0.20 sec | Time = 0.25 sec

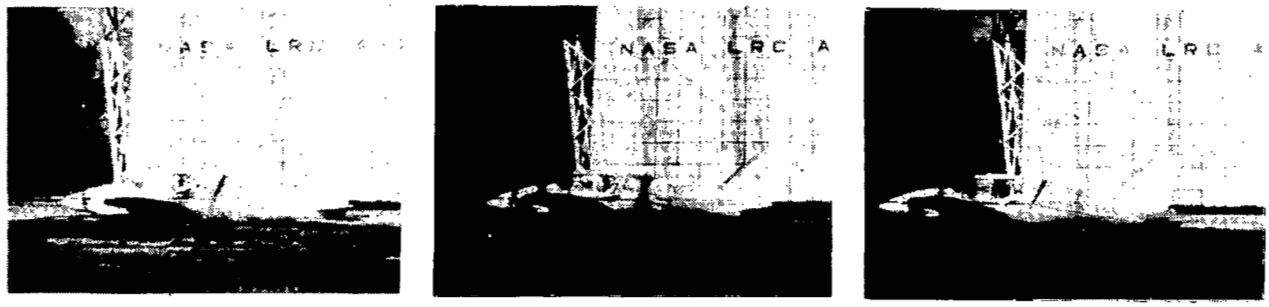

Time = 0.30 sec | Time = 0.35 sec | Time = 0.40 sec

L-81-5700.1

Figure A1.- Crash-sequence photographs of flat-impact test.

(a) Precrash forward interior view of flat-impact test airplane.

Figure A2.- Precrash and postcrash photographs of flat-impact test.

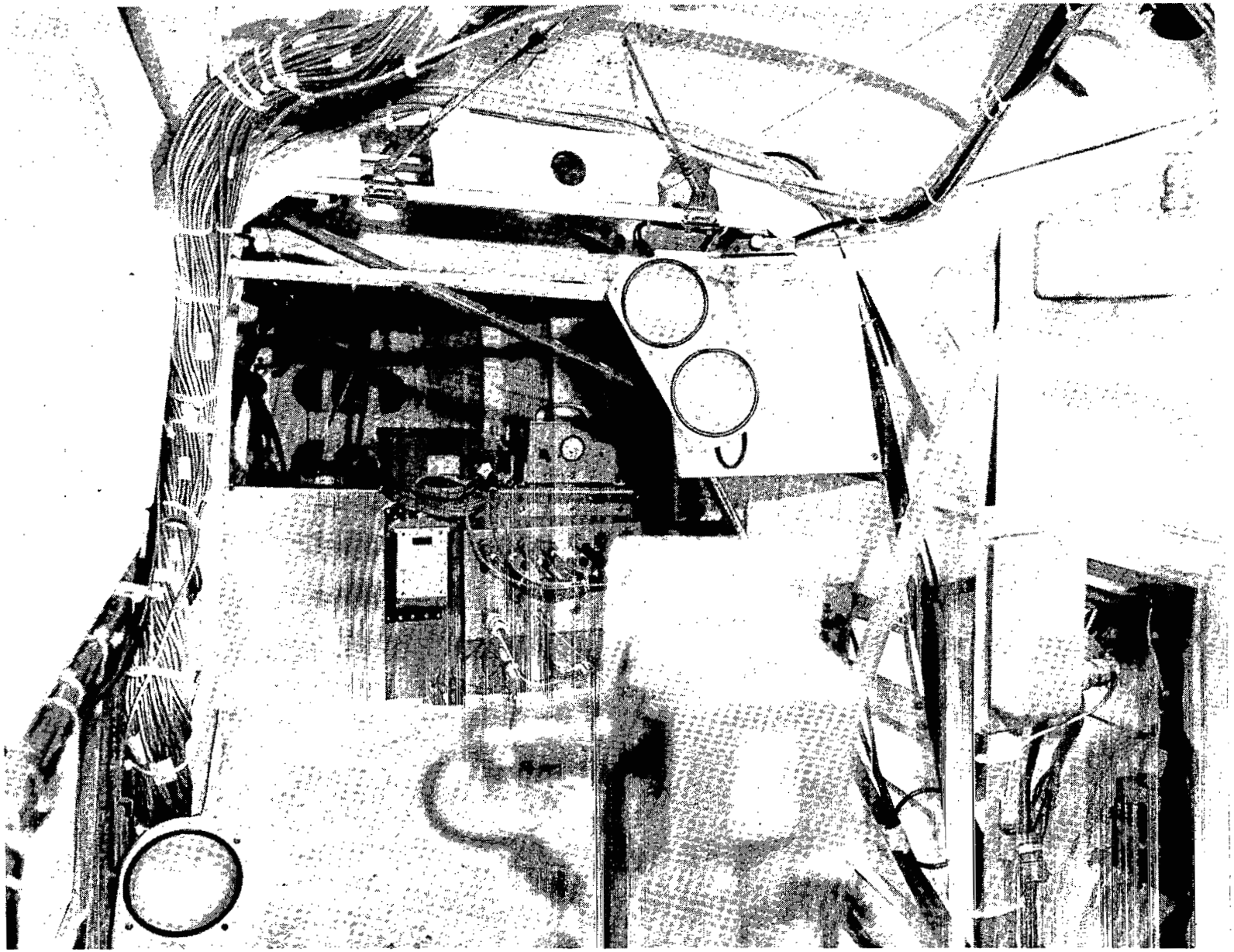

L-80-9853

(b) Precrash rear interior view of flat-impact test airplane.

Figure A2.- Continued.

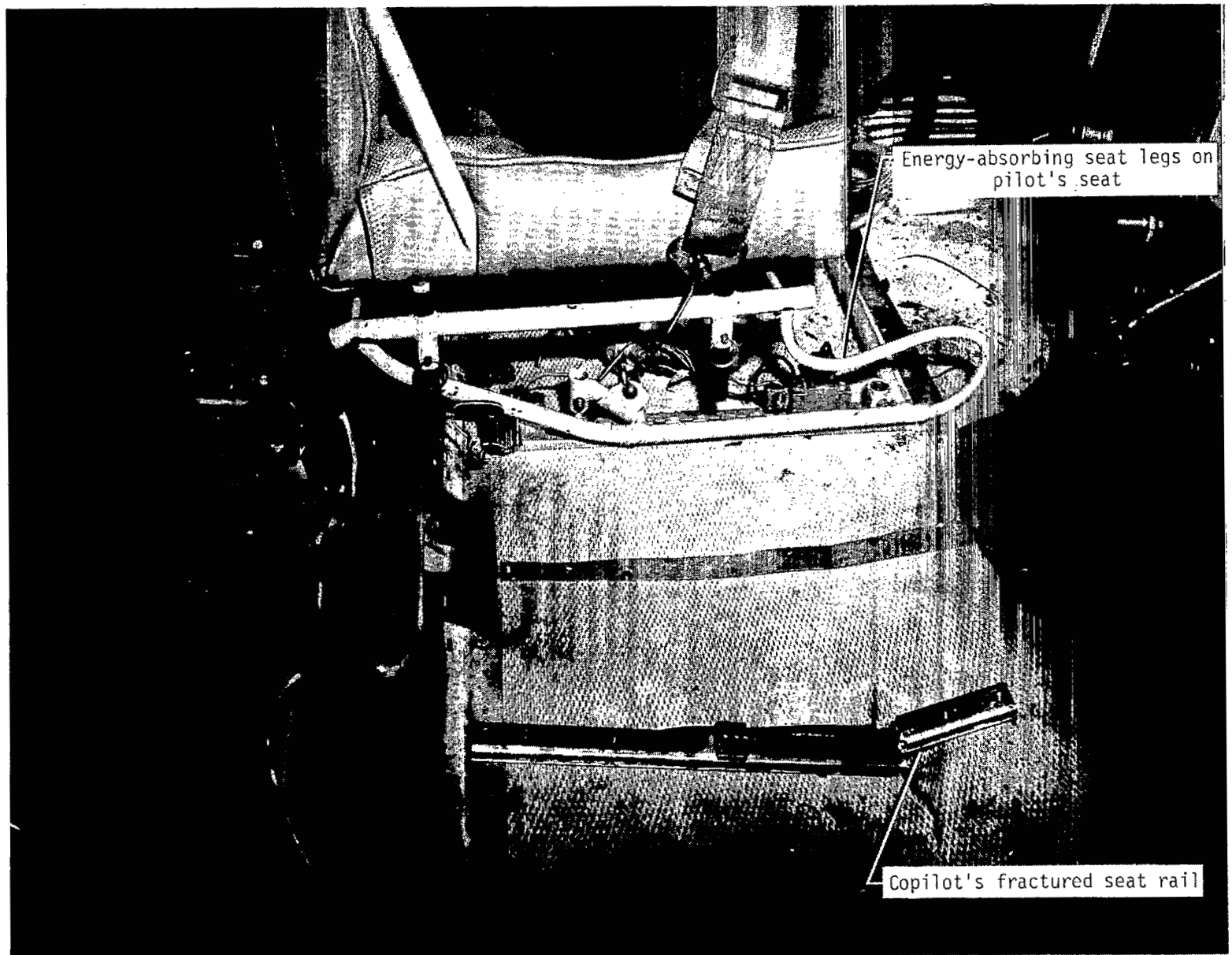

L-80-10,094.1

(c) Postcrash view of crew compartment.

Figure A2.- Continued.

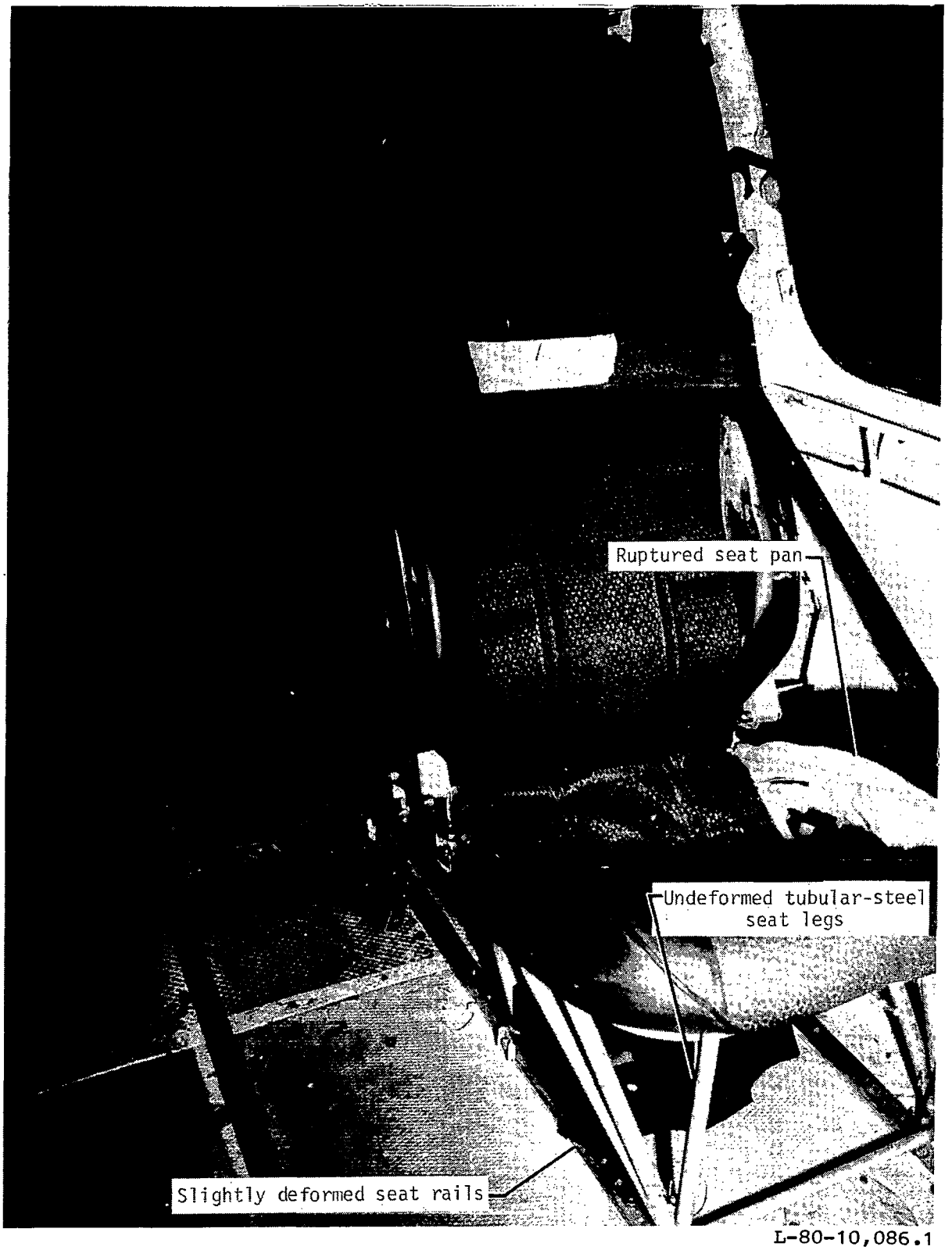

(d) Postcrash view of passenger's seat.

Figure A2.- Continued.

L-80-10,062.1

(e) Port-side view of airplane.

Figure A2.- Continued.

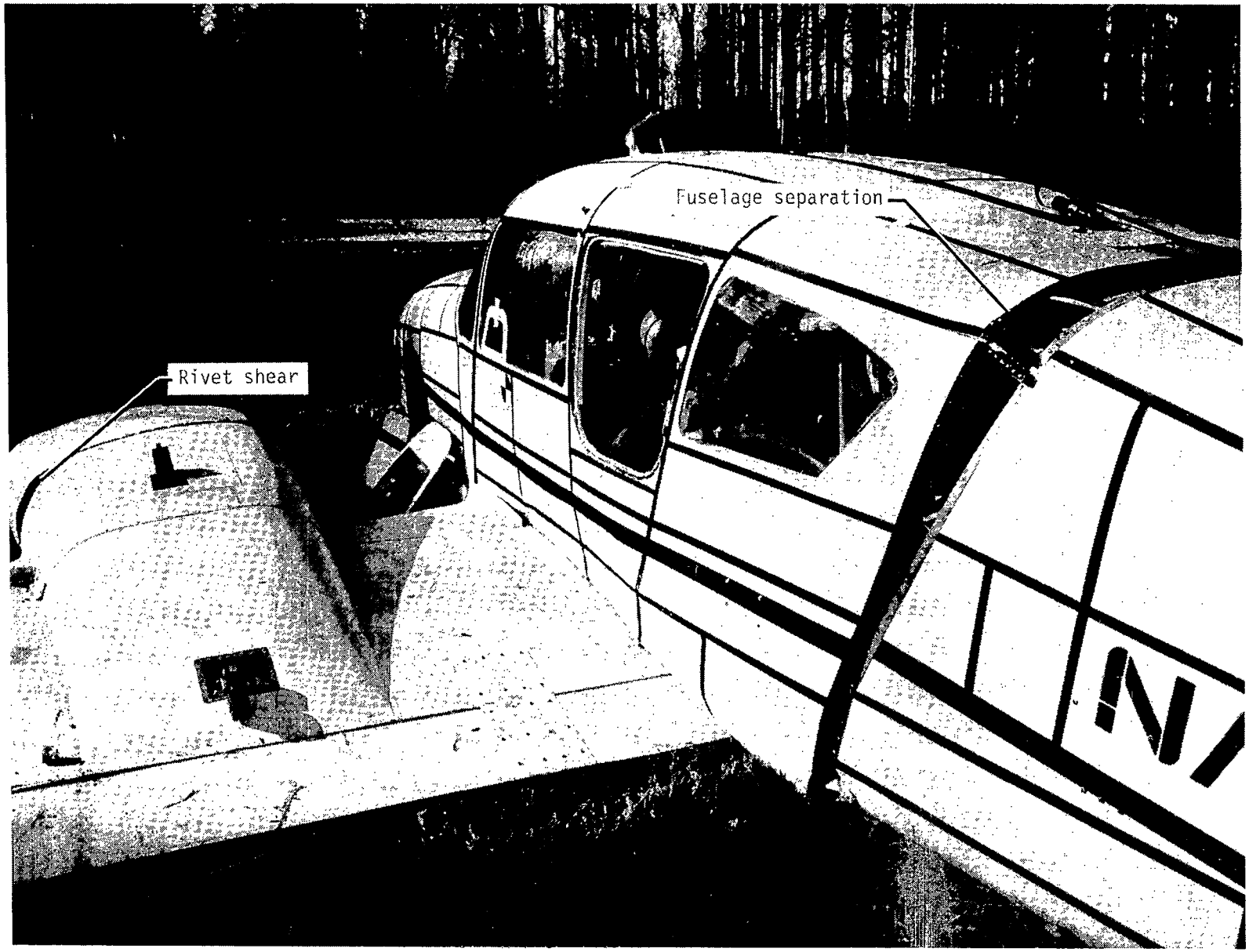

L-80-10,106.1

(f) Port-side external damage.

Figure A2.- Continued.

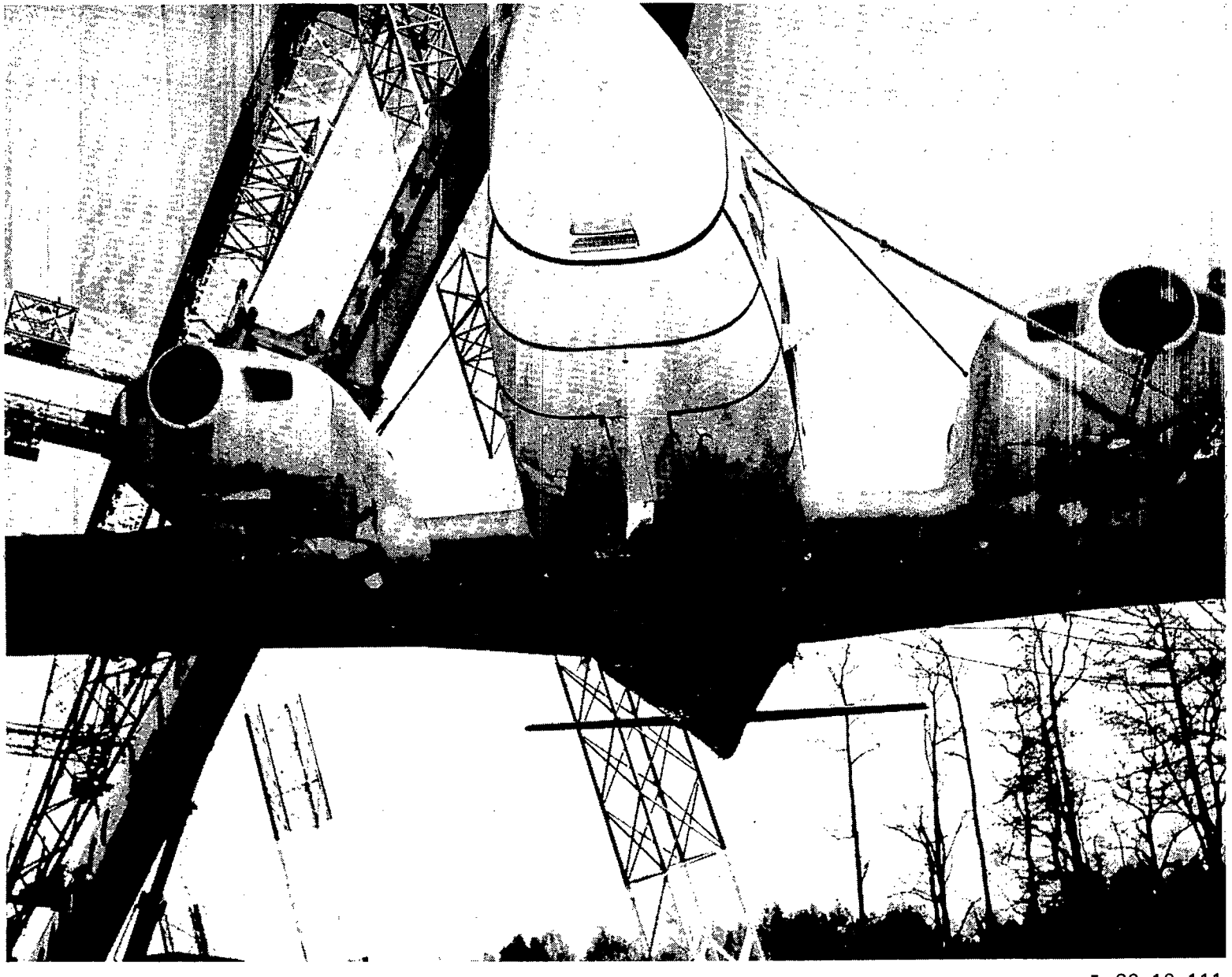

L-80-10,111

(g) Underside view of airplane showing crash damage.

Figure A2.- Concluded.

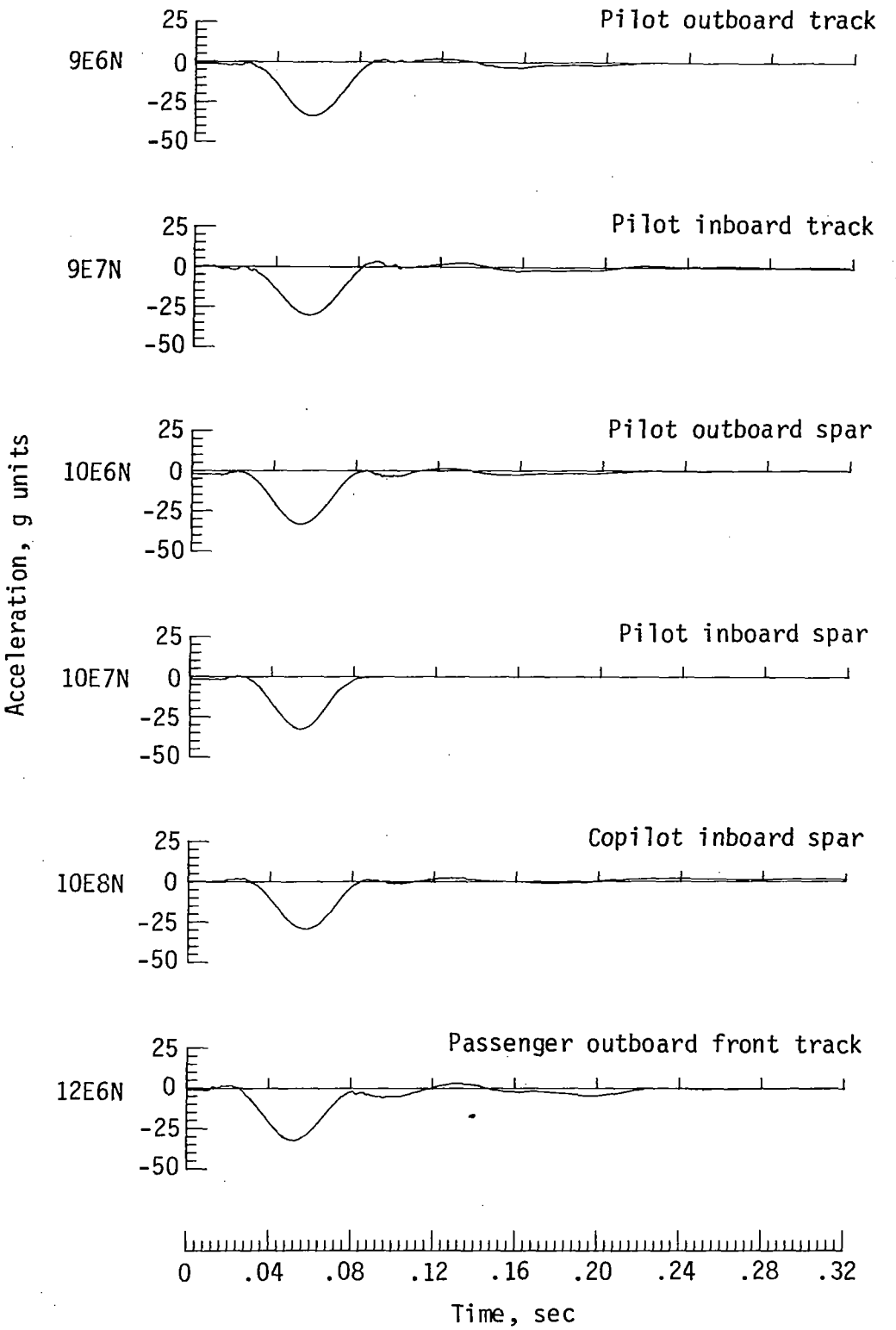

(a) Normal floor accelerations.

Figure A3.- Data for flat-impact test.

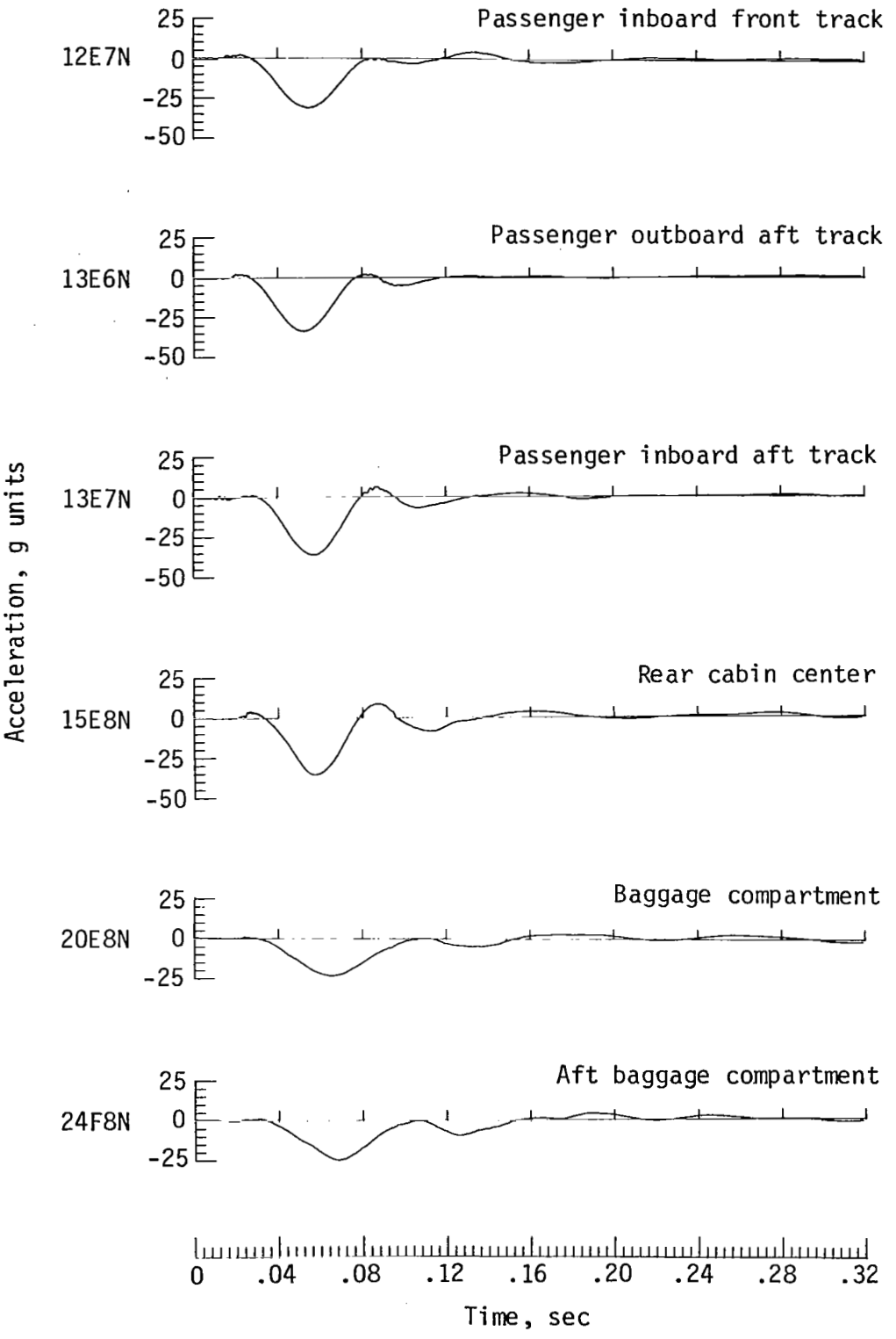

(a) Concluded.

Figure A3.- Continued.

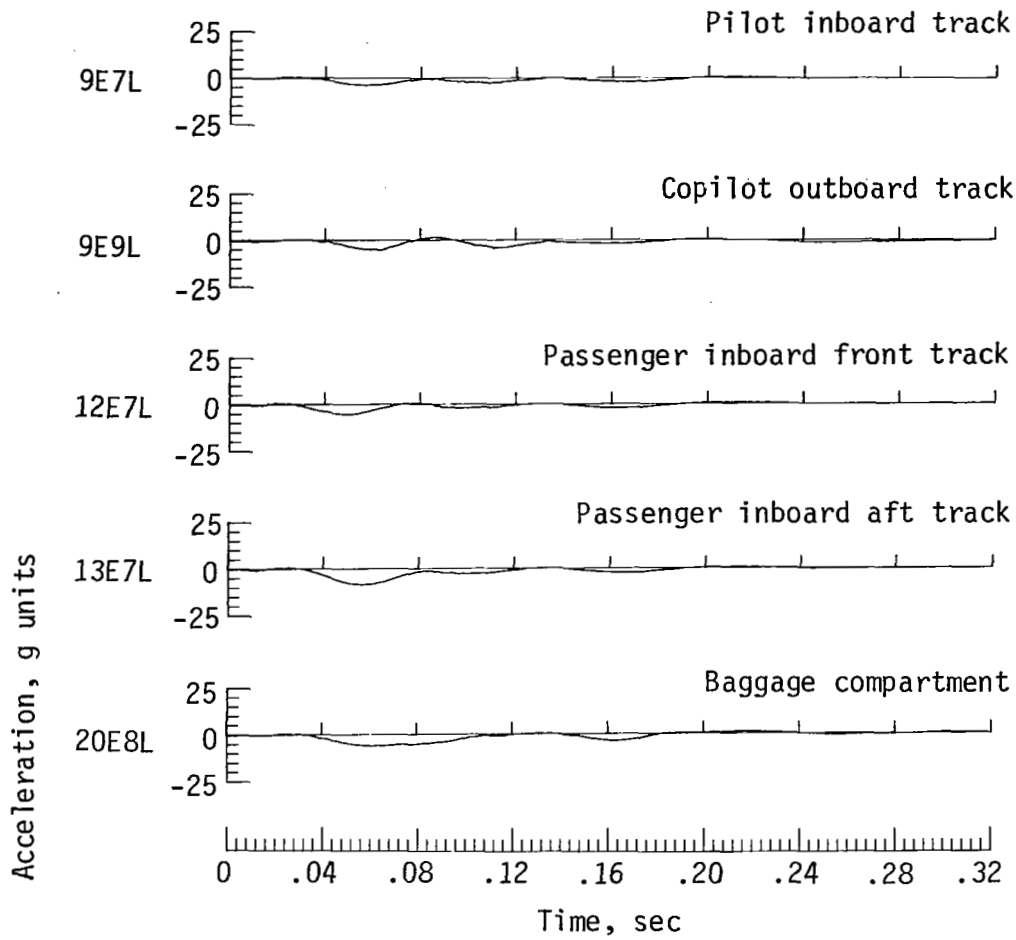

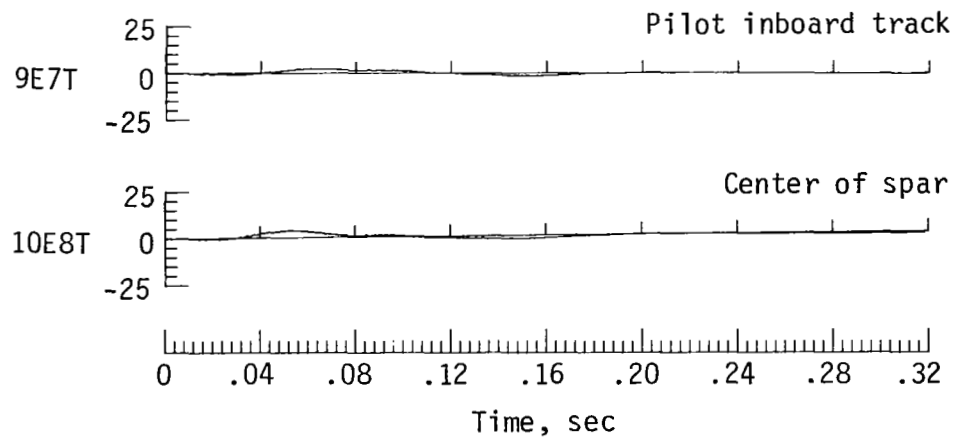

(b) Longitudinal and transverse floor accelerations.

Figure A3.- Continued.

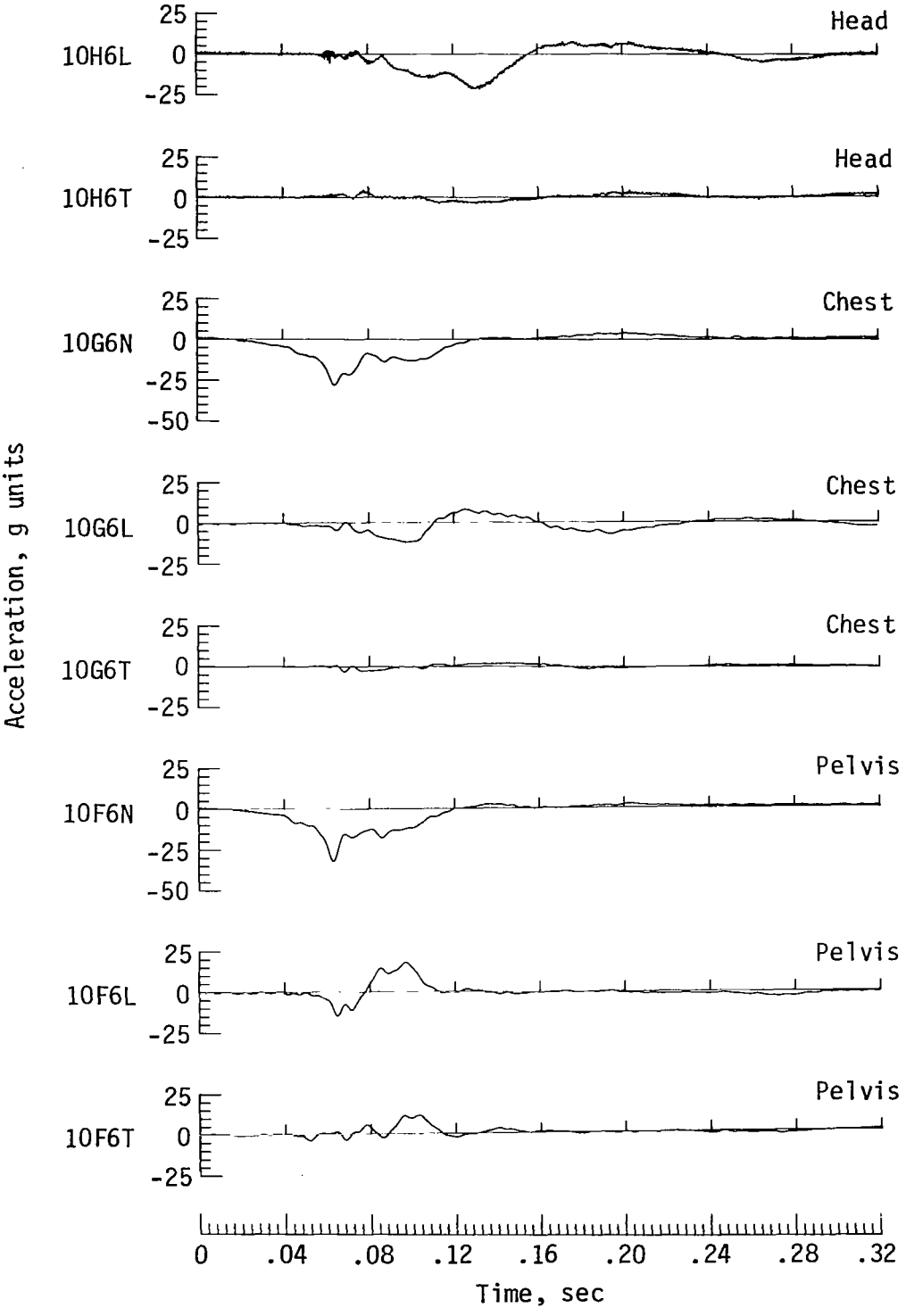

(c) Pilot accelerations.

Figure A3.- Continued.

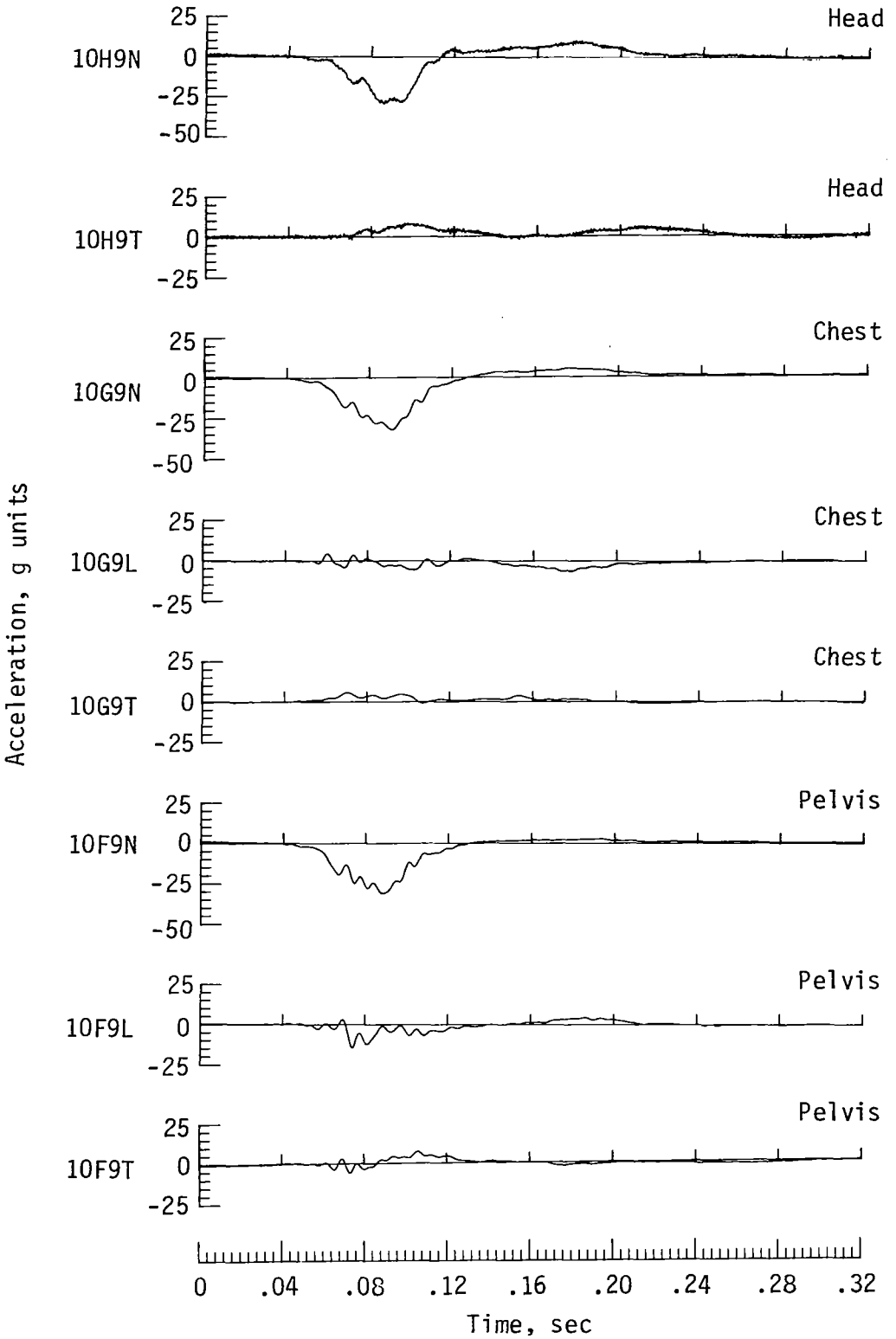

(d) Copilot accelerations.

Figure A3.- Continued.

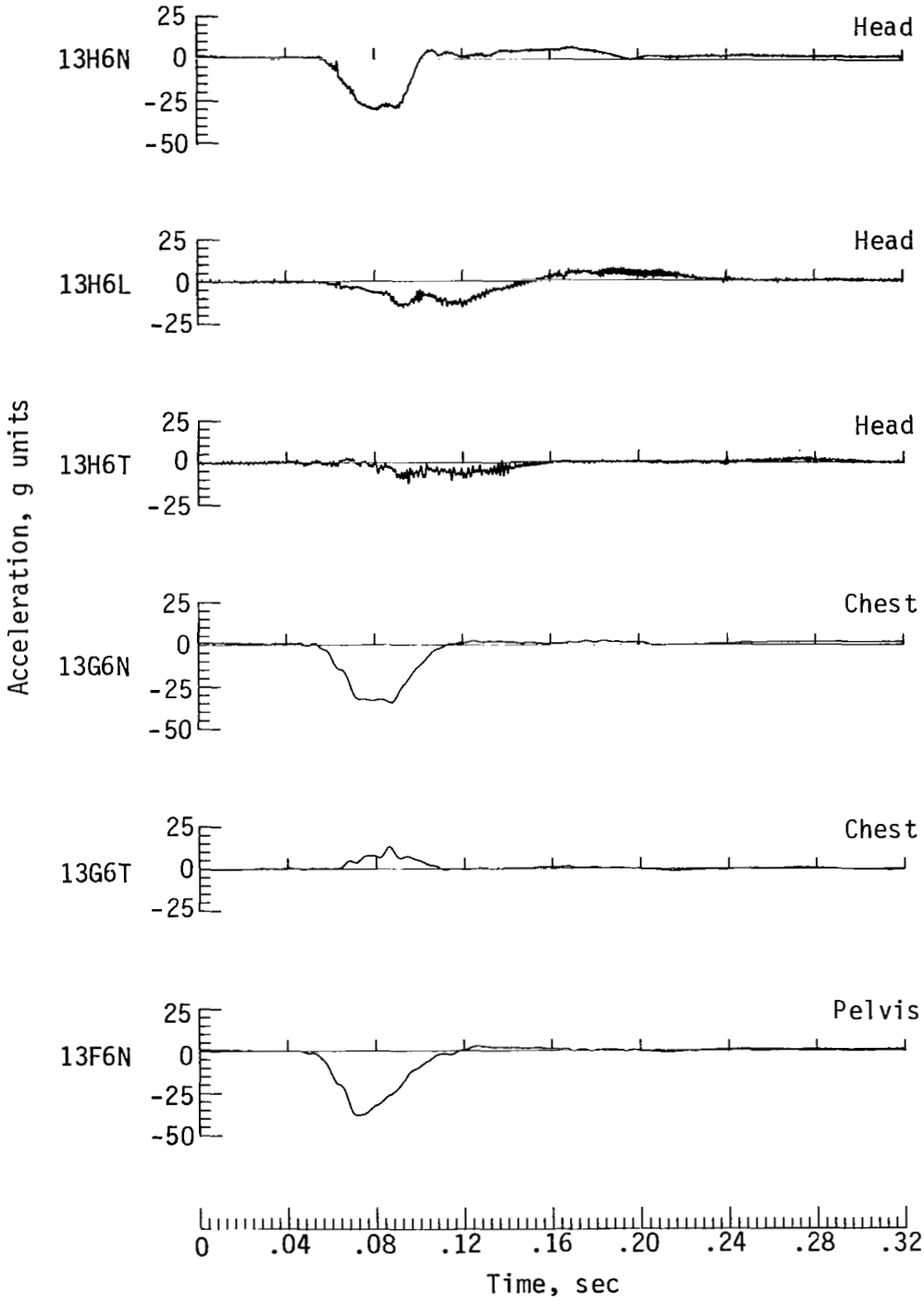

(e) Passenger accelerations.

Figure A3.- Continued.

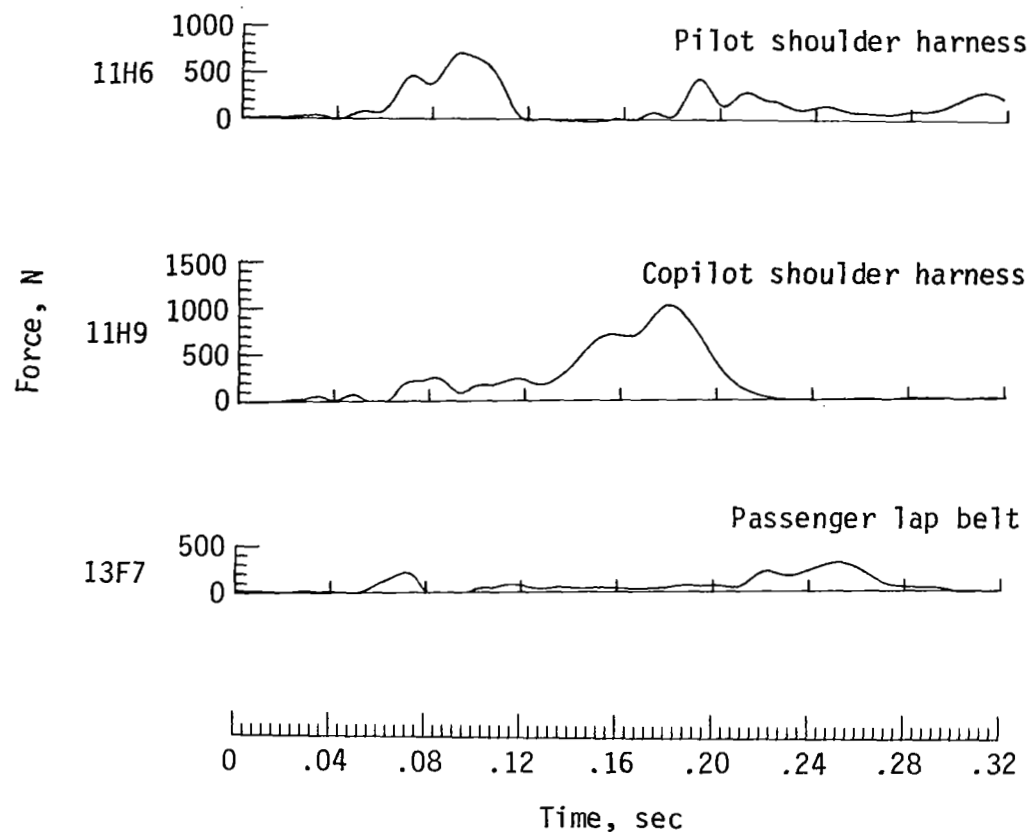

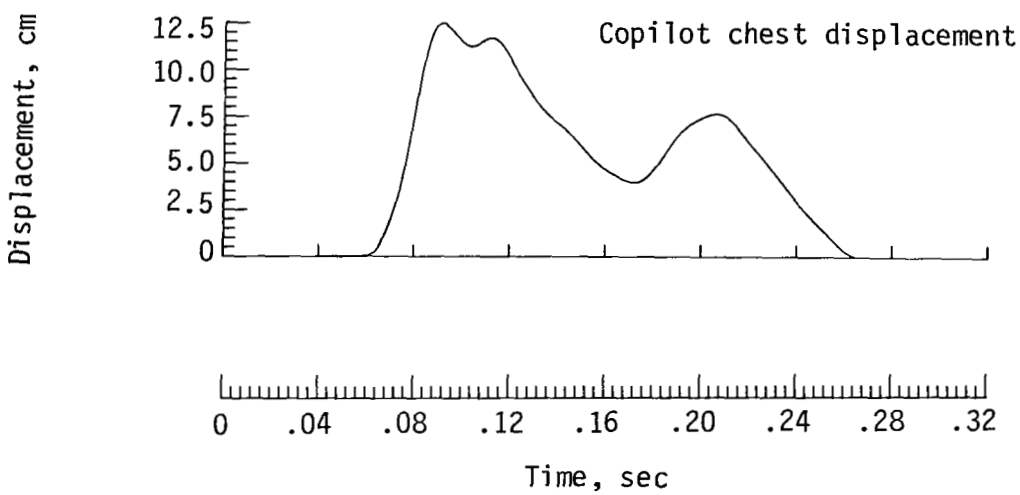

(f) Restraint loads and chest displacement data.

Figure A3.- Continued.

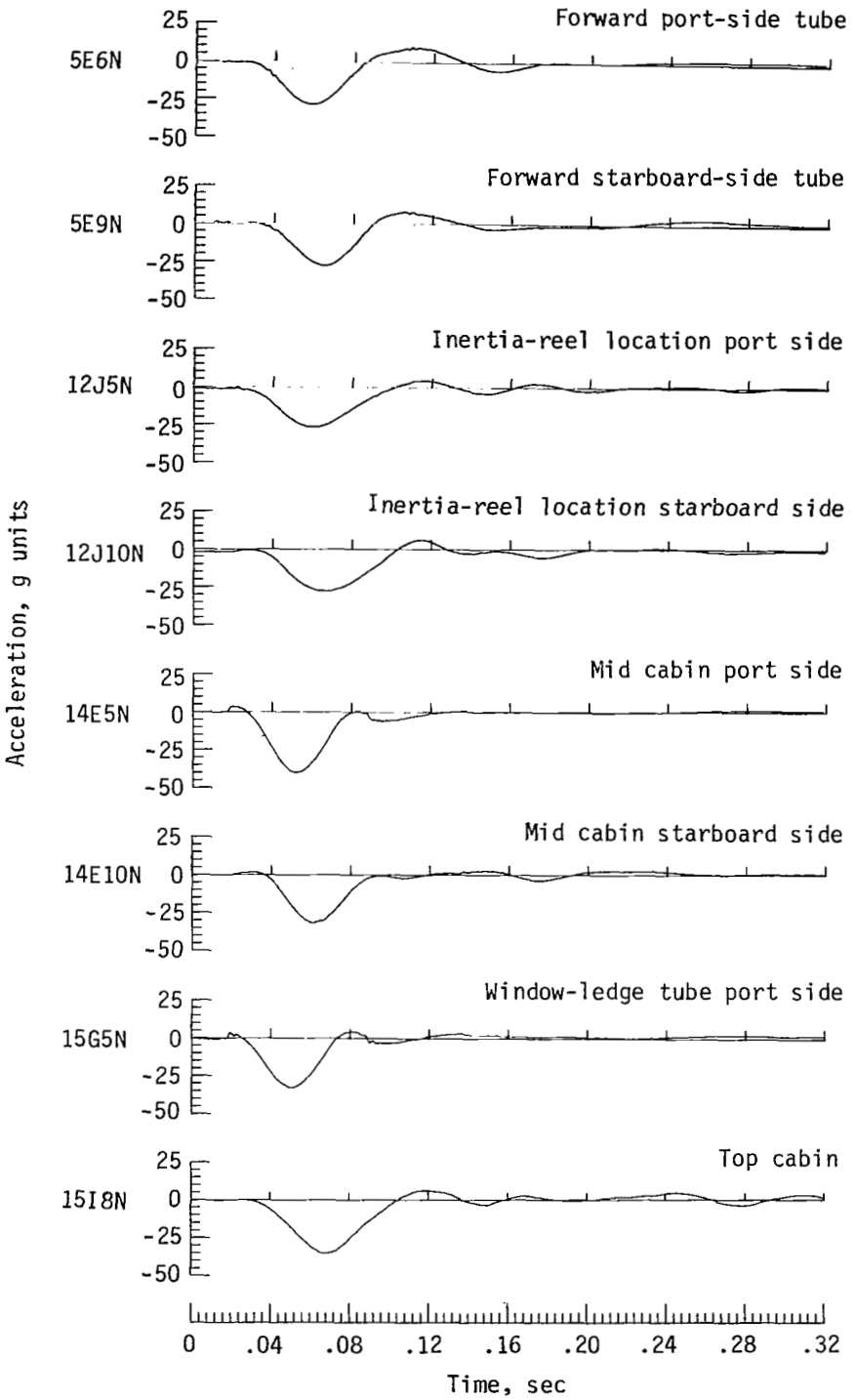

(g) Aircraft structure normal accelerations.

Figure A3.- Continued.

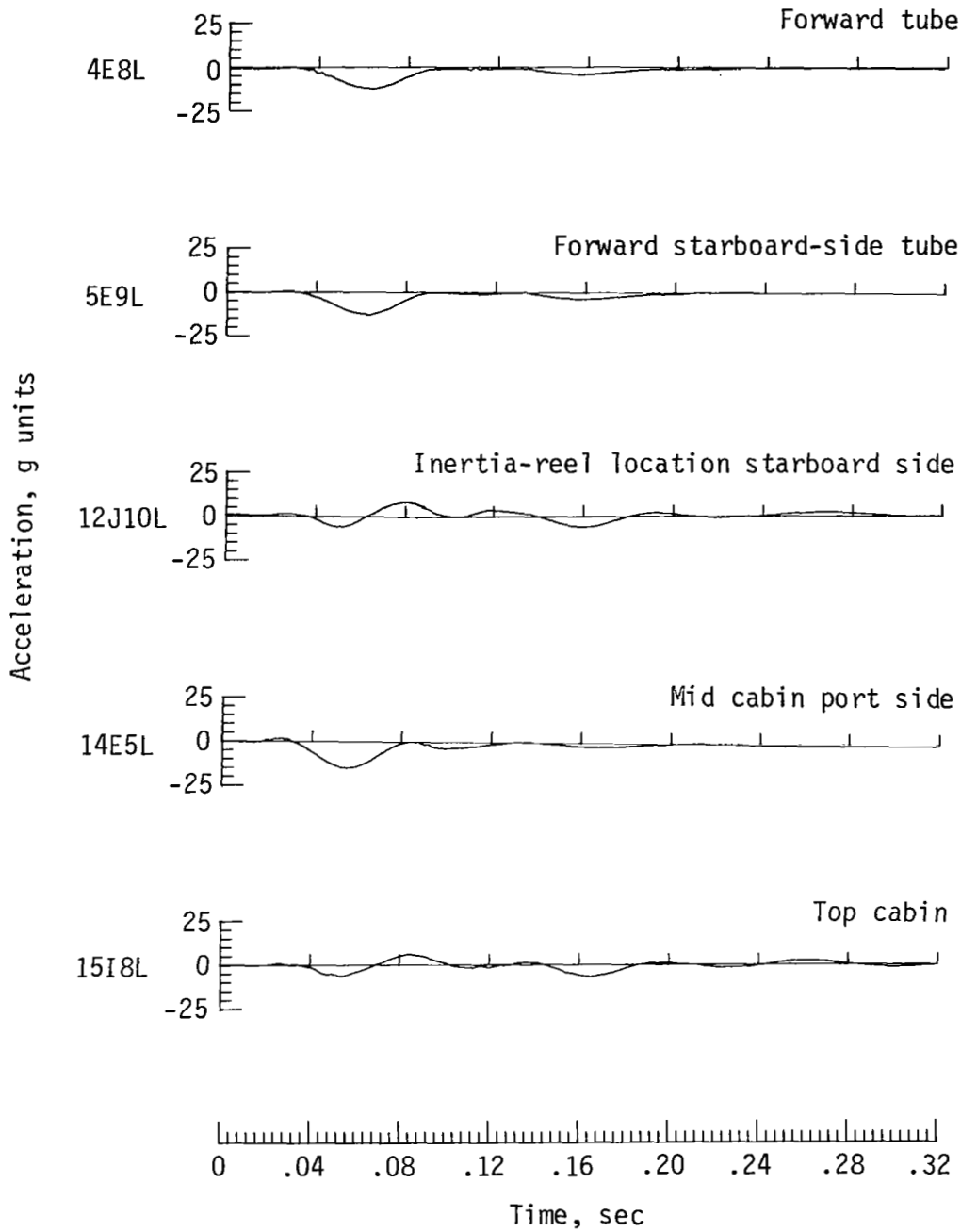

(h) Aircraft structure longitudinal accelerations.

Figure A3.- Concluded.

APPENDIX B

15° NOSE-DOWN TEST

Crash Dynamics

The crash sequence for the 15° nose-down test is illustrated in figure B1 with nine photographs taken by a scanning camera. The velocity and attitude at impact are given in figure 5(b).

At 0.05 sec, crushing of the nose structure has begun. By 0.10 sec, the anthropomorphic dummies have begun to rotate forward in their seats. At approximately 0.15 sec into the crash, the upper-body forward rotation of the crew and passenger has reached the maximum. At 0.20 sec, the dummies have begun to rebound to an upright position in their seats. The tail of the airplane has completed the downward rotation and is flat along the concrete surface by time 0.30 sec, and the nose of the airplane is pitched up. The remaining photographs in figure B1 show the airplane during slide-out.

Assessment of Damage

Postcrash photographs from the 15° nose-down test are presented in figure B2. The livable volume was maintained in the crew and passenger positions during the crash impact. The crew and passenger seats showed no apparent postcrash damage except for the rubber-membrane seat pans, which failed at several attachment points (figs. B2(a) through B2(d)). Both inboard crew seat rails were broken by the compressive loading of the legs on the rails (fig. B2(a)). The first-passenger seat rails were slightly deformed. Figure B2(e) shows an overall interior postcrash view of the cabin floor from rear to front after the seats were removed. The floor showed some deformation in the crew and passenger locations.

Buckling of the nose structure that occurred during impact is shown in figure B2(f). Also visible through the copilot's window is part of the surrounding tubular structure, which bent under compressive loading. Compression loading of the bottom of the fuselage and nacelles can be seen in figure B2(g).

Acceleration Time Histories

Accelerations, loads, and displacements measured on the airplane structure and in the occupants are given in figure B3. Normal, longitudinal, and transverse accelerations measured along the floor of the airplane are given in figures B3(a) and B3(b) as a function of time. The data are grouped according to accelerometer location and orientation. The accelerometers were oriented along the normal (Z), longitudinal (X), and transverse (Y) axes as shown in figure 4. Each location is designated by its grid coordinate corresponding to figure 6. The first number indicates the longitudinal coordinate; the first letter indicates the normal coordinate (floor to roof); the second number indicates the transverse coordinate; and the second letter indicates the accelerometer orientation with respect to the airplane body-axis system.

The maximum measured normal floor accelerations varied from 11g to 20g, with an average peak normal floor pulse of 16g, a 0.120-sec duration, and a 10.6 m/sec inte-

grated velocity change. As seen in figure B3(a) and in the sequence photographs (fig. B1), the peak acceleration occurs later in the aft cabin and baggage area than in the crew area. This result occurs because the aft cabin experiences loads only after the tail rotates downward and contacts the ground. Maximum longitudinal accelerations ranged from 3g to 9g, with an average peak longitudinal pulse of 5.5g, a 0.088-sec duration, and a 4.0 m/sec integrated velocity change of the main pulse. The remaining 22.1 m/sec horizontal velocity was dissipated by sliding friction in 84 m of travel with an average deceleration of 0.30g. Transverse floor acceleration was approximately 2g with a duration of 0.06 sec.

Normal, longitudinal, and transverse accelerations in the head, chest, and pelvis of the pilot and copilot are shown in figures B3(c) and B3(d). They experienced similar accelerations. The maximum normal pelvis acceleration for the pilot was 22g, compared with 24g for the copilot, and the maximum longitudinal acceleration was 8g for both. These normal acceleration pulses fall within current ejection-seat design limits and are expected to be only mildly injurious (ref. 17).

Normal, longitudinal, and transverse accelerations in the head, chest, and pelvis of the passenger are shown in figure B3(e). The maximum normal pelvis acceleration for the passenger was 28g, slightly higher than that measured for the crew. The higher acceleration is probably due to a stiffer passenger seat and stronger subfloor in the passenger area. The maximum longitudinal accelerations were 6g in the pelvis and 14g in the chest.

The pilot's forward chest motion was 17.5 cm with a 1200 N peak shoulder-harness load (fig. B3(f)). The pilot's shoulder-harness inertia reel locked after 1.5 cm of strap reel-out. Similarly, the copilot's shoulder-harness inertia-reel strap extended 1.4 cm before locking with a maximum shoulder-harness load of 1100 N (fig. B3(f)). These displacements were all measured using pull-wire displacement transducers (fig. 9(c)). The maximum passenger shoulder-harness load was 1190 N (fig. B3(f)). All lap-belt load data were lost for this test.

Figures B3(g) and B3(h) contain miscellaneous acceleration traces presented for completeness.

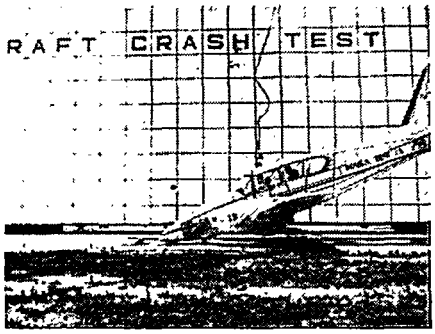

Time = 0.0 sec

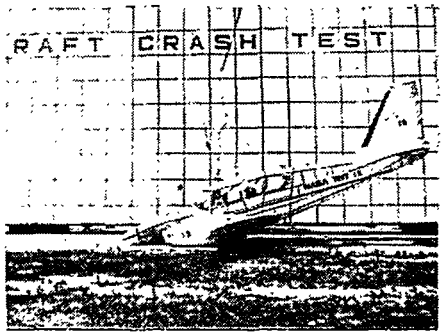

Time = 0.05 sec

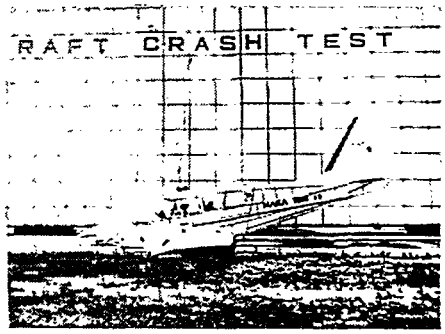

Time = 0.10 sec

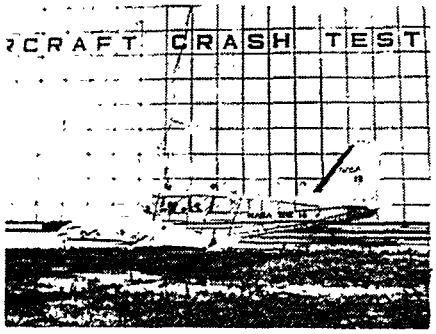

Time = 0.15 sec

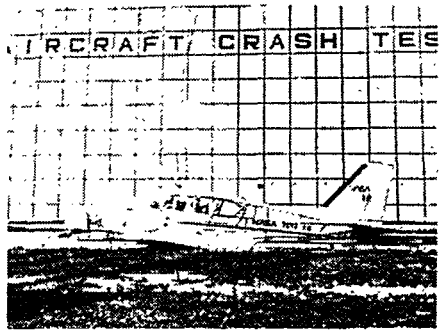

Time = 0.20 sec

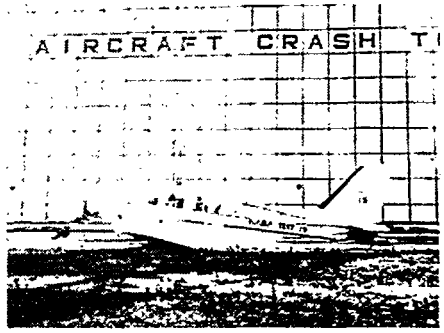

Time = 0.25 sec

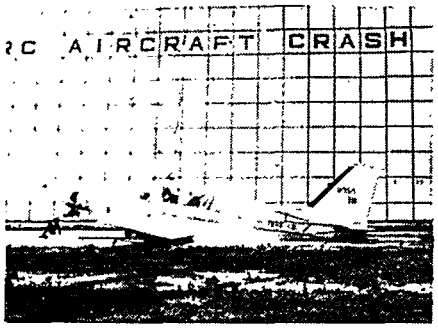

Time = 0.30 sec

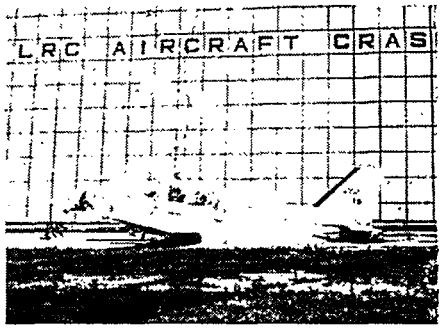

Time = 0.35 sec

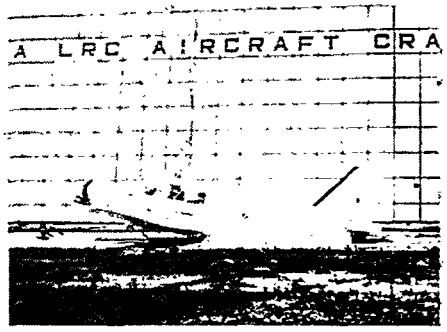

Time = 0.40 sec

L-82-170

Figure B1.- Crash-sequence photographs of 15° nose-down test.

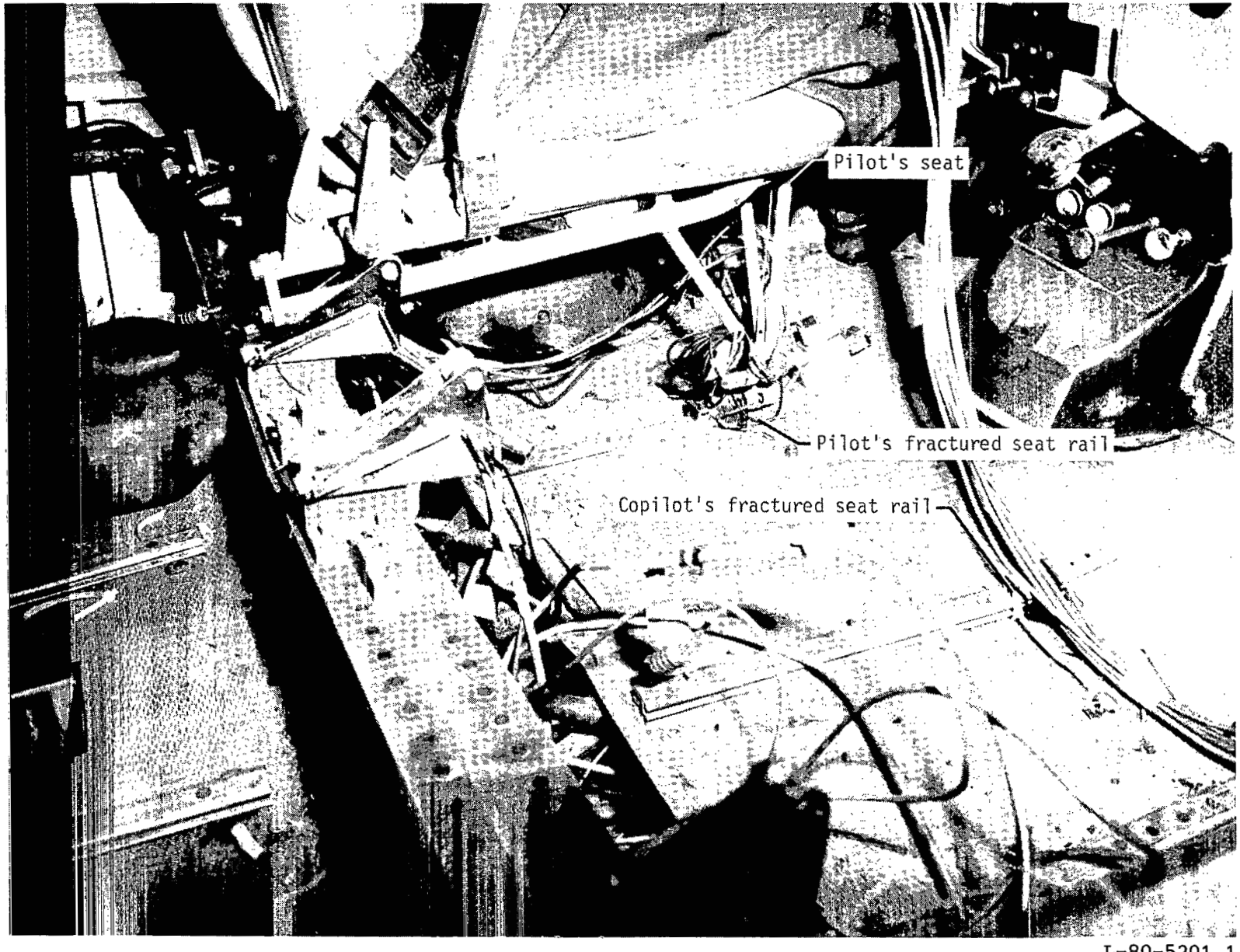

(a) Postcrash view of crew compartment.

Figure B2.- Postcrash photographs of 15° nose-down test.

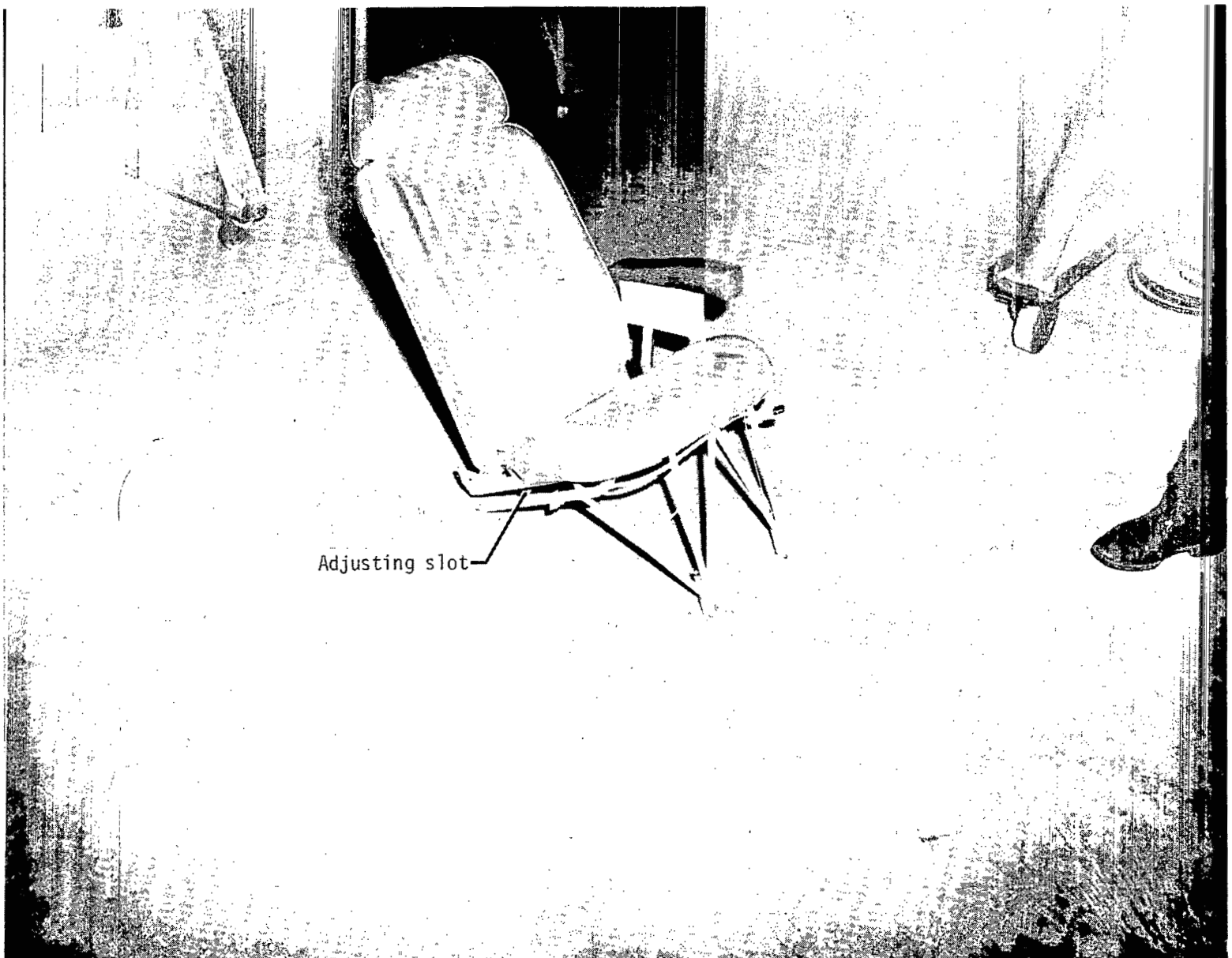

(b) Postcrash view of copilot's seat.

Figure B2.- Continued.

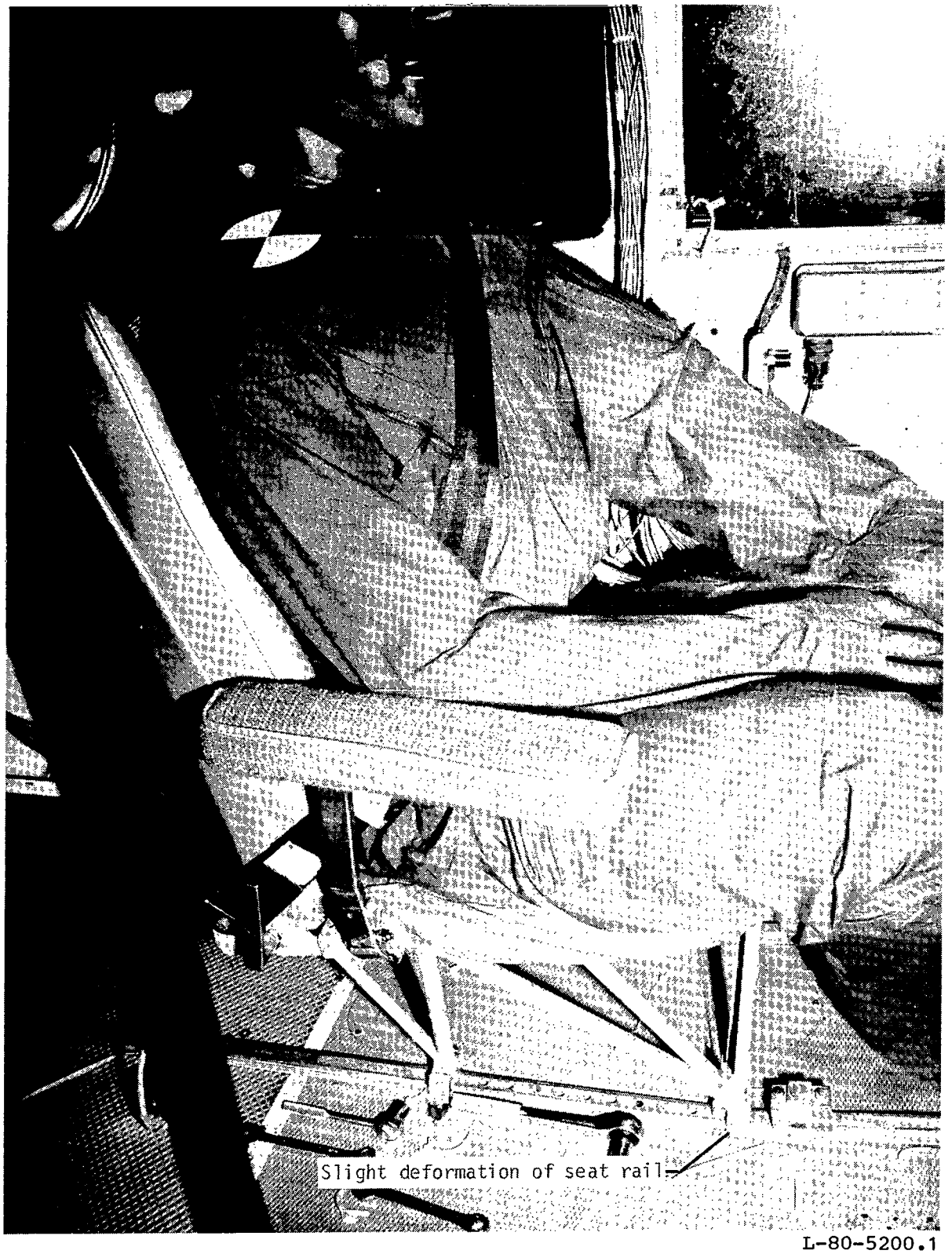

(c) Postcrash close-up of passenger's seat.

Figure B2.- Continued.

L-80-5214

(d) Postcrash view of passenger's seat.

Figure B2.- Continued.

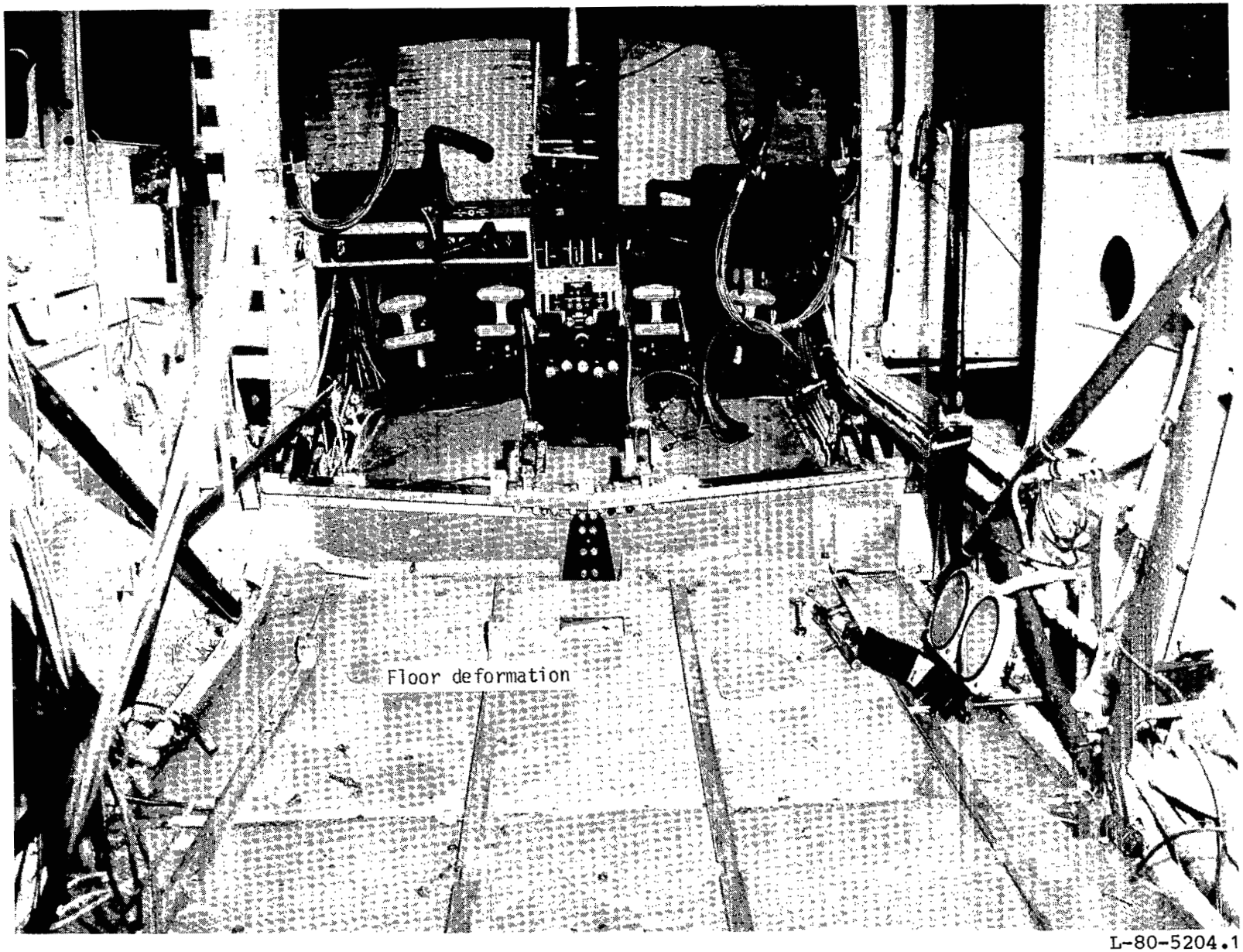

(e) Postcrash view of cabin after seat removal.

Figure B2.- Continued.

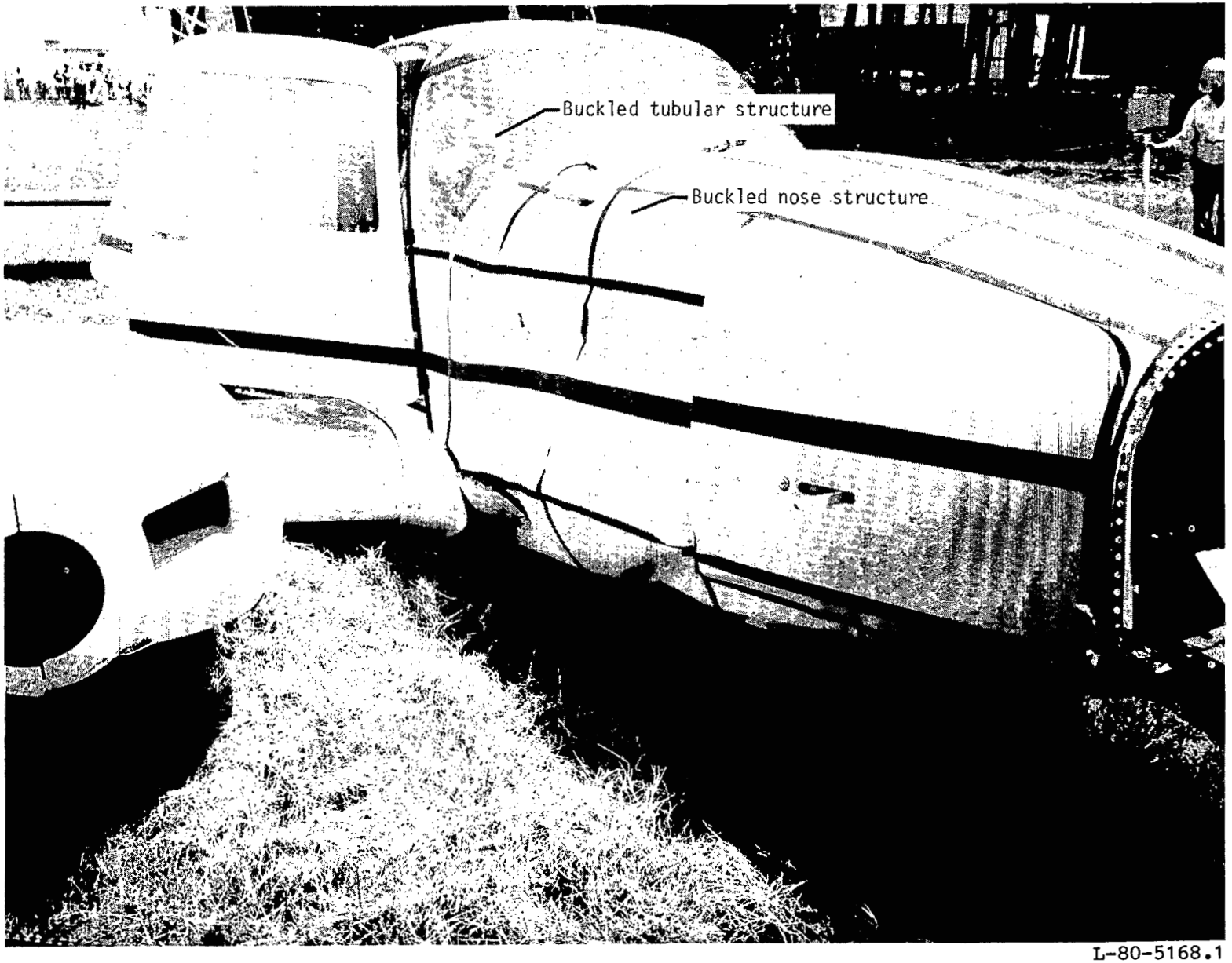

L-80-5168.1

(f) Starboard view of airplane.

Figure B2.- Continued.

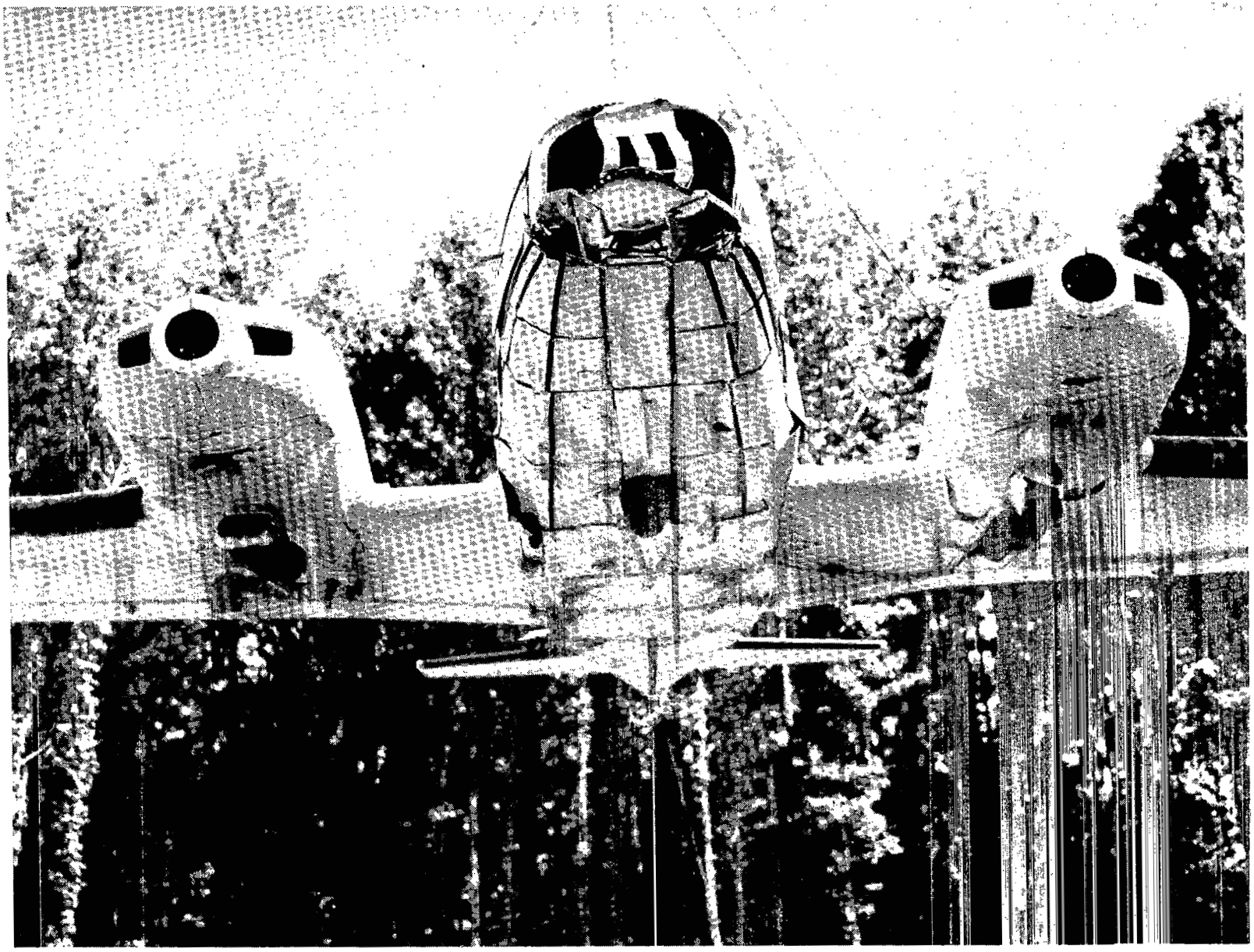

L-80-5037

(g) Underside view of damage to fuselage and nacelles.

Figure B2.- Concluded.

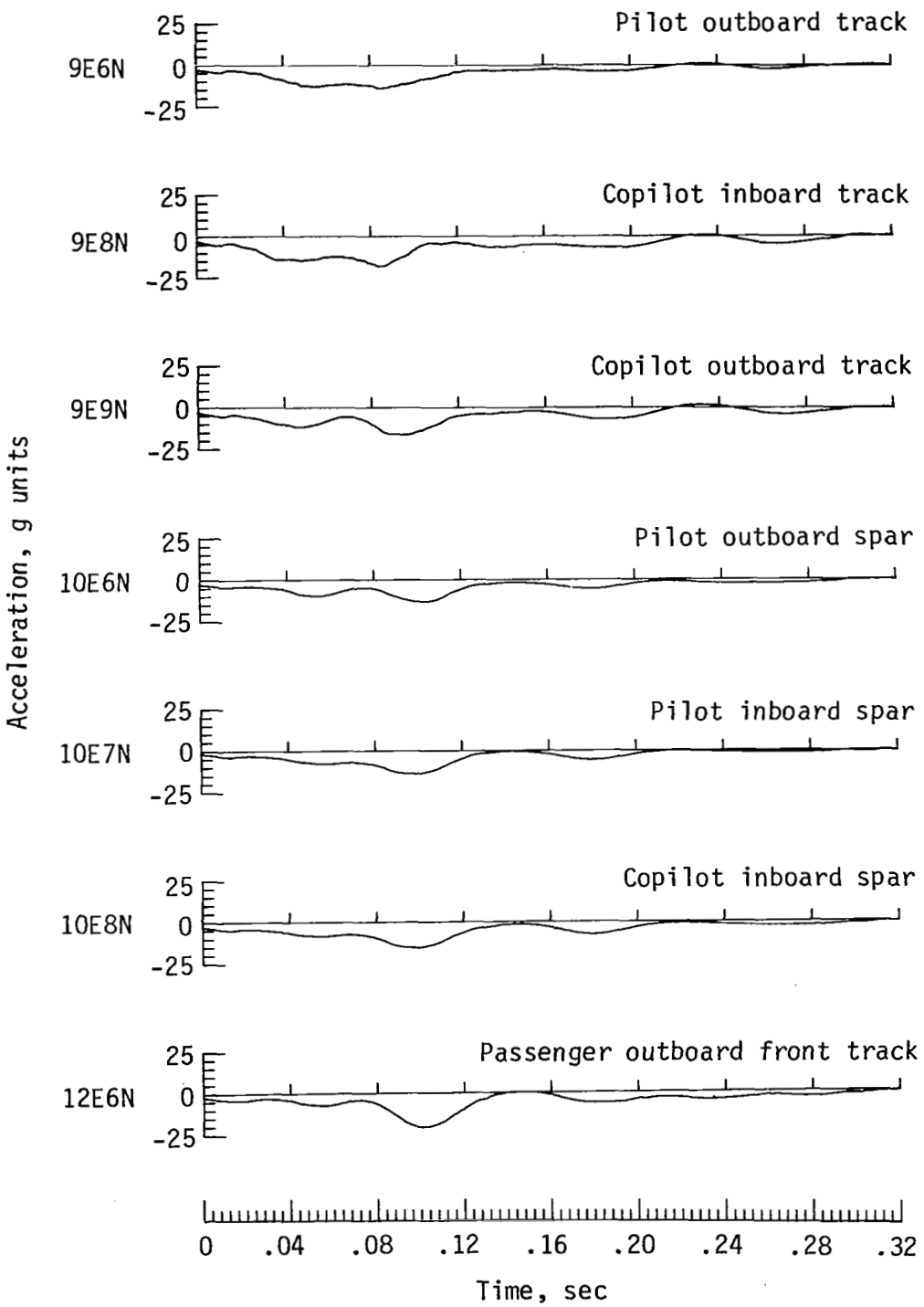

(a) Normal floor accelerations.

Figure B3.- Data from 15° nose-down test.

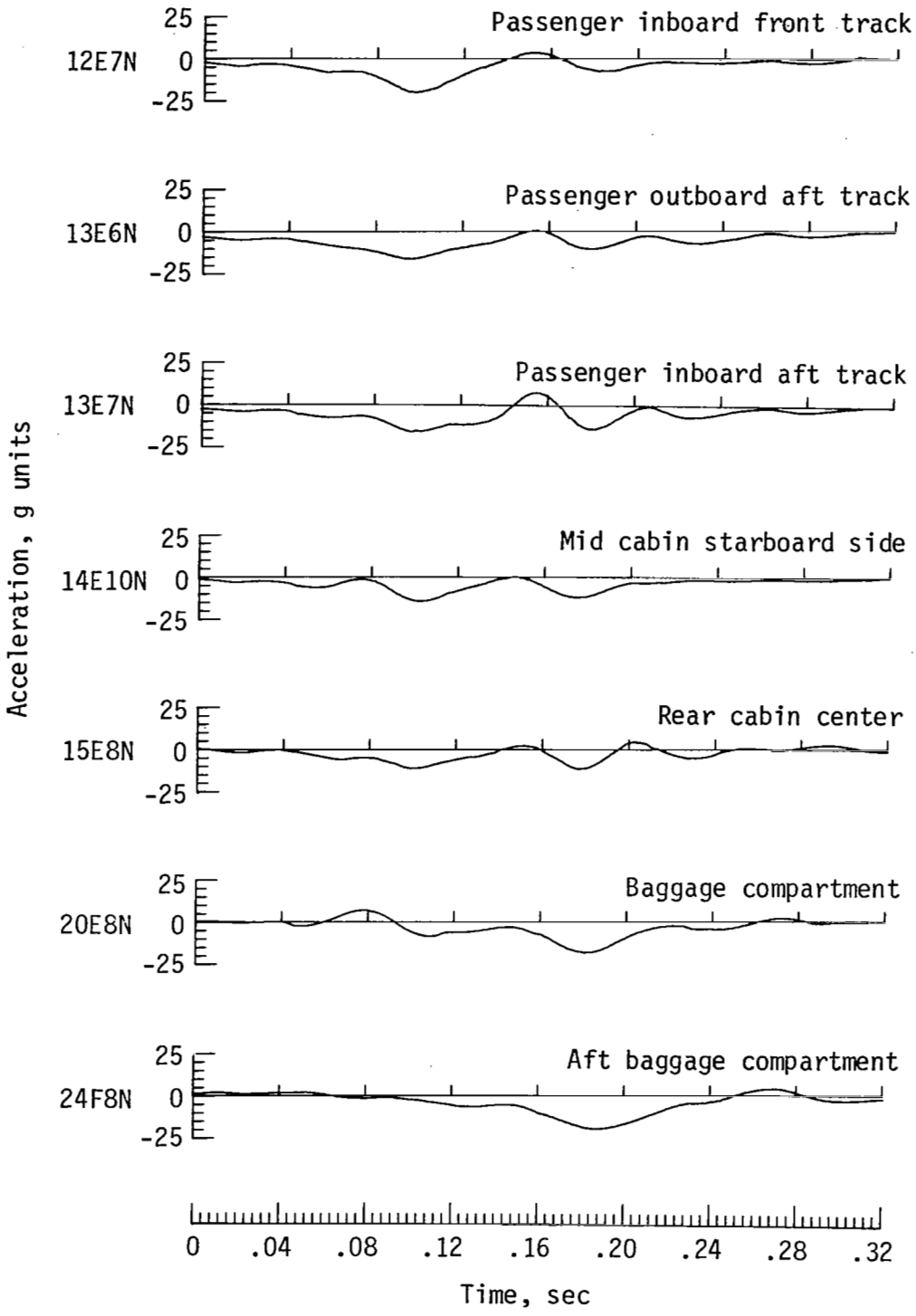

(a) Concluded.

Figure B3.- Continued.

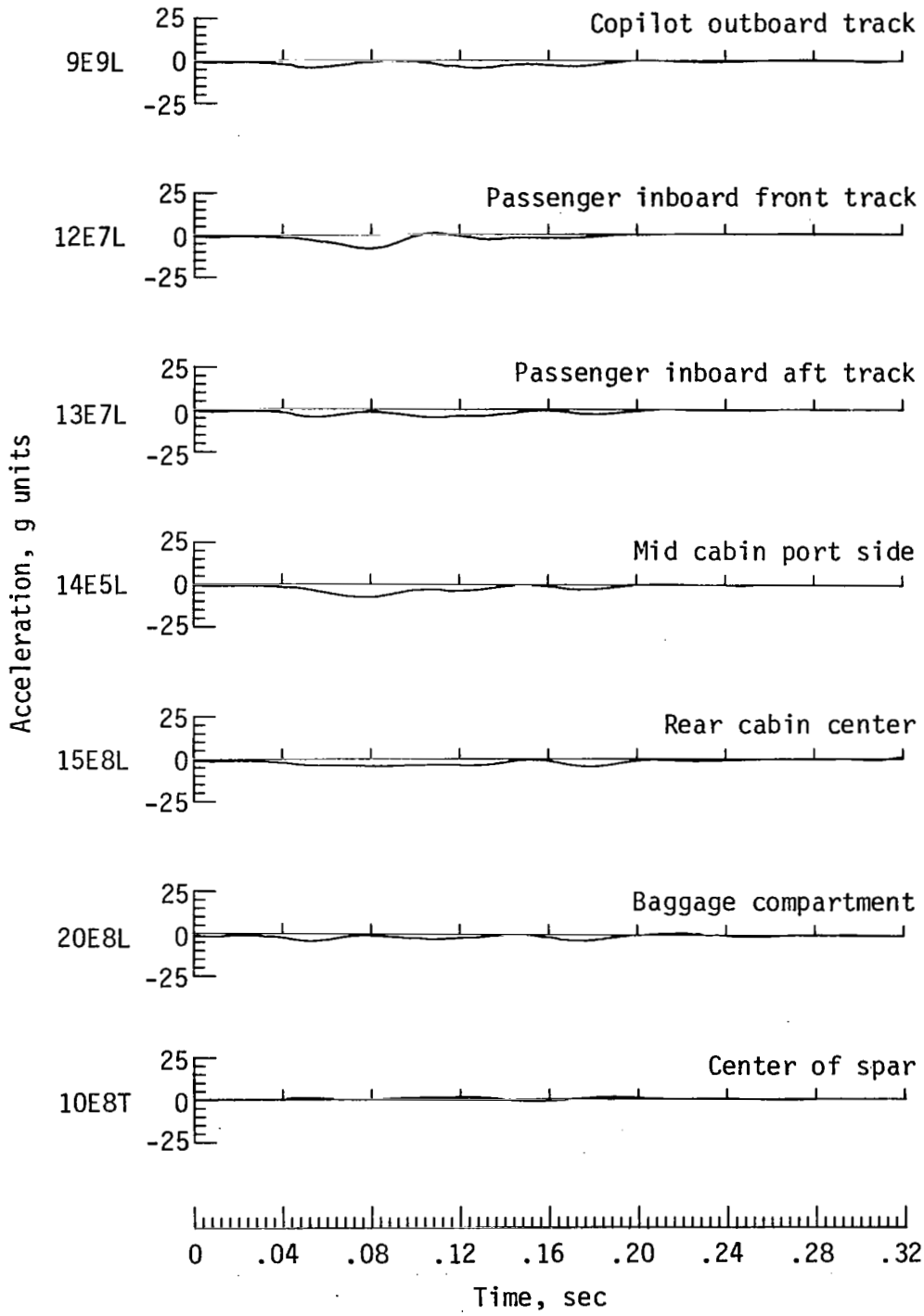

(b) Longitudinal and transverse floor accelerations.

Figure B3.- Continued.

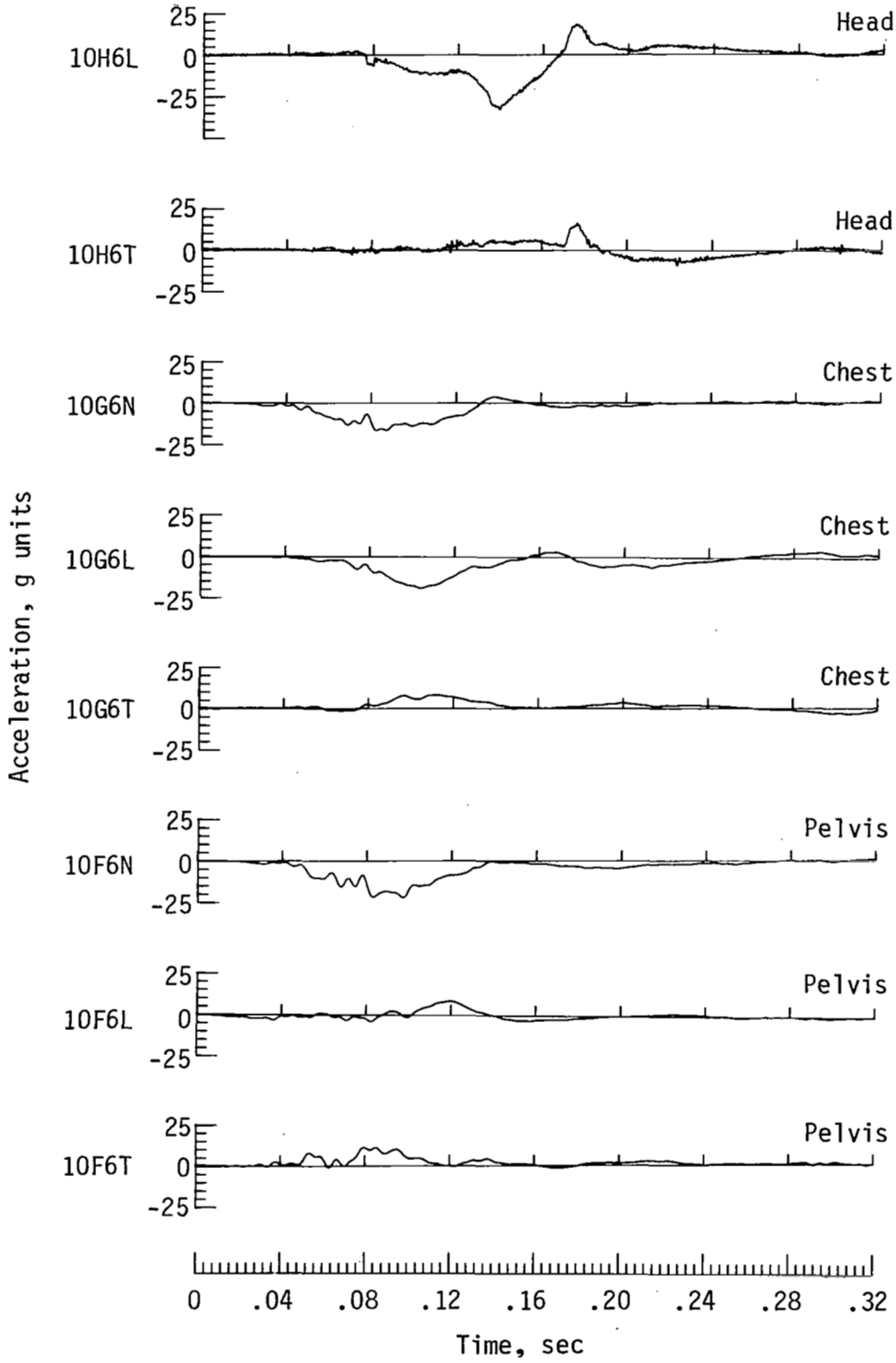

(c) Pilot accelerations.

Figure B3.- Continued.

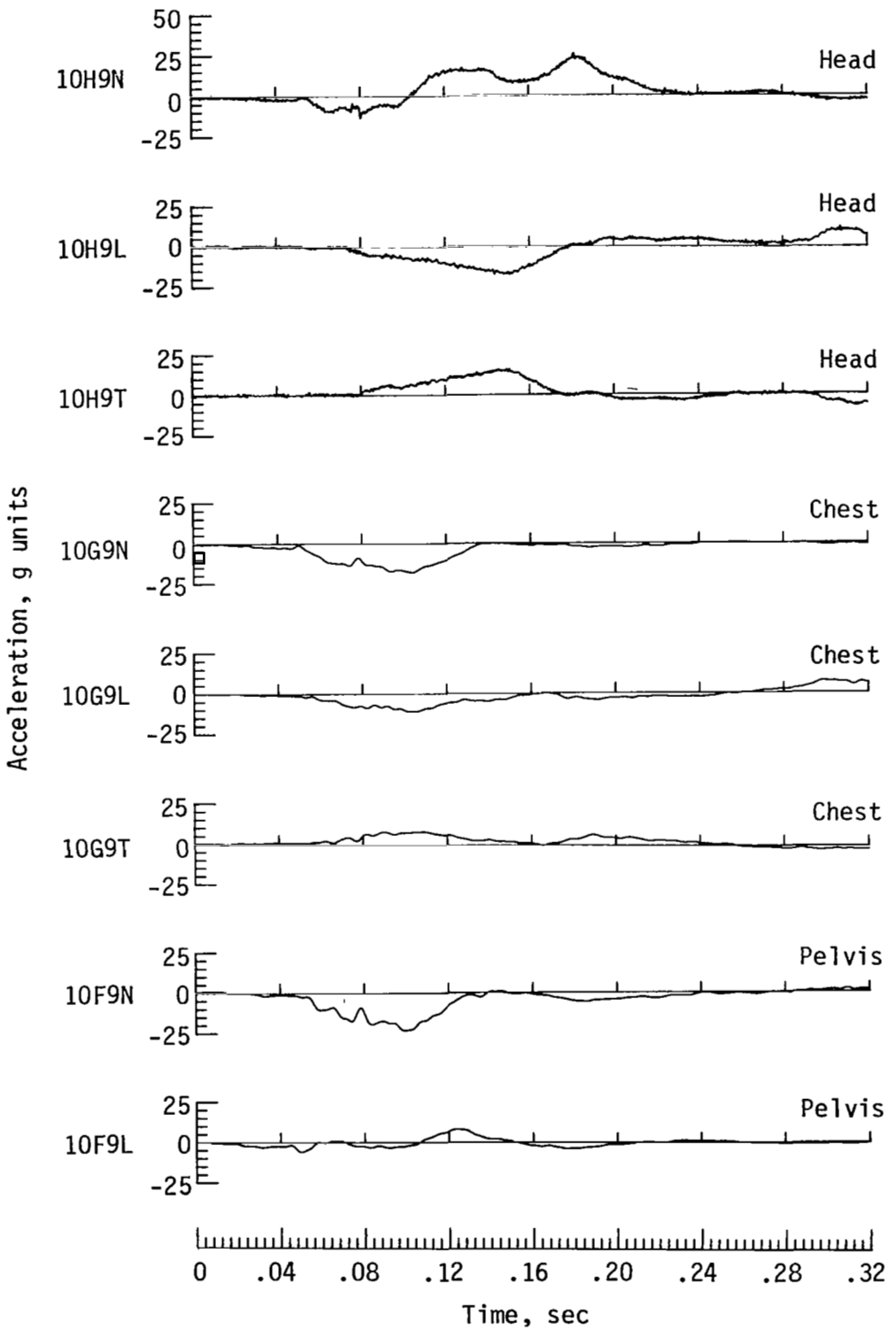

(d) Copilot accelerations.

Figure B3.- Continued.

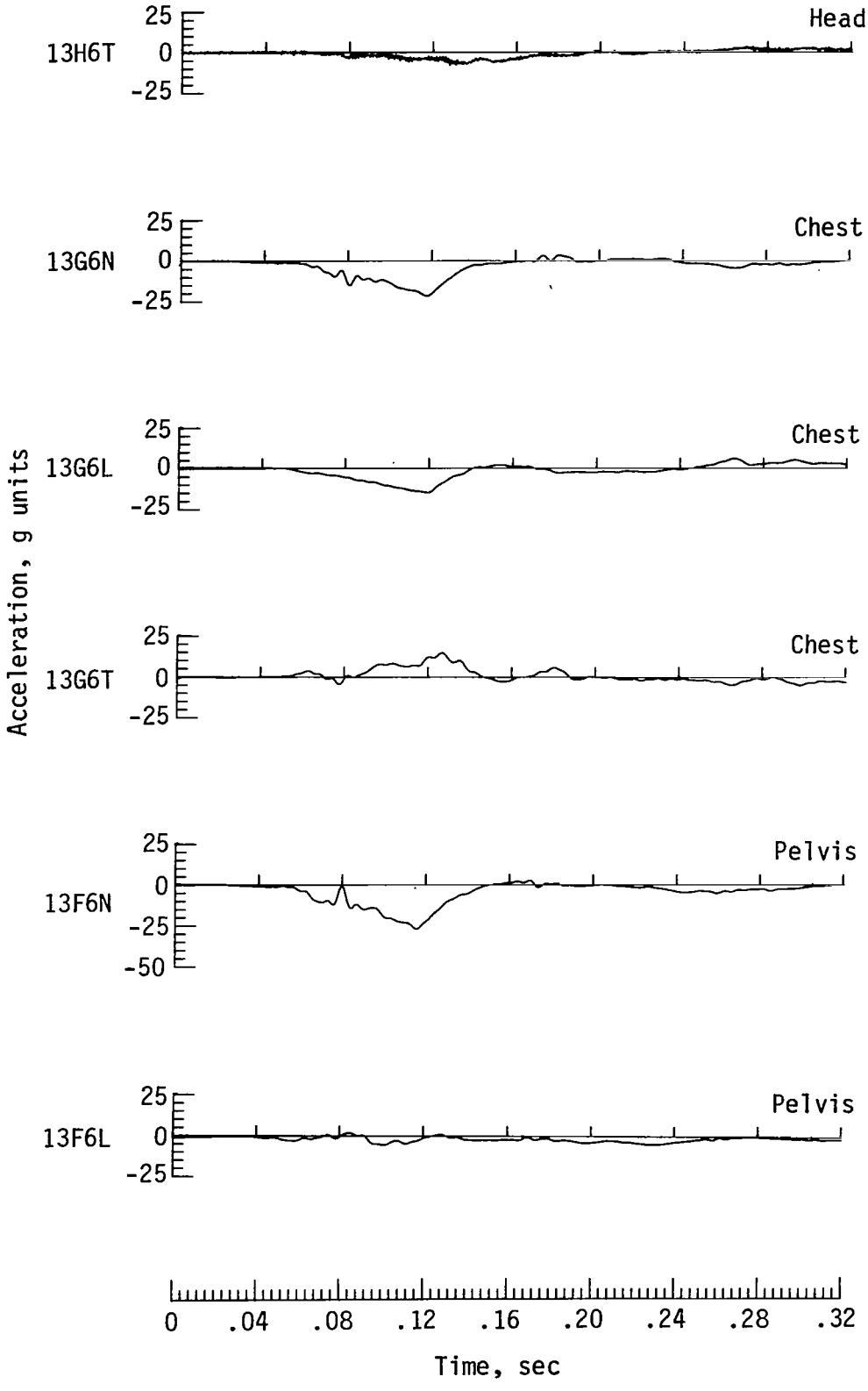

(e) Passenger accelerations.

Figure B3.- Continued.

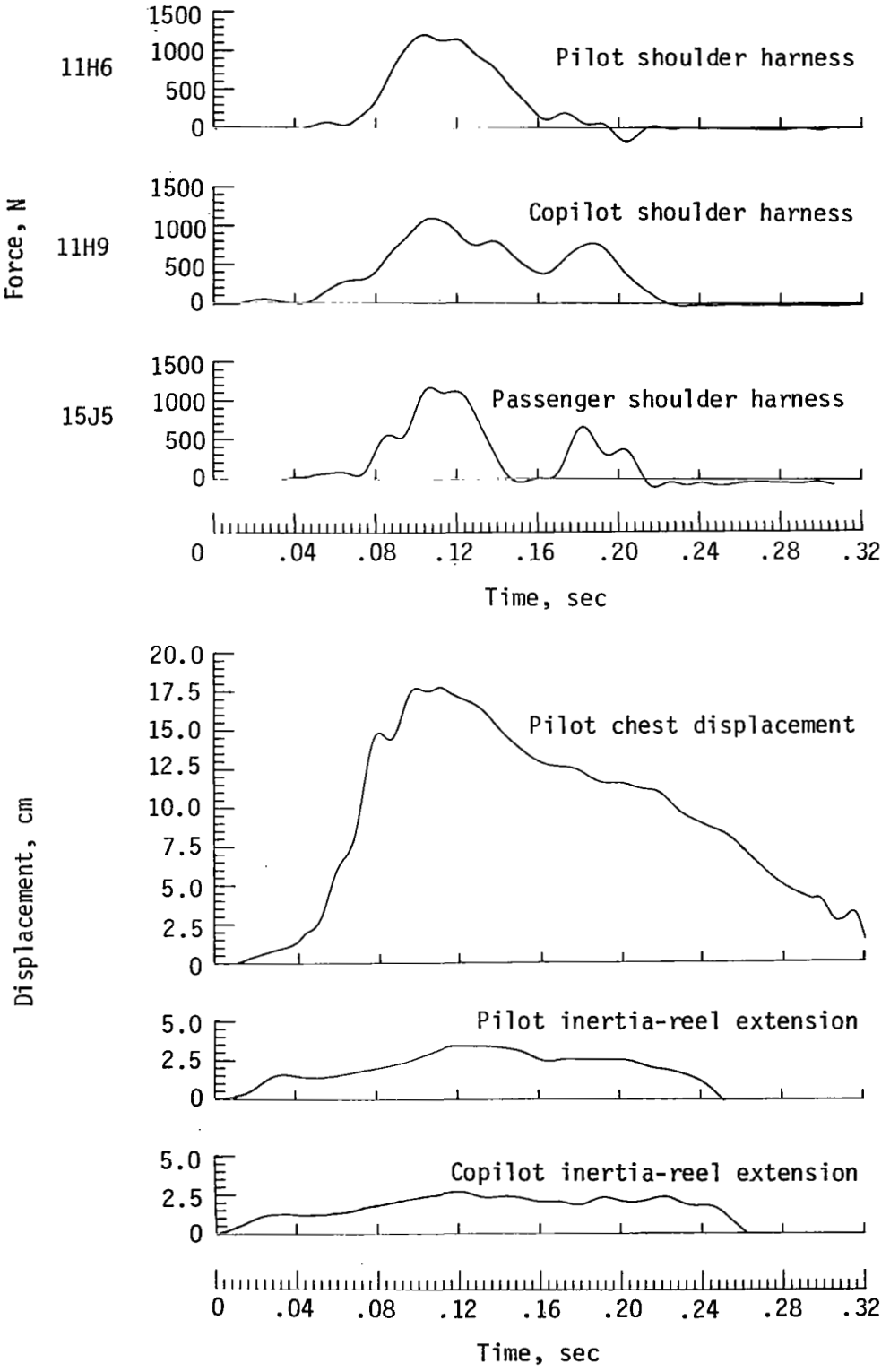

(f) Restraint loads and chest and inertia-reel displacement data.

Figure B3.- Continued.

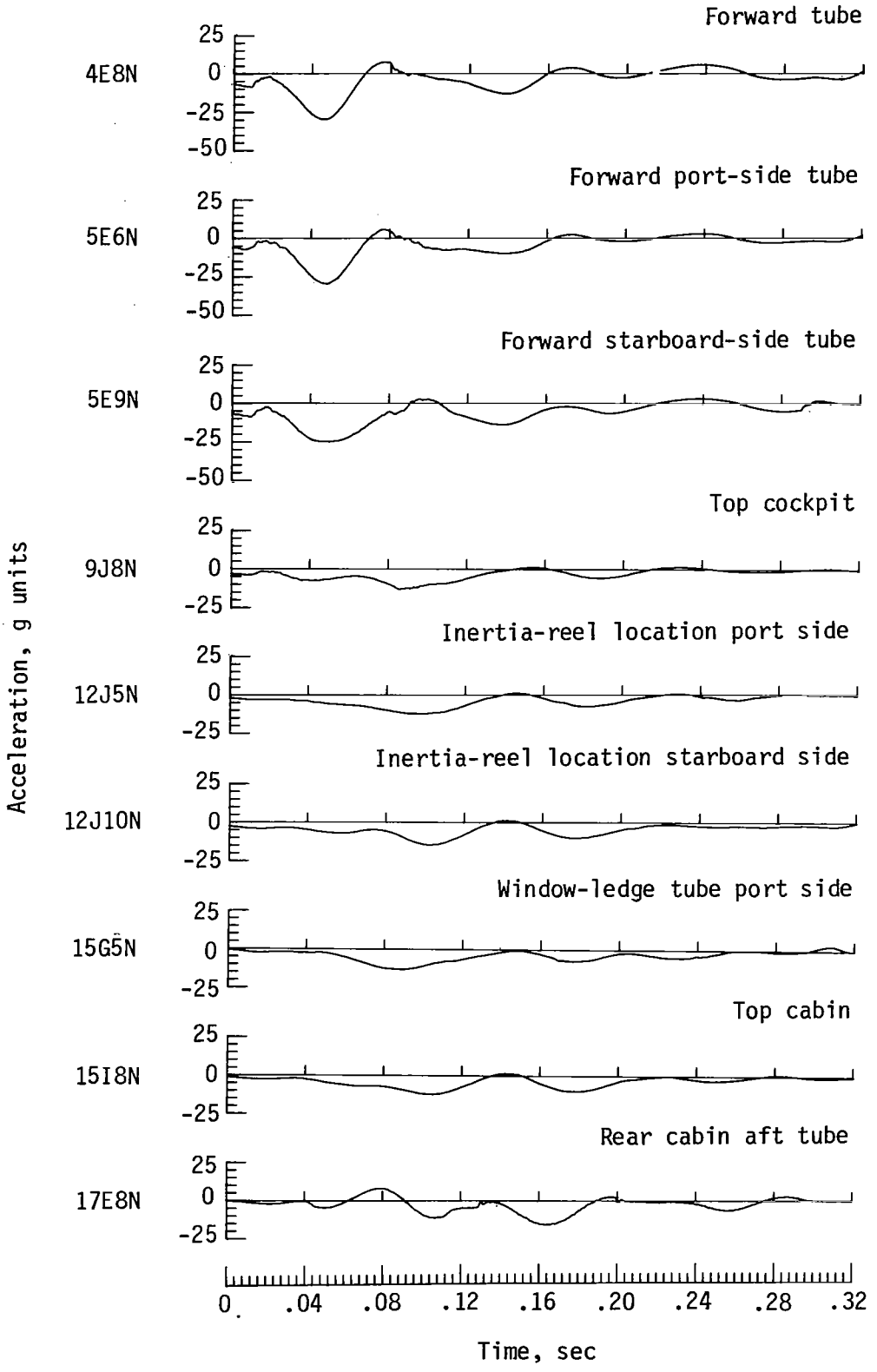

(g) Aircraft structure normal accelerations.

Figure B3.- Continued.

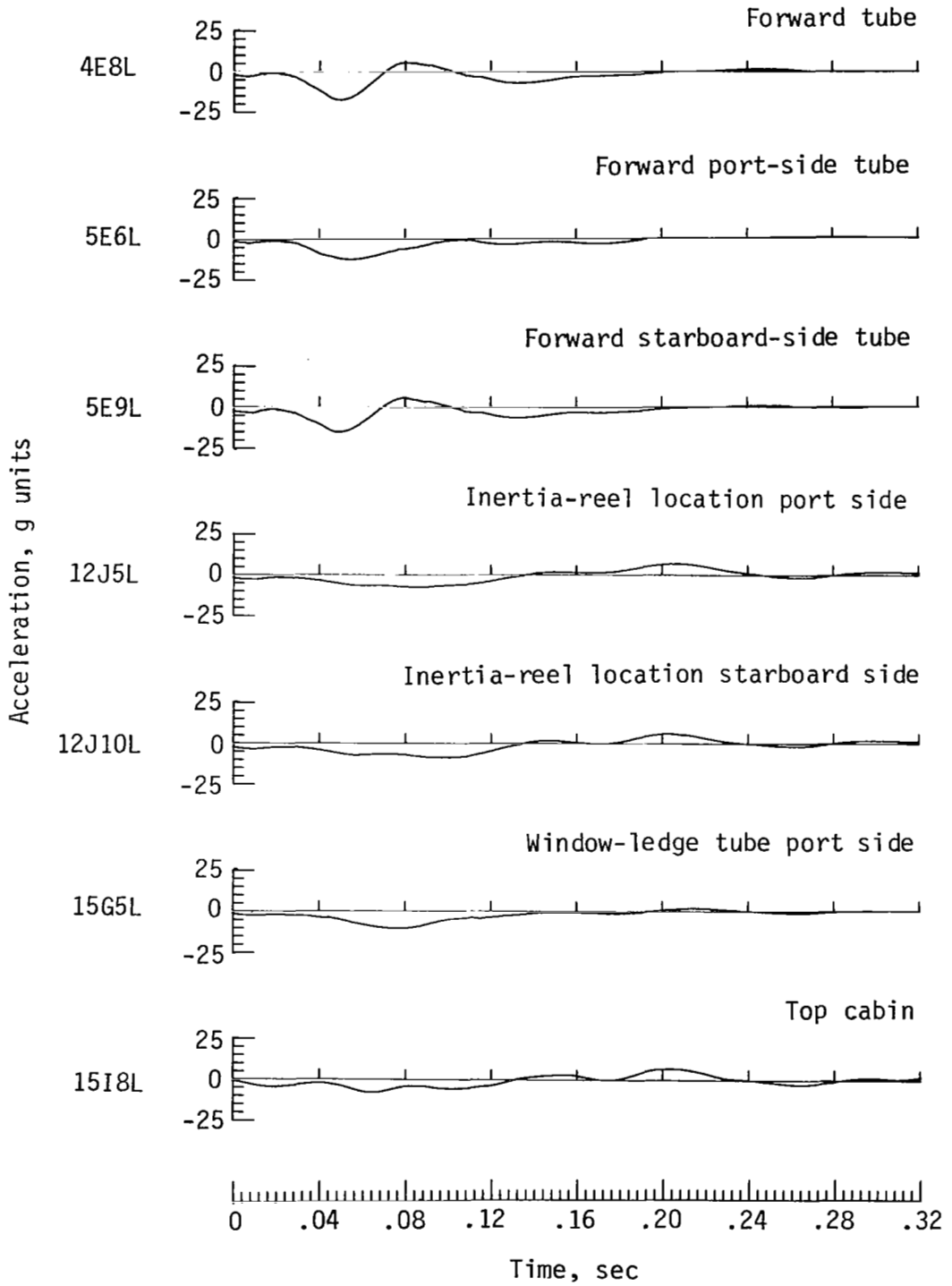

(h) Aircraft structure longitudinal accelerations.

Figure B3.- Concluded.

APPENDIX C

30° NOSE-DOWN TESTS

Crash Dynamics

The two 30° nose-down tests were the most severe of the four crash tests conducted. In the first 30° nose-down test, a substantial amount of data was lost because of the severe impact and its effect upon the instrumentation. A second test similar to the first was conducted to supplement the data. Unfortunately, the data from the second test exhibited the same problems experienced in the first test (i.e., noise spikes, shorts, severed wires, and voltage shifts).

The crash sequences for the 30° nose-down tests are illustrated in figures C1 and C2. The impact parameters are given in figure 5(c) for the first 30° nose-down test and in figure 5(d) for the second 30° nose-down test. The sequence photographs show that similar external damage occurred in the two tests. At 0.05 sec and 0.10 sec, extensive crushing of the nose and nacelles is evident for both tests. At 0.10 sec, the dummies have begun to rotate forward in their seats, and initial deformation of the cabin roof has occurred. At 0.15 sec, the wings and fuselage forward of the main spar are essentially flat on the concrete test surface, but the fuselage aft of the main spar is at a 20° angle to the ground and still has a vertical velocity component. This situation caused severe deformation of the cabin roof, particularly in the second 30° nose-down test. In the remaining photographs, as the aircraft slides out, the tail rotates downward to become parallel with the impact surface (causing the nose to pitch up), and the cabin roof returns to the original shape.

Assessment of Damage

Postcrash photographs of damage that occurred during impact in the two 30° nose-down tests are presented in figure C3. The livable volume in the first 30° nose-down test was maintained, although the cabin roof buckled inward during the impact. The deformation of the cabin roof was more extreme in the second 30° nose-down tests, and the livable volume in the crew and passenger areas was encroached upon. The increased mass (300 kg) of the second aircraft probably contributed to the greater deformation in the crew area.

Postcrash photographs of the crew seats are shown in figures C3(a) through C3(c). The crew seats are adjustable fore and aft and are locked in place with pins in the front legs, which are secured into the seat track. No back legs are necessary, since the rear seat-pan frame is supported by a roller-bracket assembly attached to the main spar. The roller fits into the adjusting slot of the seat pan with forward seat travel limited by the stop at the end of the slot. Damage to the crew seats was similar in these two tests; the front legs buckled during impact and were detached from the seat rails, allowing the seats to move forward in the adjusting slot. In the second test, the pilot's seat moved as far forward as possible in the slot and then tore the bracket off the main spar. Part of the damaged brackets, which are still attached to the roller, are visible in figure C3(c). The rubber-membrane seat pans in all of the crew seats failed. In the second test, the pilot's seat cushion ruptured. Pilot and copilot seat rails for each test are shown in figures C3(d) and C3(e). The pilot's inboard seat rail and both of the copilot's seat rails were broken in the first test. In the second test, both of the pilot's seat

rails were broken. Also, the photographs show that the thin-gauge aluminum floor in the crew area was torn in both crash tests.

Postcrash photographs of the passenger seats are shown in figures C3(f) through C3(h). The passenger seats in both tests showed little damage upon postcrash inspection. The rubber-membrane seat pans failed in these seats, just as they had done in the crew seats. The passenger's seat in the first test and the second passenger's seat in the second test remained attached to the seat rails during the impact; however, the first passenger's seat in the second test completely detached from the seat rails. This passenger came to rest facing the port side of the airplane still strapped to the seat (fig. C3(g)).

Postcrash inspection of the first passenger's seat in the second 30° nose-down test revealed that the bolt in each rear-leg attachment clamp was not fully tightened. This situation allowed the rear-leg attachments to spread, and consequently the seat disengaged from the track. In the first test, the passenger's outboard seat rail cracked, pulled up in the rear, and depressed in the front. The passenger seat rails in the second test showed similar deformation, but did not fracture.

Overall damage to the instrument panel, floor, and tubular-steel truss structure in each test is shown in figures C3(i) through C3(l). The tubular-truss structure was bent and fractured in many of the same locations for the two tests. In the second test, the tubular-truss structure bent inward into the leg of the second passenger (fig. C3(l)).

Damage to the port side of the airplanes is shown in figures C3(m) and C3(n). This damage was similar in the two tests but more severe in the second test. Separation occurred along the side of the fuselage and along the fuselage-wing junction. Some plexiglas windows were broken during the impact. On the starboard side of the airplane in both tests, the door detached from the fuselage and was lying on the wing. Also, the steel tubular-truss structure bent outward and penetrated the side of the fuselage.

Similar compression loading of the bottom of the fuselage and nacelles in both tests is shown in figures C3(o) and C3(p). In the first test, the port-side engine mounts failed, and the engine can be seen on the ground in figure C3(o).

Acceleration Time Histories

Accelerations, loads, and displacements measured on the airplane structure and in the occupants for both 30° nose-down tests are shown in figure C4. Normal, longitudinal, and transverse accelerations measured on the floor of the airplane are shown in figures C4(a) and C4(b) for the first 30° nose-down test and in figures C4(k) and C4(l) for the second 30° nose-down test. The data are grouped according to accelerometer location and orientation. The accelerometers were oriented along the normal (Z), longitudinal (X), and transverse (Y) axes as shown in figure 4. Each location is designated by its grid coordinate corresponding to figure 6. The first number indicates the longitudinal coordinate; the first letter indicates the normal coordinate (floor to roof); the second number indicates the transverse coordinate; and the second letter indicates the accelerometer orientation with respect to the airplane body-axis system.

The average normal and longitudinal crash pulses were similar for the two tests. In the first test, the average normal floor pulse in the cabin area was 27.2g peak,

0.083 sec time duration, and 11.3 m/sec integrated velocity change. For the second test, the average normal floor pulse was 29.9g peak, 0.096 sec time duration, and 12.3 m/sec integrated velocity change. In both tests, the peak acceleration occurred later for the aft cabin and baggage area, since loading in this area occurred after the tail rotated downward and contacted the ground. The average longitudinal floor pulse for the first test was 15.2g peak, 0.090 sec time duration, and 8.2 m/sec integrated velocity change of the main pulse. The remaining 15.5 m/sec horizontal velocity was dissipated by sliding friction in approximately 59.5 m with an average deceleration of 0.21g. In the second test, the average longitudinal floor pulse was 14g peak, 0.112 sec time duration, and 10.5 m/sec integrated velocity change of the main pulse. The airplane in the second test slid out 57.5 m to dissipate the remaining 13.0 m/sec horizontal velocity, giving an average deceleration of 0.15g. The average transverse acceleration in the first test was 5g over 0.068 sec and 8g over 0.140 sec in the second test.

The normal, longitudinal, and transverse accelerations for the occupants were measured relative to the head, chest, and pelvis of the dummy. Accelerations experienced by the pilot and copilot in the first 30° nose-down test are given in figures C4(c) and C4(d). Accelerations experienced by the pilot and copilot were similar. The pilot's maximum normal pelvis acceleration was 47g compared with 46g for the copilot. Maximum longitudinal chest acceleration was 24g for the pilot and 22g for the copilot. Maximum longitudinal pelvis acceleration was 12g for the pilot and 11g for the copilot.

Accelerations experienced by the passenger in the first test are shown in figure C4(e). Maximum normal accelerations were 52g in the pelvis, which is slightly higher than those of the crew. Maximum chest accelerations were 26g normal and 55g longitudinal. The passenger did not have a shoulder harness. As a result, the passenger's head hit the back of the pilot's seat during the crash test, producing a peak head acceleration of over 100g.

Restraint loads and chest and inertia-reel extensions are shown in figures C4(f) through C4(h) for the first 30° nose-down test. Maximum loads in the pilot's shoulder harness and lap belt were 2700 N and 2000 N, respectively. The displacement transducer trace indicated that the pilot's inertia-reel shoulder harness extended about 9.5 cm before latching. The copilot's forward chest motion was 32 cm with a peak shoulder-harness load of 4780 N. The copilot's shoulder-harness inertia reel locked after 6.5 cm of strap pullout. Maximum loads in his lap belt were 2080 N. The maximum load in the passenger's lap belt was 3300 N (fig. C4(g)).

Miscellaneous acceleration traces presented for completeness are contained in figures C4(i) and C4(j).

Normal, longitudinal, and transverse accelerations for the pilot, first passenger (seated behind the pilot), and the second passenger are given in figures C4(m) through C4(o) for the second test. As in all other tests, accelerations are measured relative to the head, chest, and pelvis of the dummy.

In the second 30° nose-down test, the maximum normal accelerations experienced by the pilot were 36g in the chest and 58g in the pelvis. The normal pelvis acceleration was higher in the second test but was for a shorter time than the accelerations experienced by the crew in the first test. The maximum forward chest motion of the pilot was 38 cm (pilot's seat detached during this crash test), and inertia-reel shoulder-harness strap extended a maximum of 7.5 cm. Restraint load measurements were lost for the pilot's lap belt and shoulder harness.

The second passenger wore a lap belt and shoulder harness; the first passenger wore a lap belt only. The inertia reel on the second passenger's shoulder harness was locked with a pin to prevent interference with camera coverage of the first passenger. One purpose of this crash test was to compare passenger response with and without a shoulder harness. It was not anticipated that the first passenger's seat would detach from the rails (as discussed in the previous section); since this was the case, a direct comparison between the first and second passenger was not possible. It is believed that the second passenger's seat in this test remained attached to the structure primarily because the leg attachment was properly tightened. In addition, the second passenger's shoulder harness was connected to the fuselage, which tended to counteract the forward overturning moment of the seat experienced by the first passenger as he rotated forward.

The second passenger experienced higher longitudinal pelvis accelerations (30g) than the first passenger (13g) because the second passenger's seat remained attached to the structure during the impact. The first passenger's seat detached during the crash test, causing him to hit the back of the pilot's seat. This resulted in very high head (45g normal, 72g longitudinal) and chest accelerations (96g longitudinal). The second passenger experienced an unexpected 70g normal head acceleration. This acceleration was caused by contact between the head and knees during the crash. As seen in high-speed motion pictures taken onboard the airplane during the test, the second passenger sunk into his seat during the impact; at the same time, his legs rebounded from the floor and his head pitched forward, impacting his knees. However, the first passenger was without upper-torso restraint and received a more severe head impact.

The second passenger's maximum chest forward motion was 17.5 cm, and as mentioned previously, his inertia reel was pinned. The first passenger's chest forward motion was 67.5 cm. The maximum load was 2900 N in the second passenger's lap belt and 1630 N in the first passenger's lap belt (fig. C4(l)). The load measurement in the second passenger's shoulder harness was lost.

Miscellaneous acceleration traces presented for completeness are contained in figure C4(p).

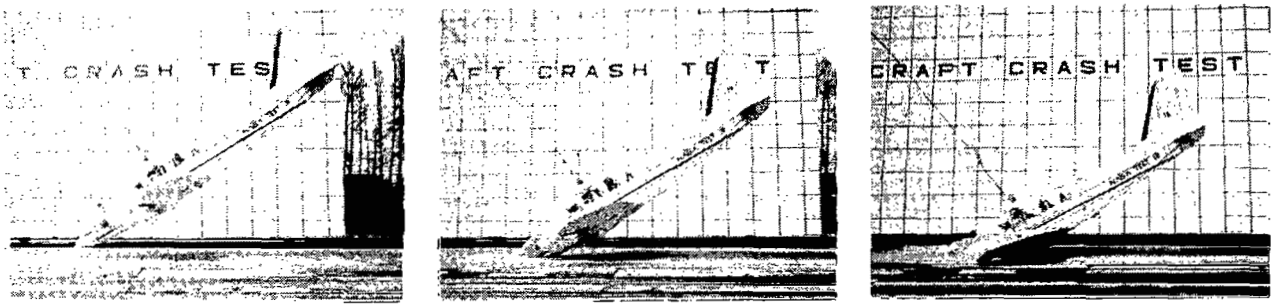

Time = 0.0 sec | Time = 0.05 sec | Time = 0.10 sec

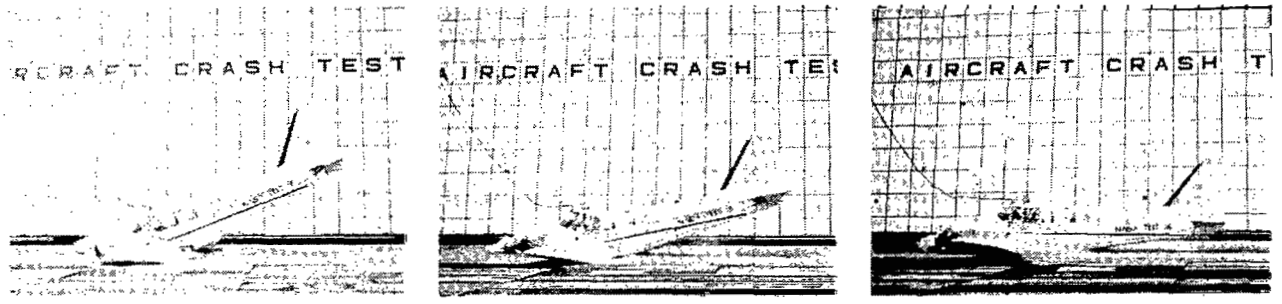

Time = 0.15 sec | Time = 0.20 sec | Time = 0.25 sec

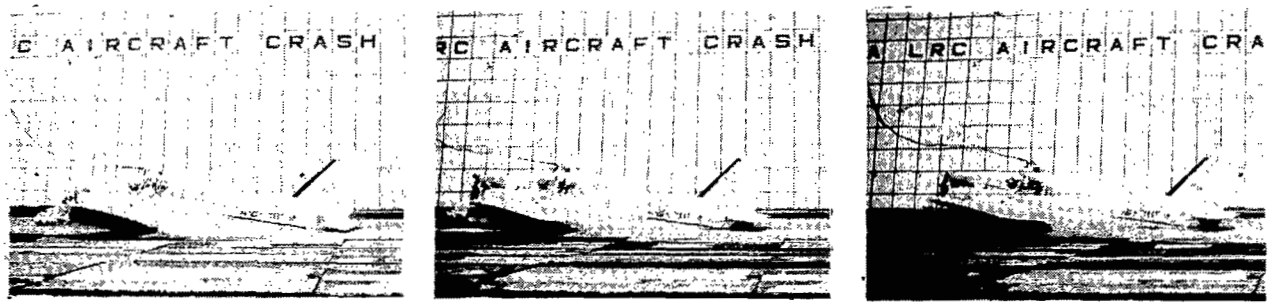

Time = 0.30 sec | Time = 0.35 sec | Time = 0.40 sec

L-81-5699.1

Figure C1.- Crash-sequence photographs of first 30° nose-down test.

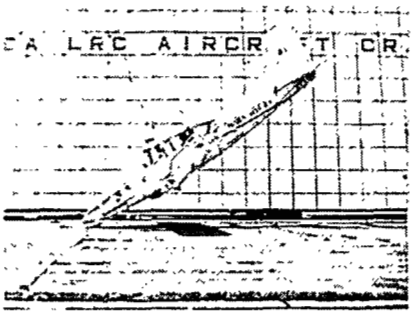

Time = 0.0 sec

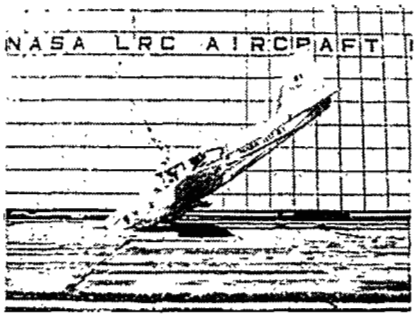

Time = 0.05 sec

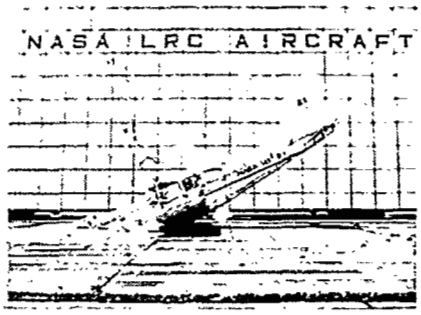

Time = 0.10 sec

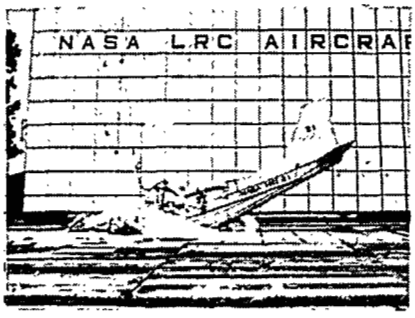

Time = 0.15 sec

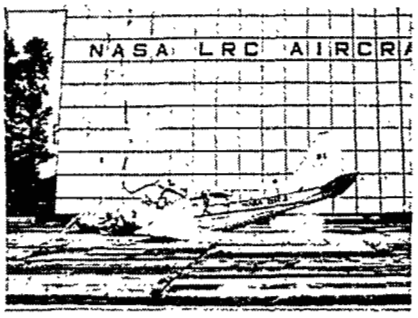

Time = 0.20 sec

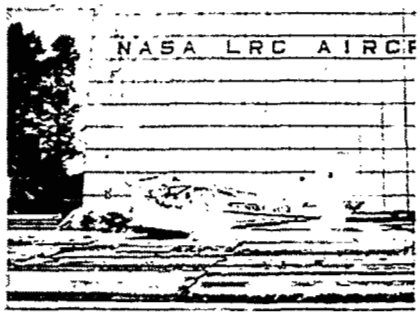

Time = 0.25 sec

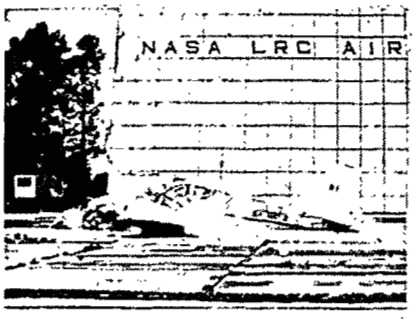

Time = 0.30 sec

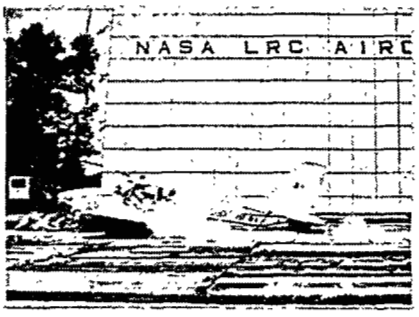

Time = 0.35 sec

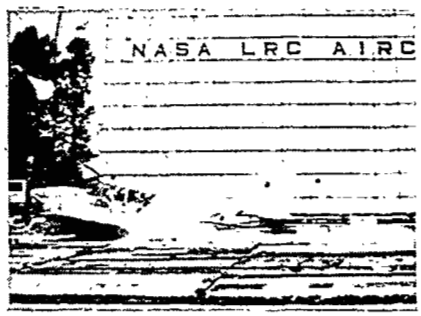

Time = 0.40 sec

L-82-171

Figure C2.- Crash-sequence photographs of second 30° nose-down test.

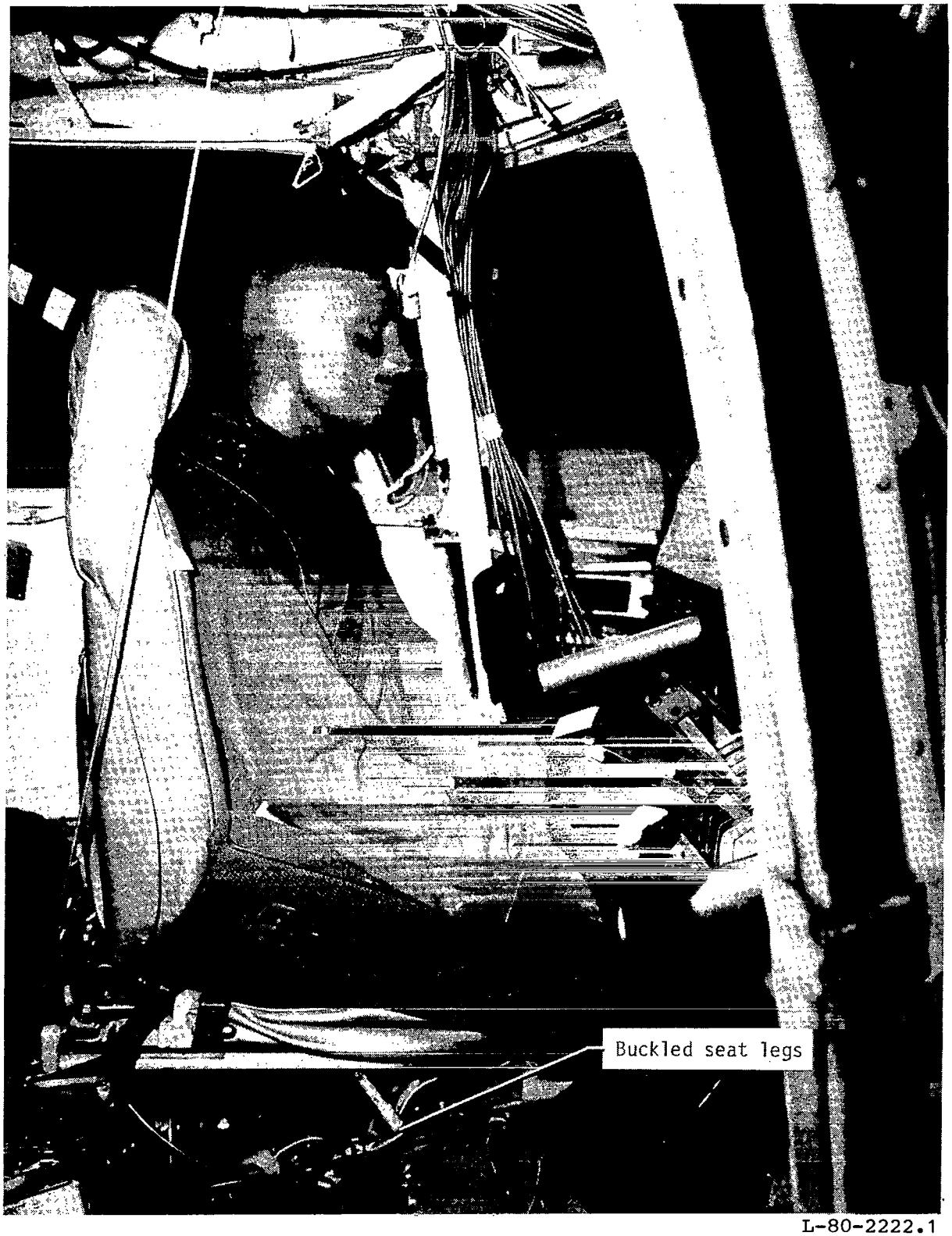

L-80-2222.1

(a) Postcrash view of pilot's seat in first 30° nose-down test.

Figure C3.- Postcrash photographs of 30° nose-down tests.

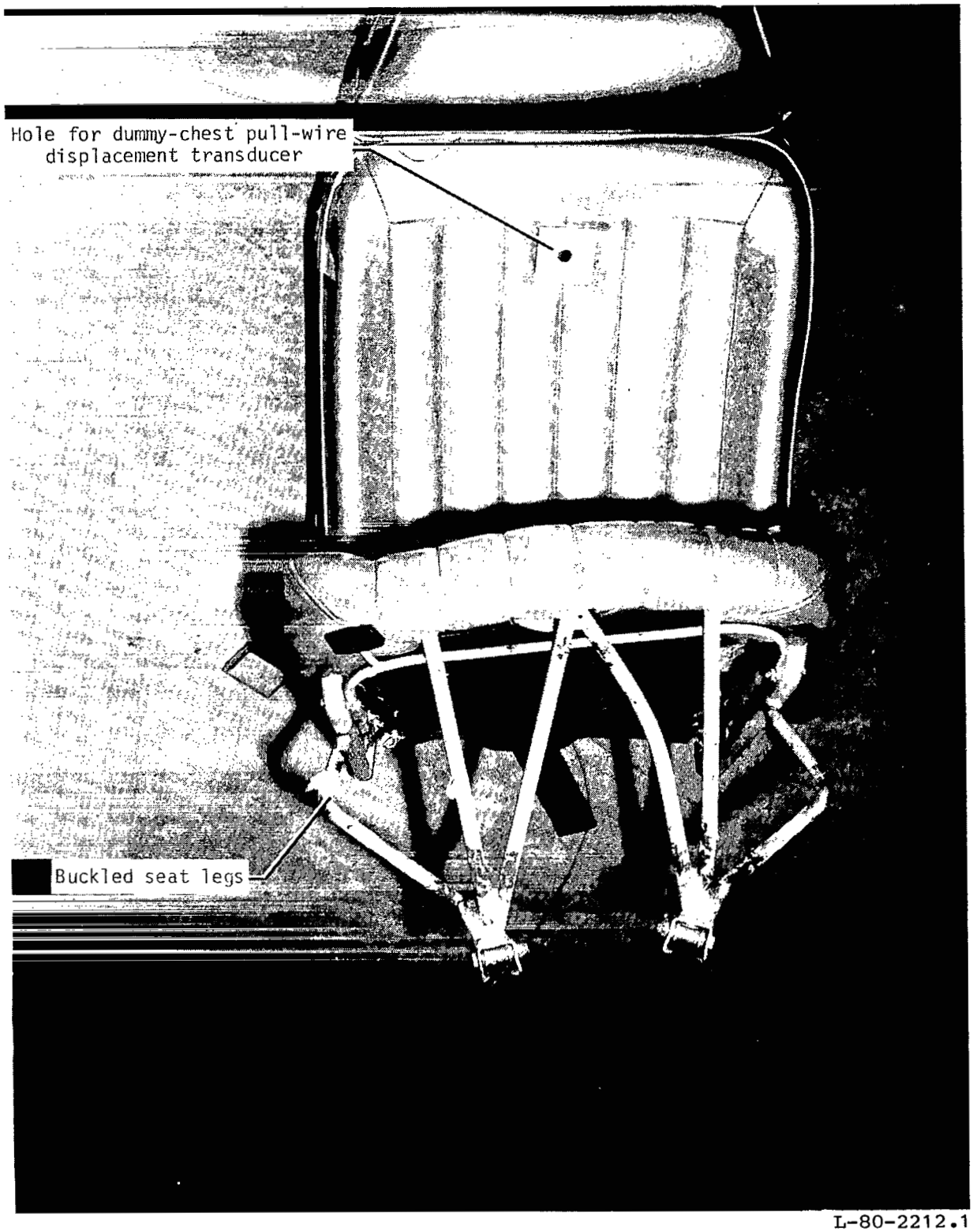

(b) Damage sustained by pilot's seat in first 30° nose-down test.

Figure C3.- Continued.

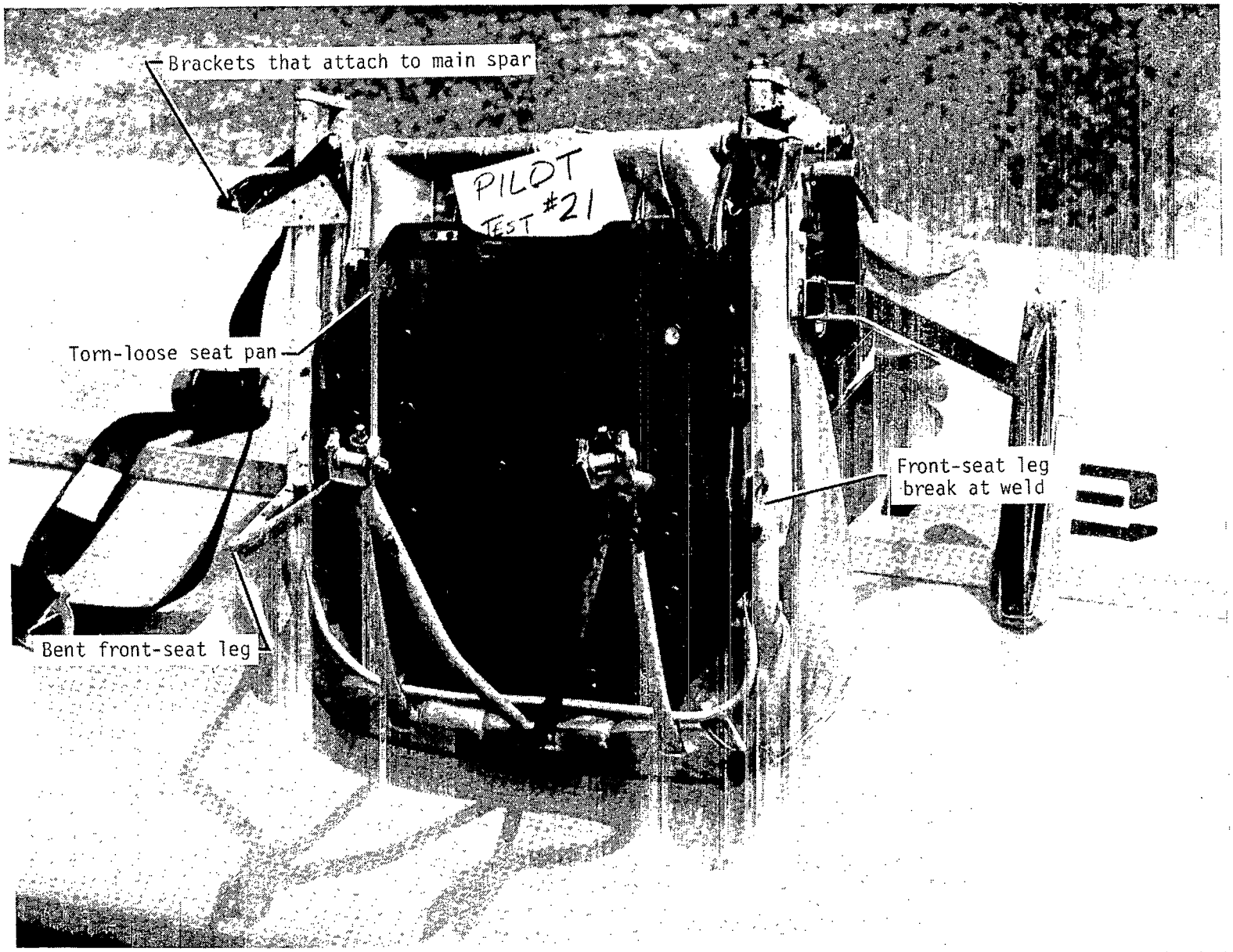

L-81-5832.1

(c) Damage sustained by pilot's seat in second 30° nose-down test.

Figure C3.- Continued.

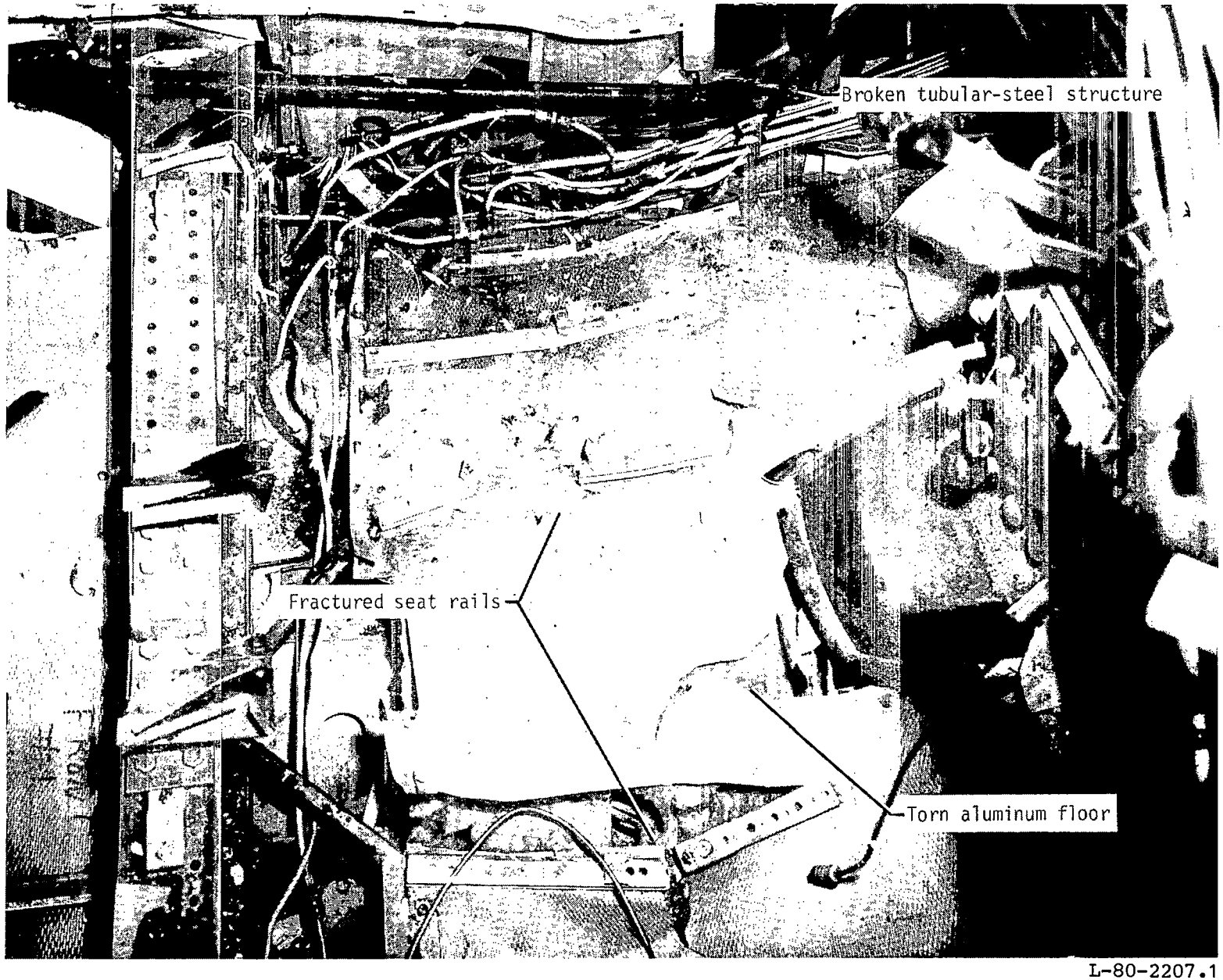

(d) Postcrash view of crew floor area from first 30° nose-down test.

Figure C3.- Continued.

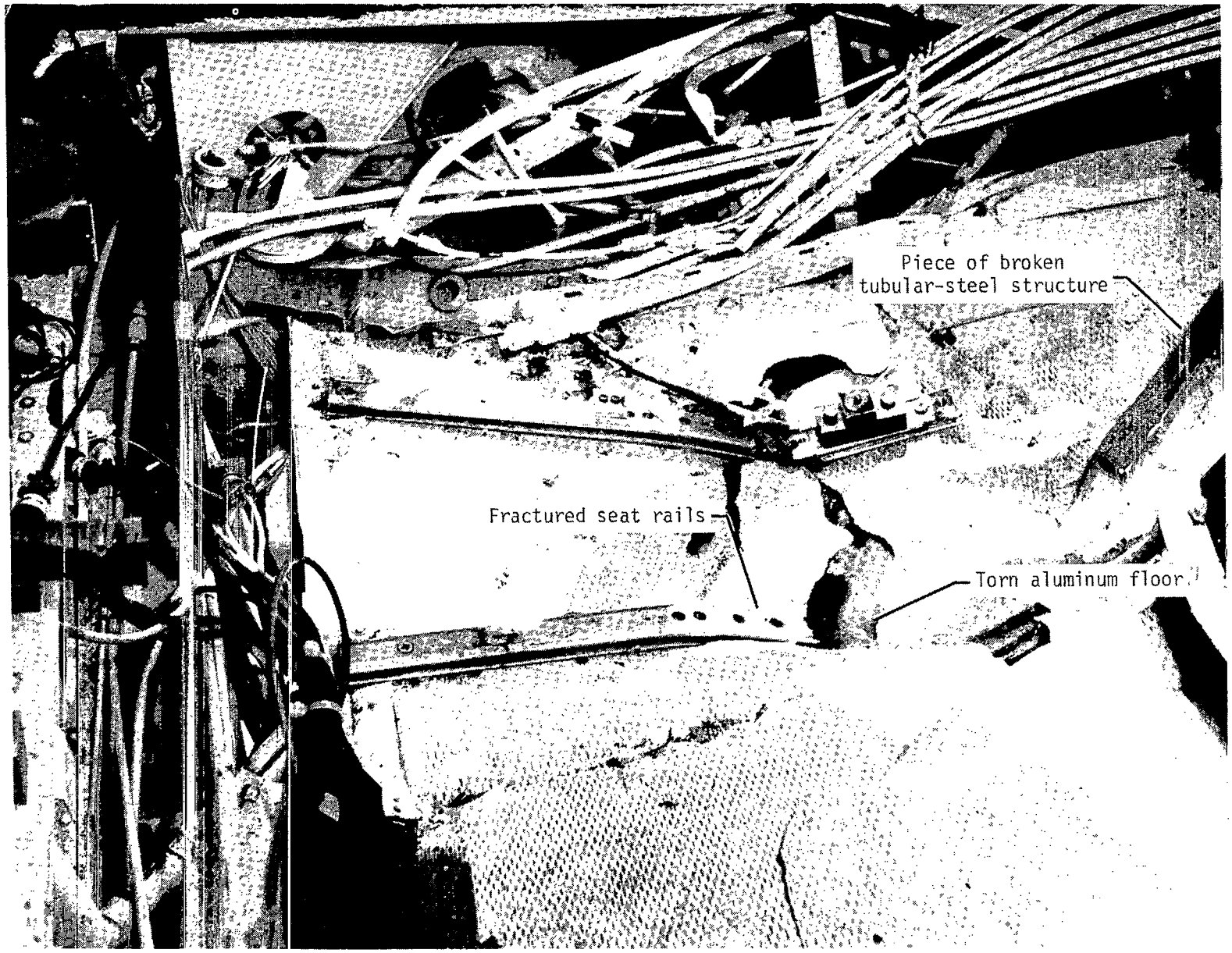

L-81-5827.1

(e) Postcrash view of pilot's position in second 30° nose-down test.

Figure C3.- Continued.

L-80-2217.1

(f) Postcrash view of passenger's seat in first 30° nose-down test.

Figure C3.- Continued.

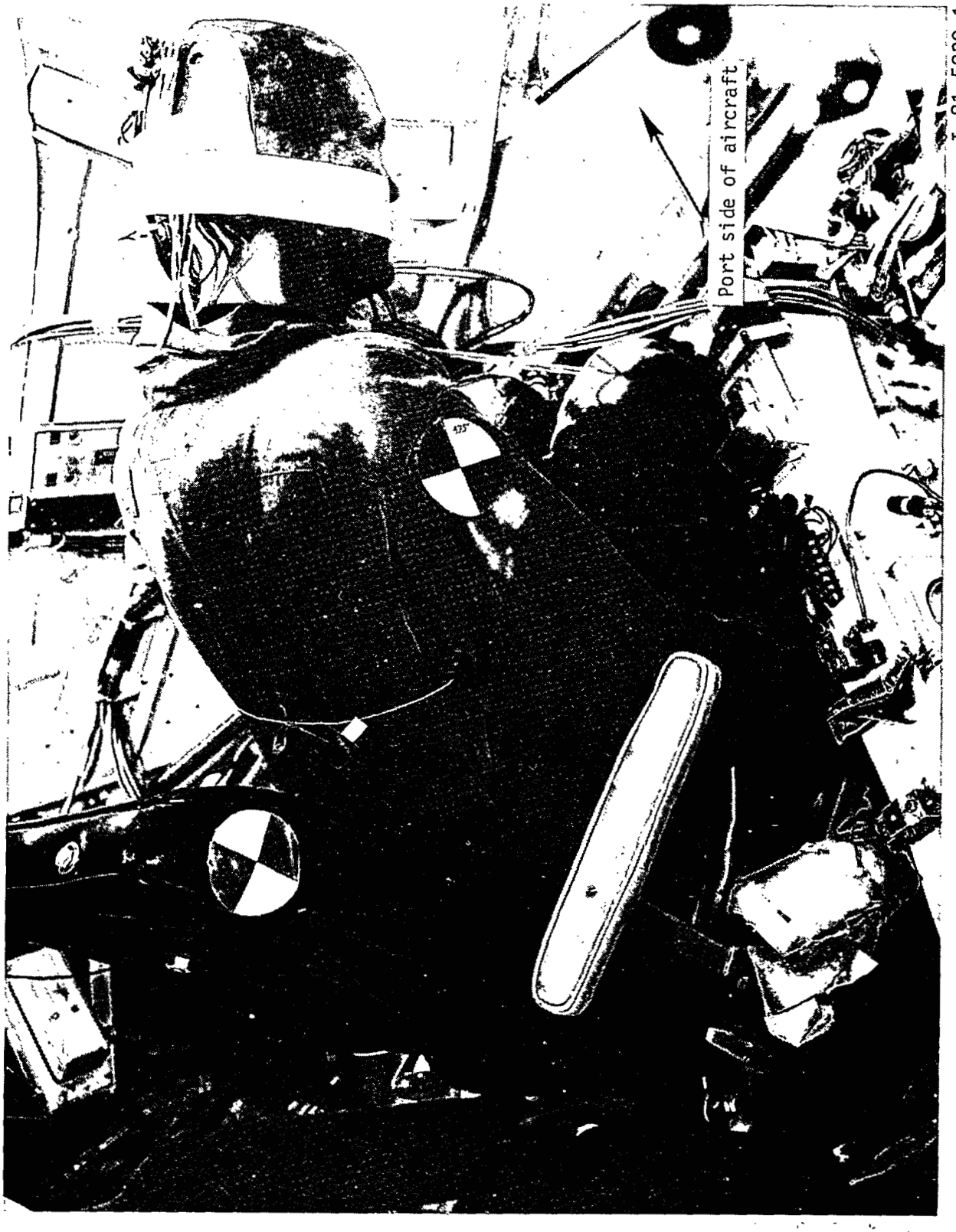

(g) First passenger's position after second 30° nose-down test.

Figure C3.- Continued.

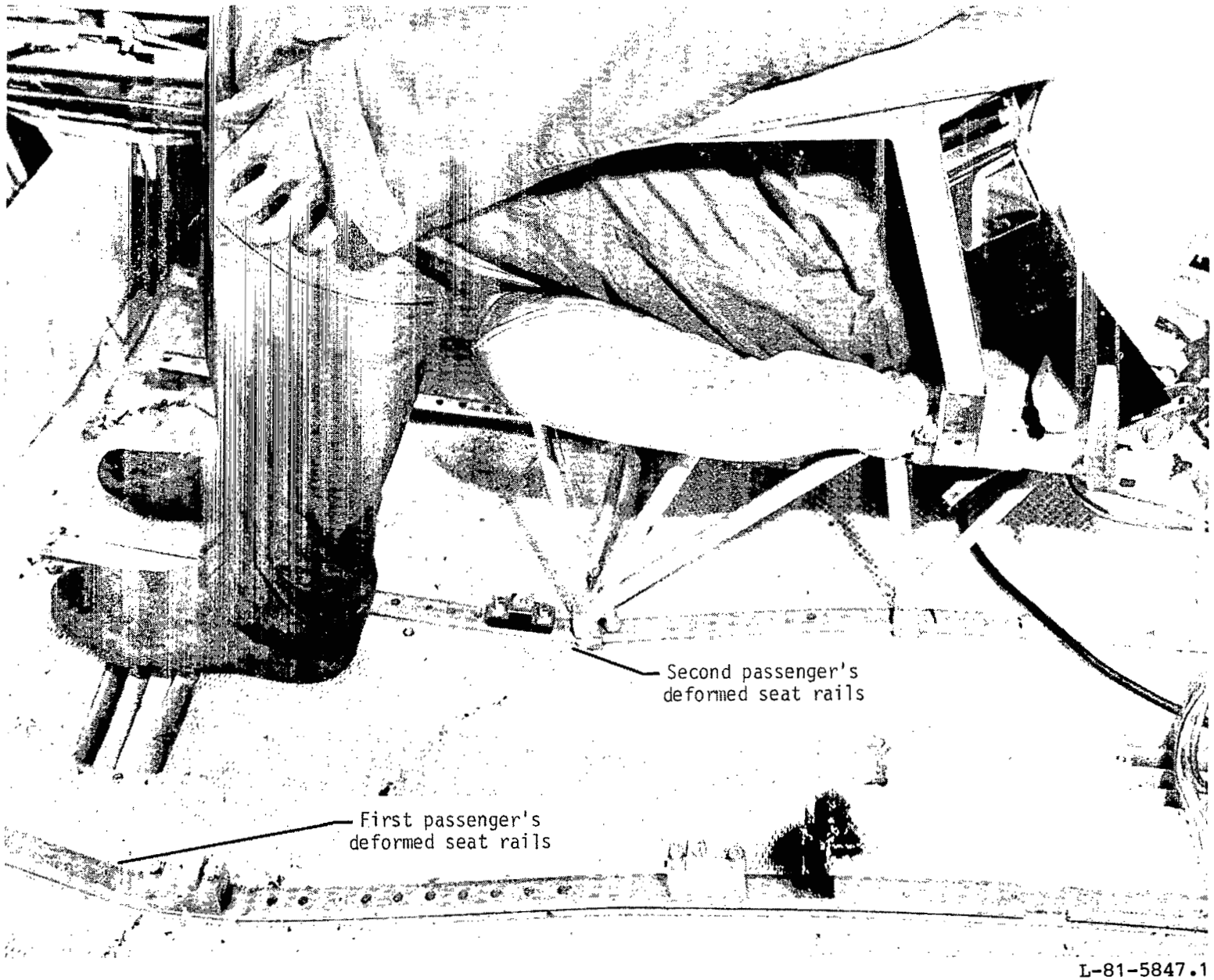

(h) Second passenger's seat in second 30° nose-down test.

Figure C3.- Continued.

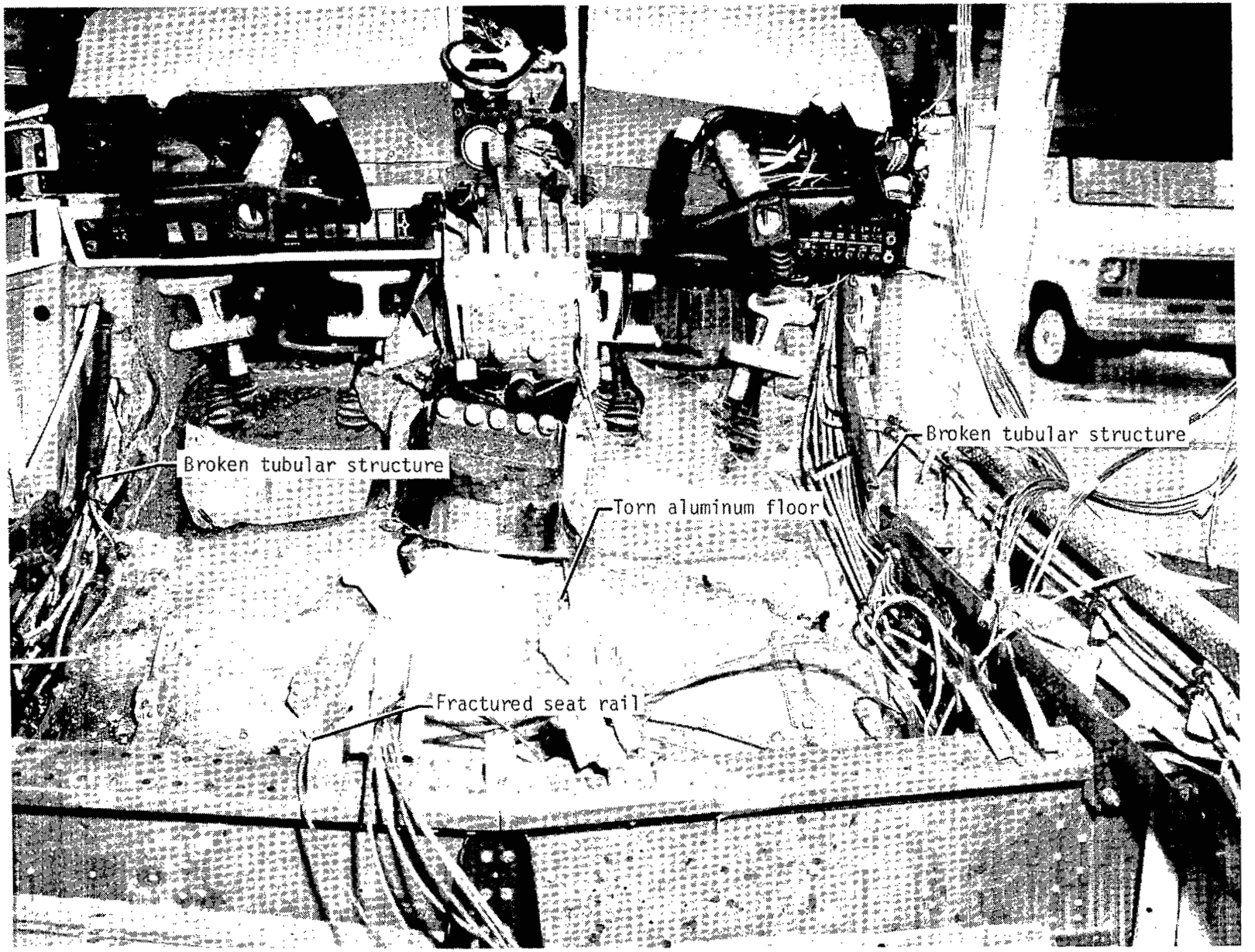

L-80-2209.1

(i) Forward view of cabin after first 30° nose-down test.

Figure C3.- Continued.

(j) Postcrash view of cabin after first 30° nose-down test.

Figure C3.- Continued.

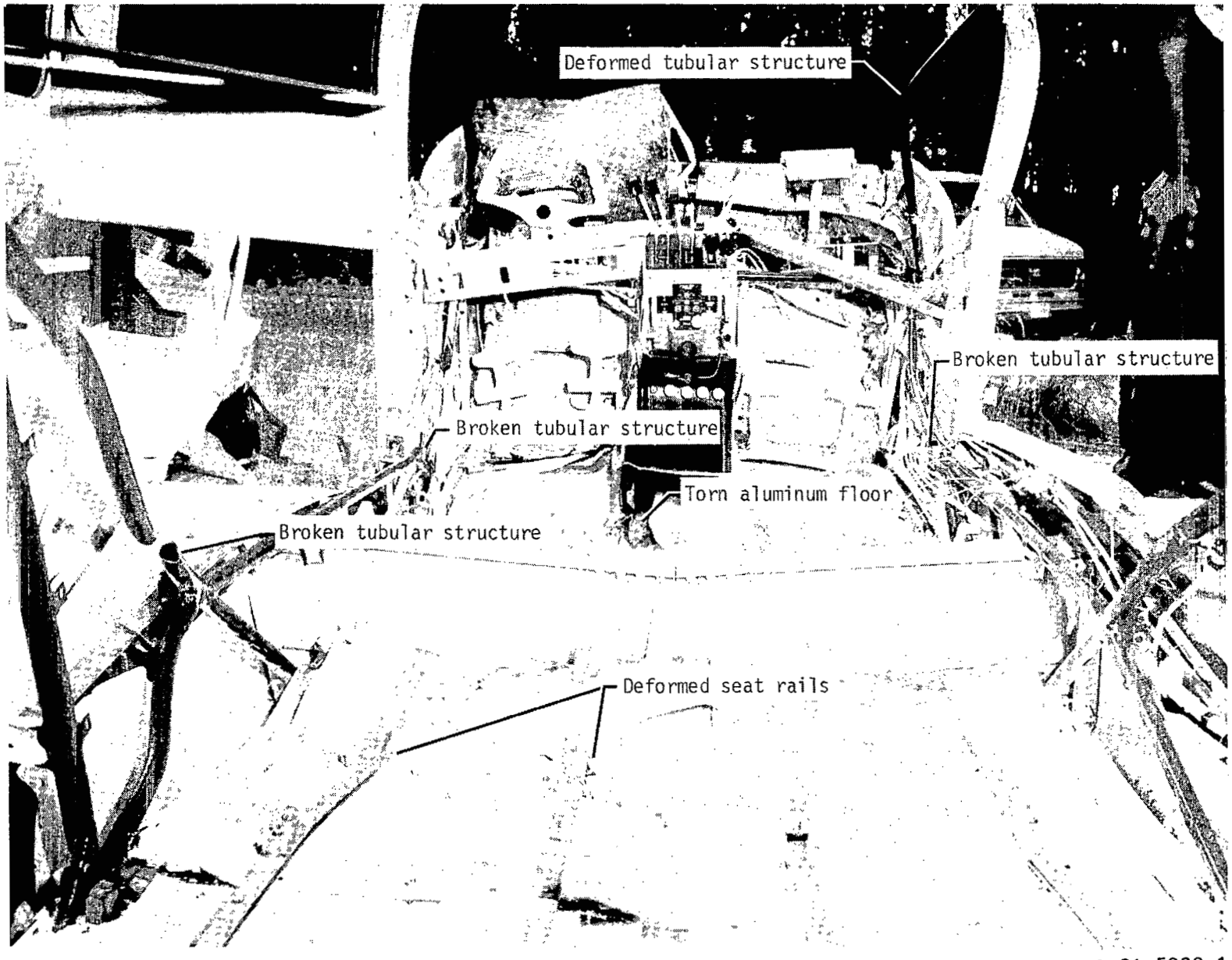

(k) Forward view of cabin after second 30° nose-down test.

Figure C3.- Continued.

(1) Second passenger's position after second 30° nose-down test.

Figure C3.- Continued.

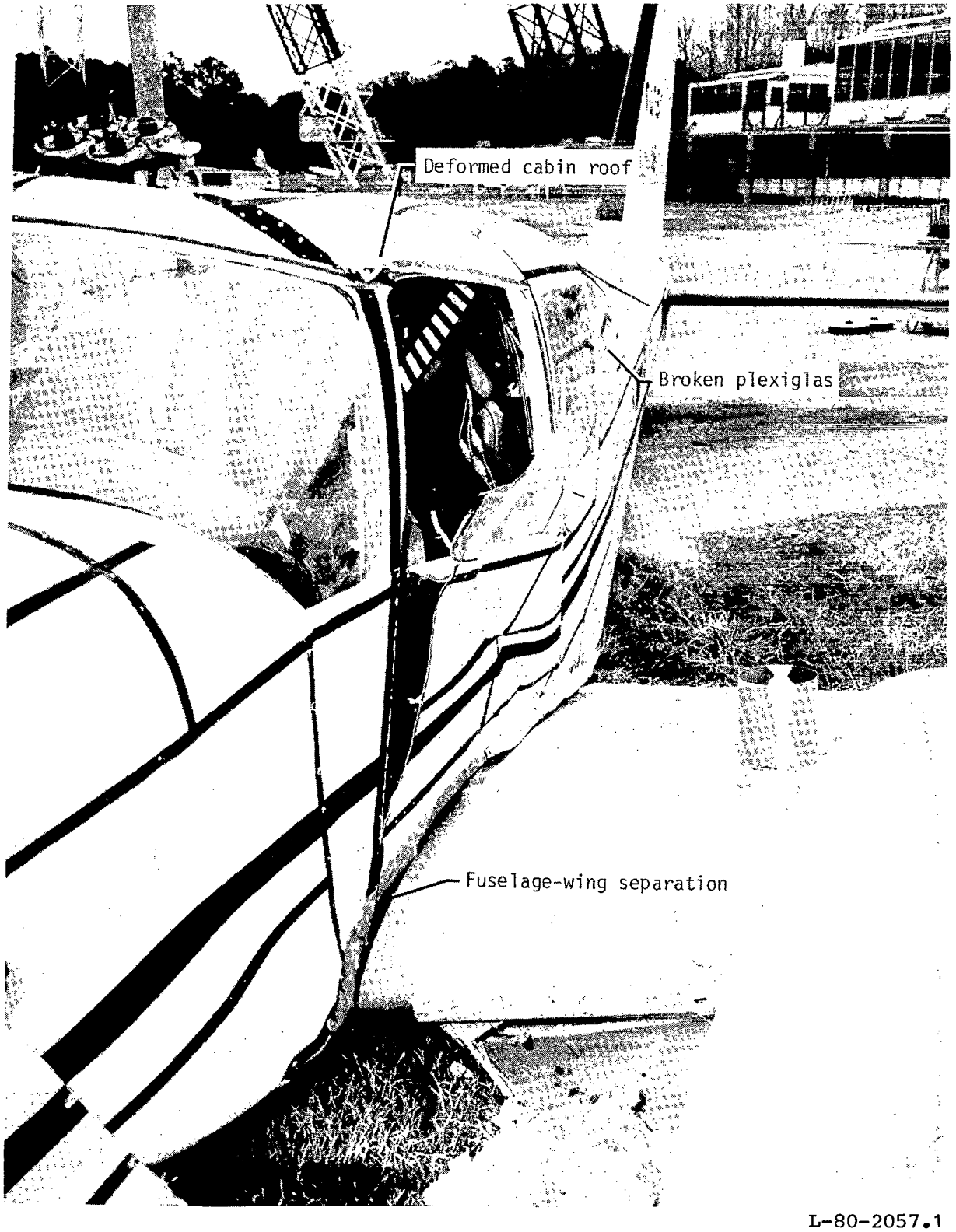

L-80-2057.1

(m) Port-side view of airplane after first 30° nose-down test.

Figure C3.- Continued.

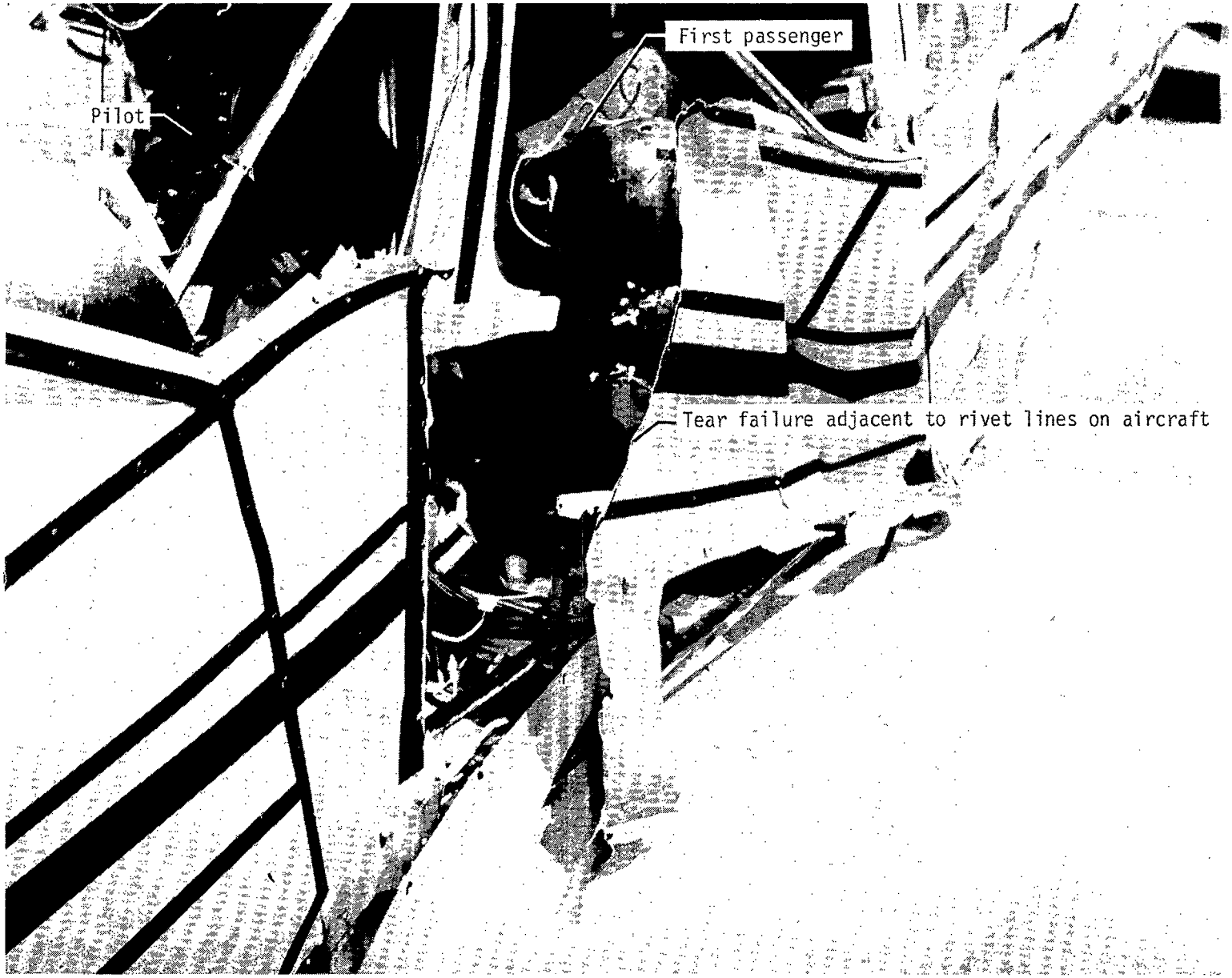

(n) Port-side view of airplane after second 30° nose-down test.

Figure C3.- Continued.

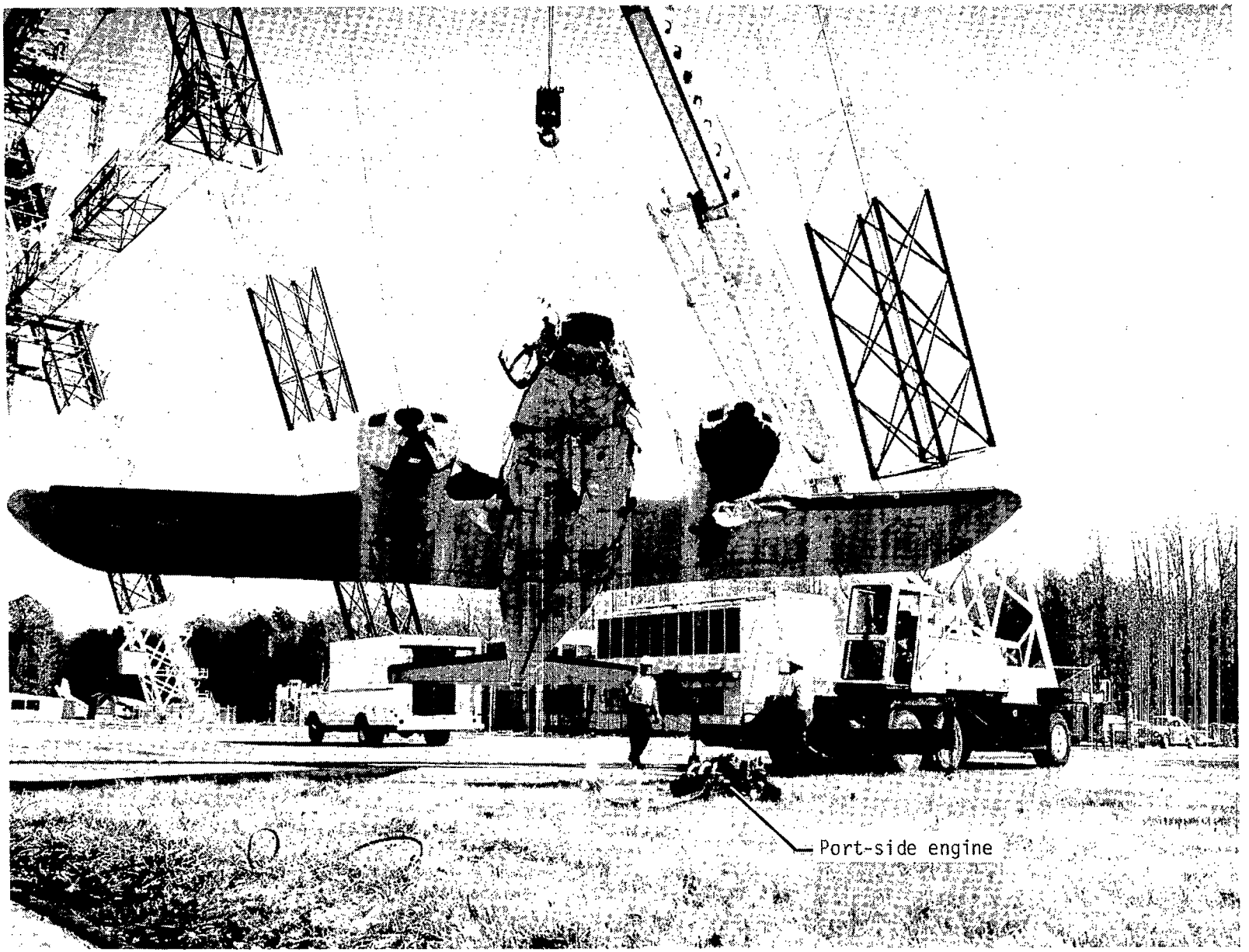

L-80-2076.1

(o) Underside view of airplane after first 30° nose-down test.

Figure C3.- Continued.

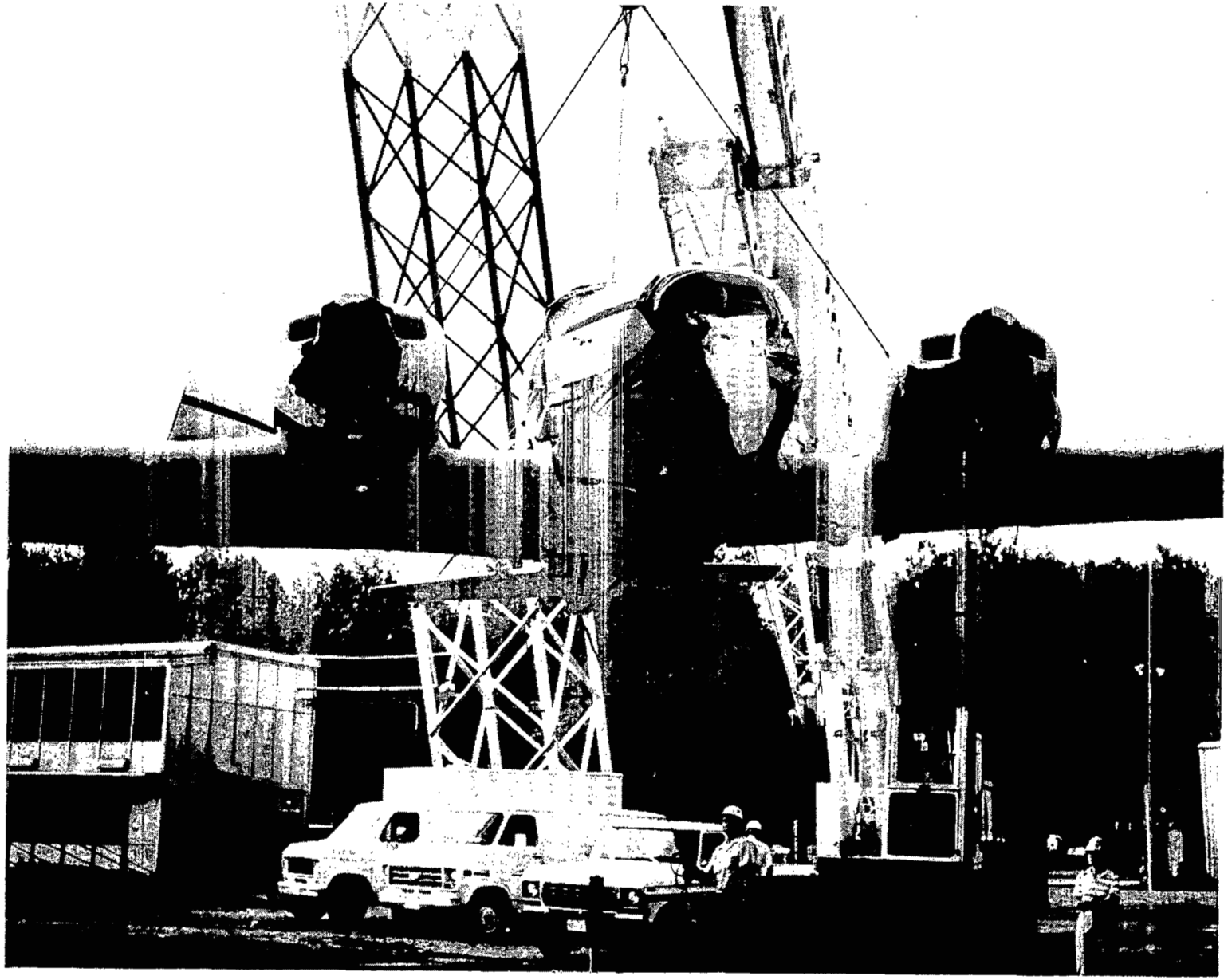

L-81-6536

(p) Underside view of airplane after second 30° nose-down test.

Figure C3.- Concluded.

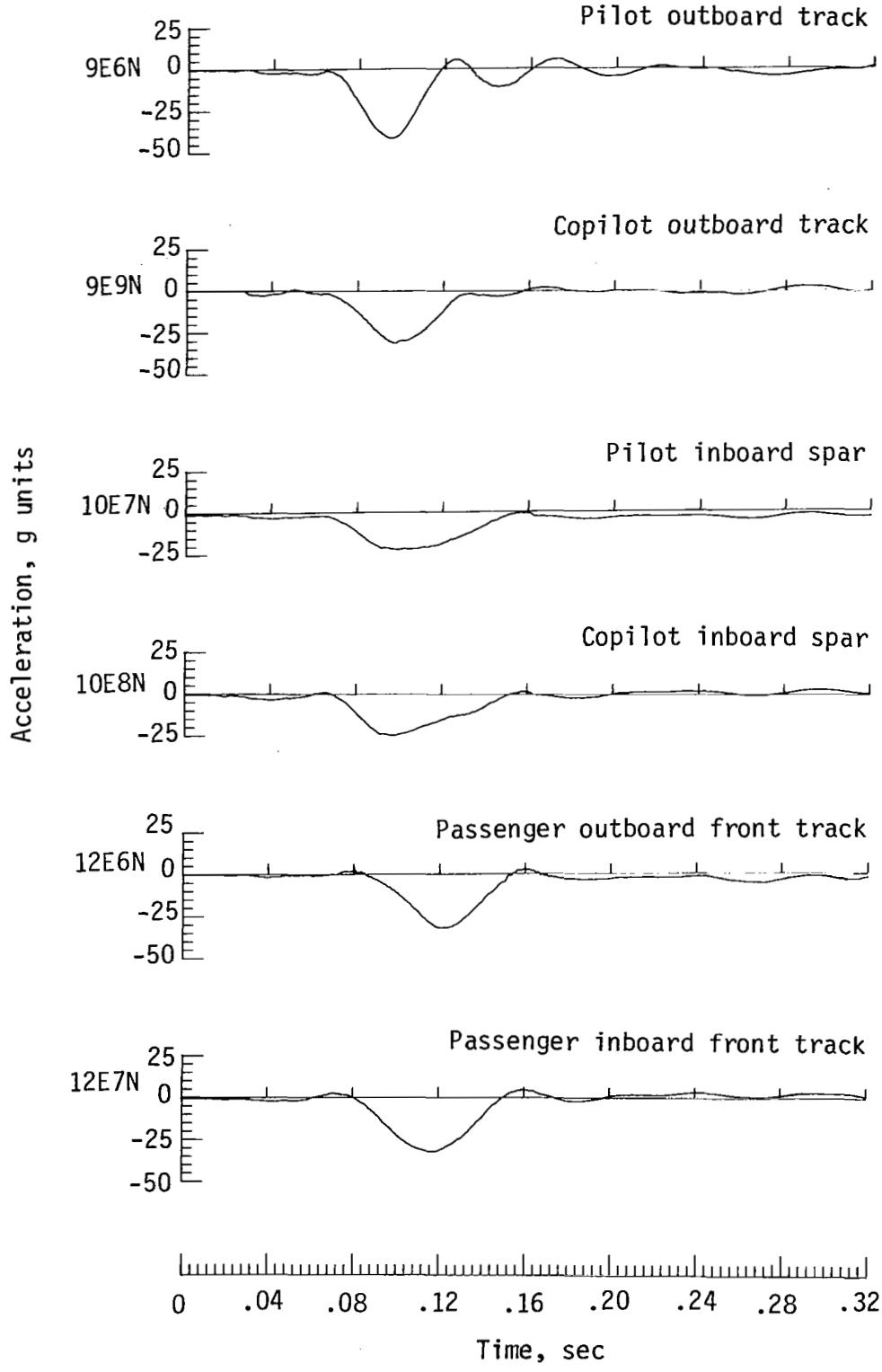

(a) Normal floor accelerations for first 30° nose-down test.

Figure C4.- Data from 30° nose-down tests.

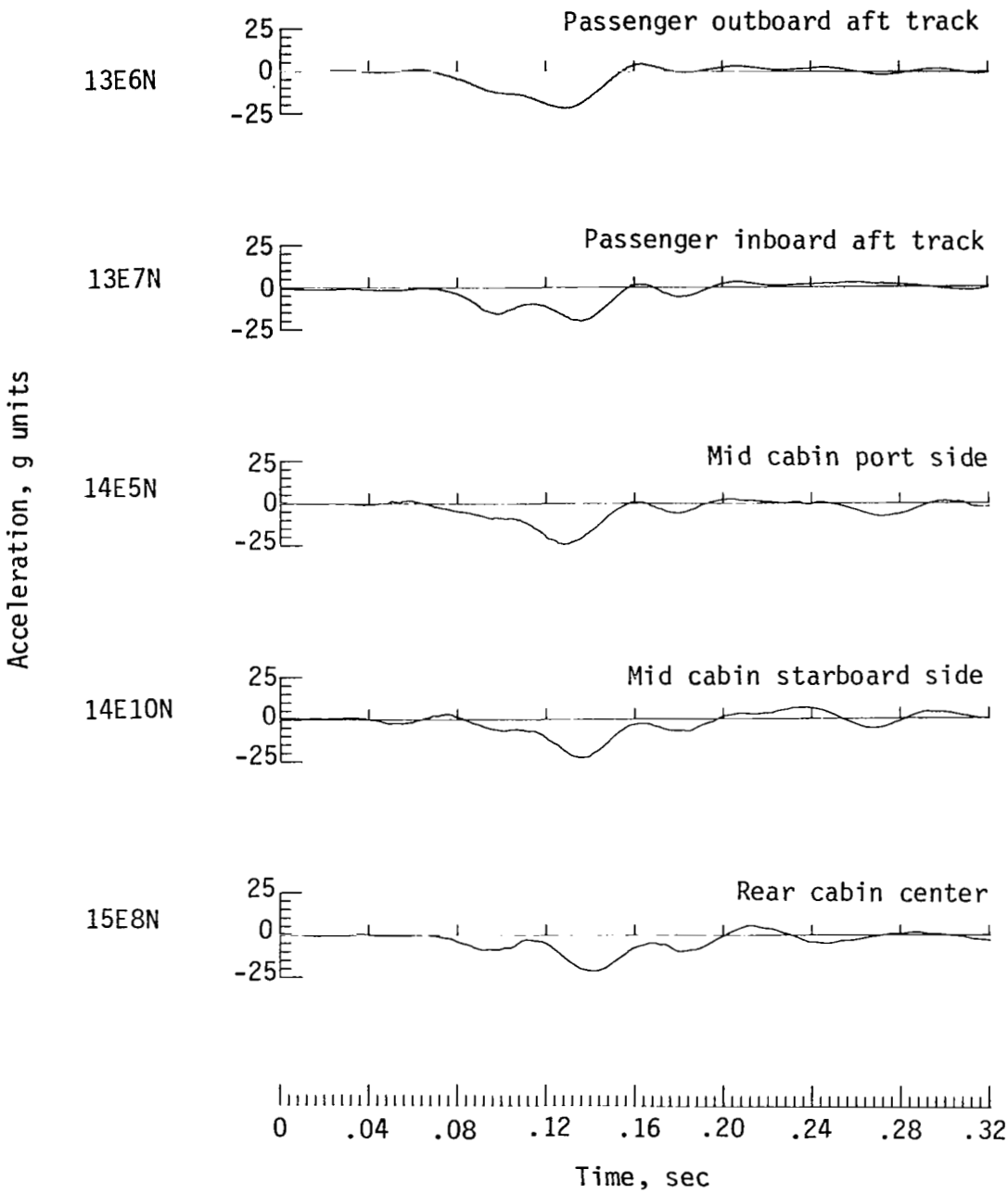

(a) Concluded.

Figure C4.- Continued.

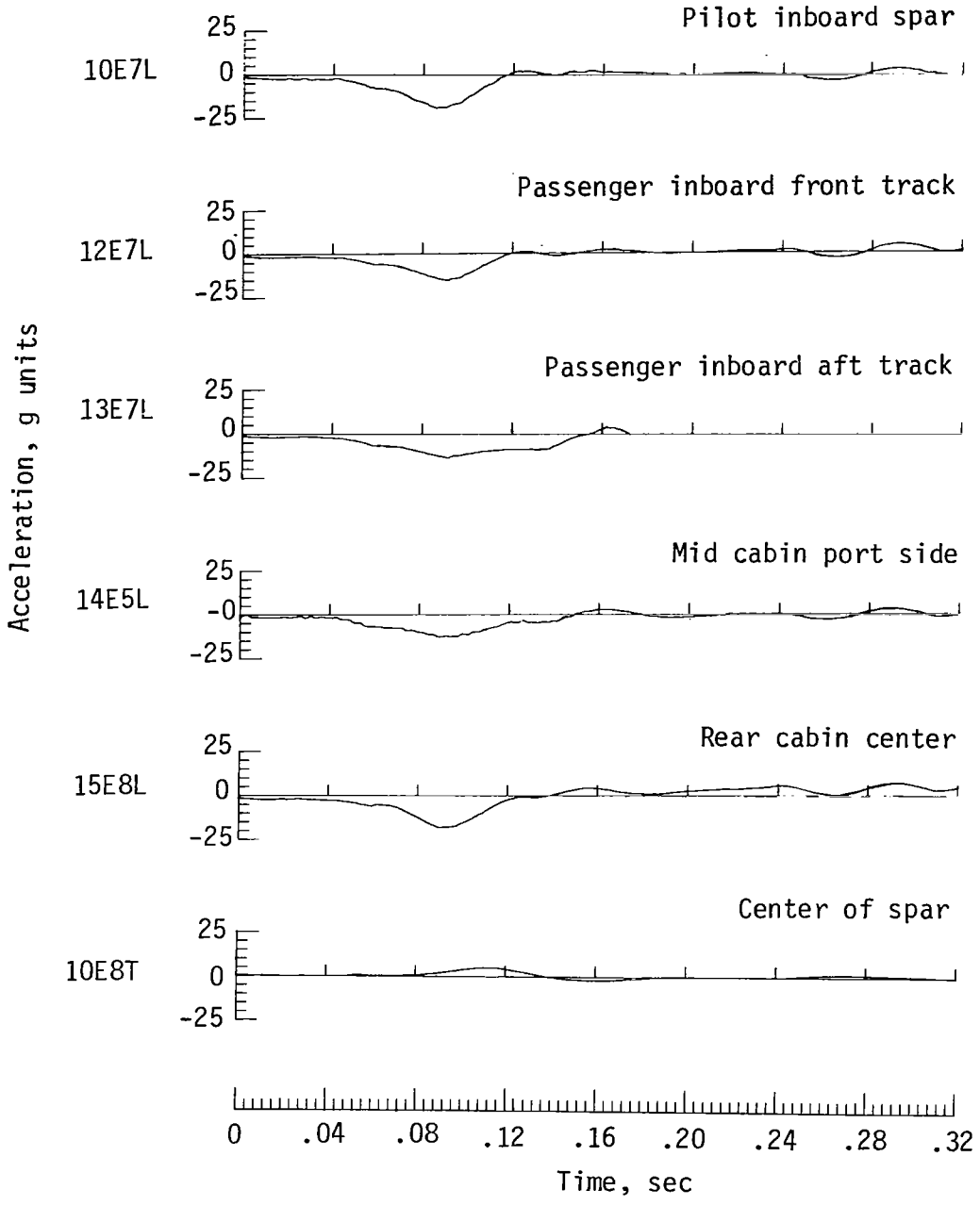

(b) Longitudinal and transverse floor accelerations for first 30° nose-down test.

Figure C4.- Continued.

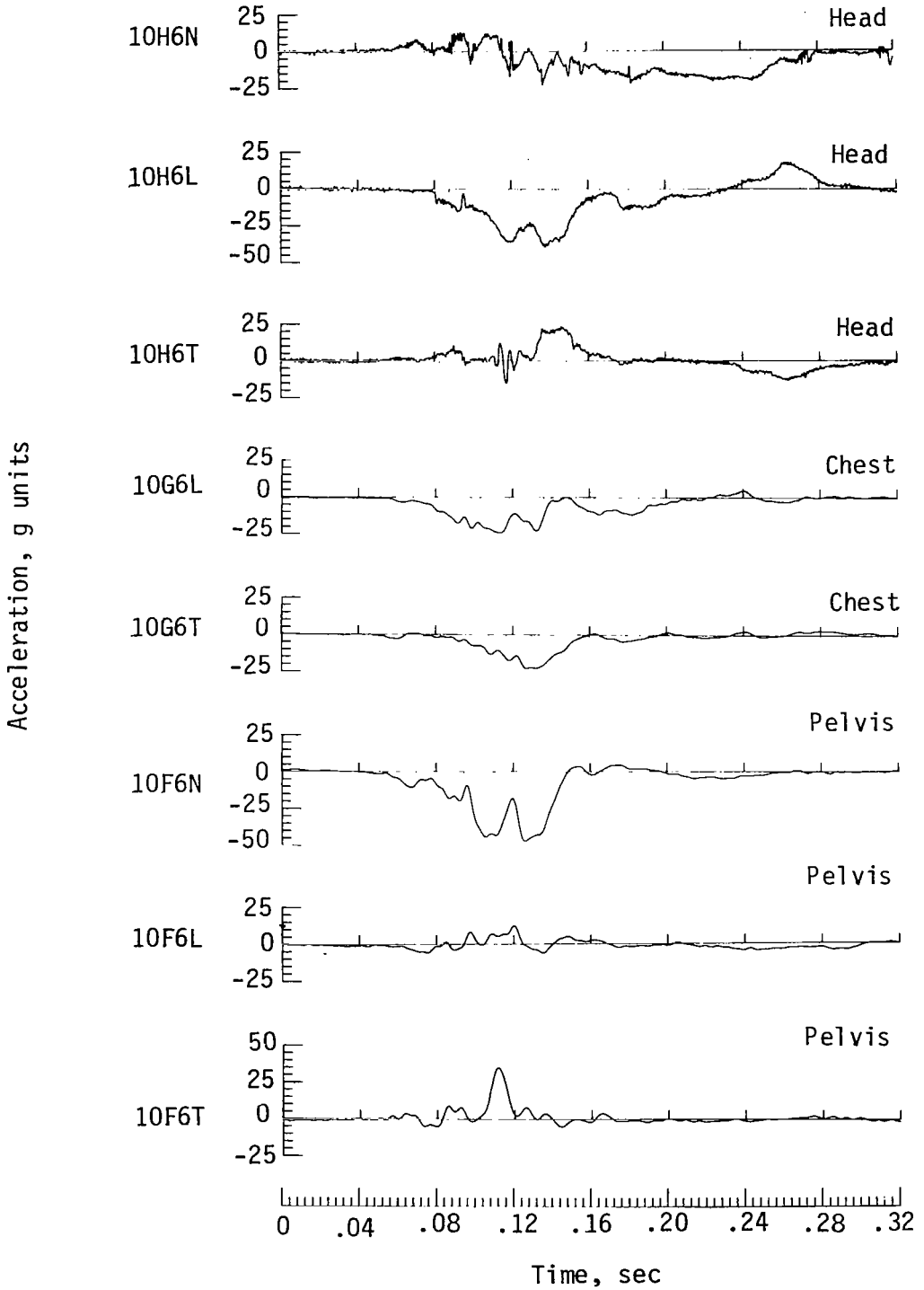

(c) Pilot accelerations for first 30° nose-down test.

Figure C4.- Continued.

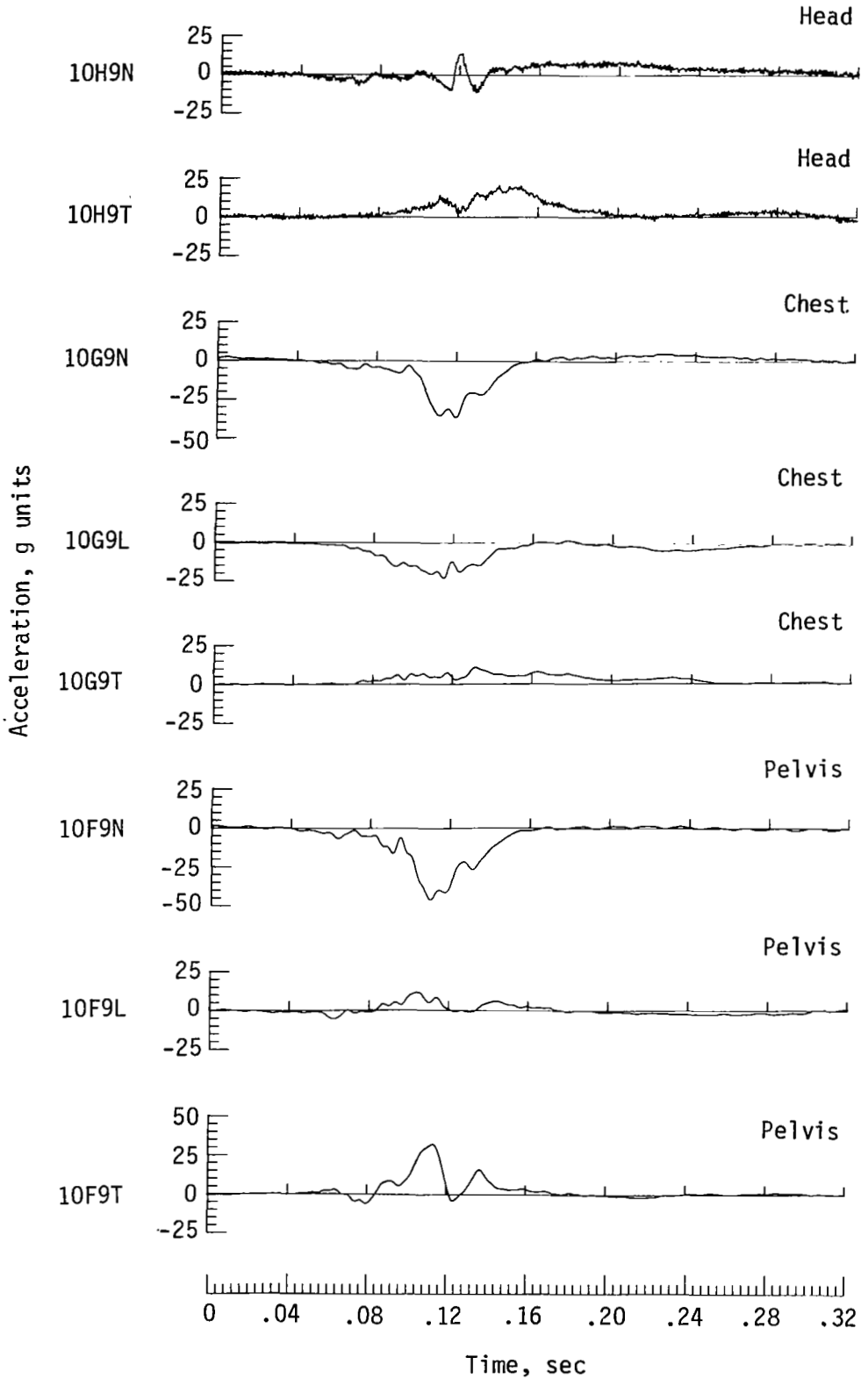

(d) Copilot accelerations for first 30° nose-down test.

Figure C4.- Continued.

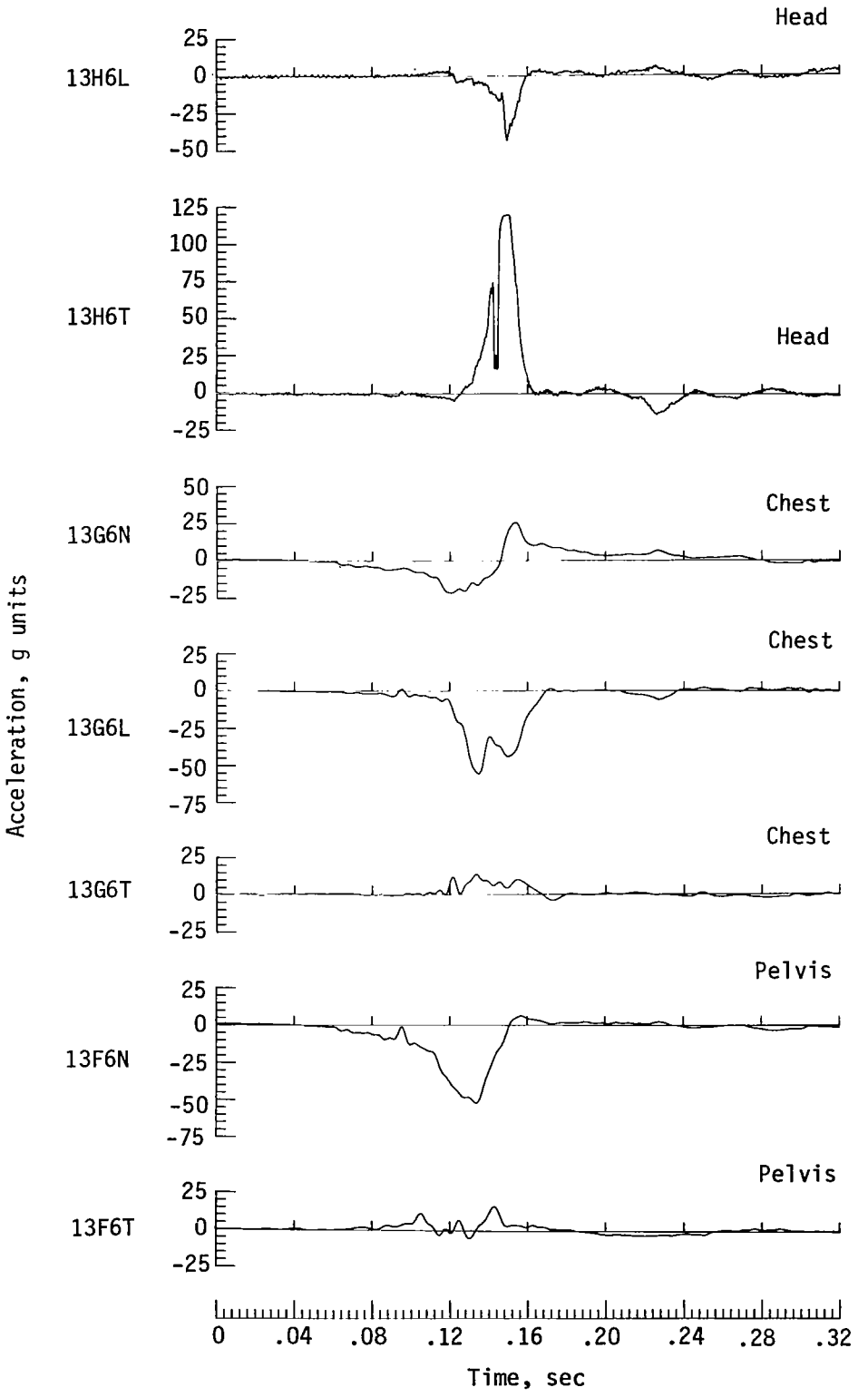

(e) Passenger accelerations for first 30° nose-down test.

Figure C4.- Continued.

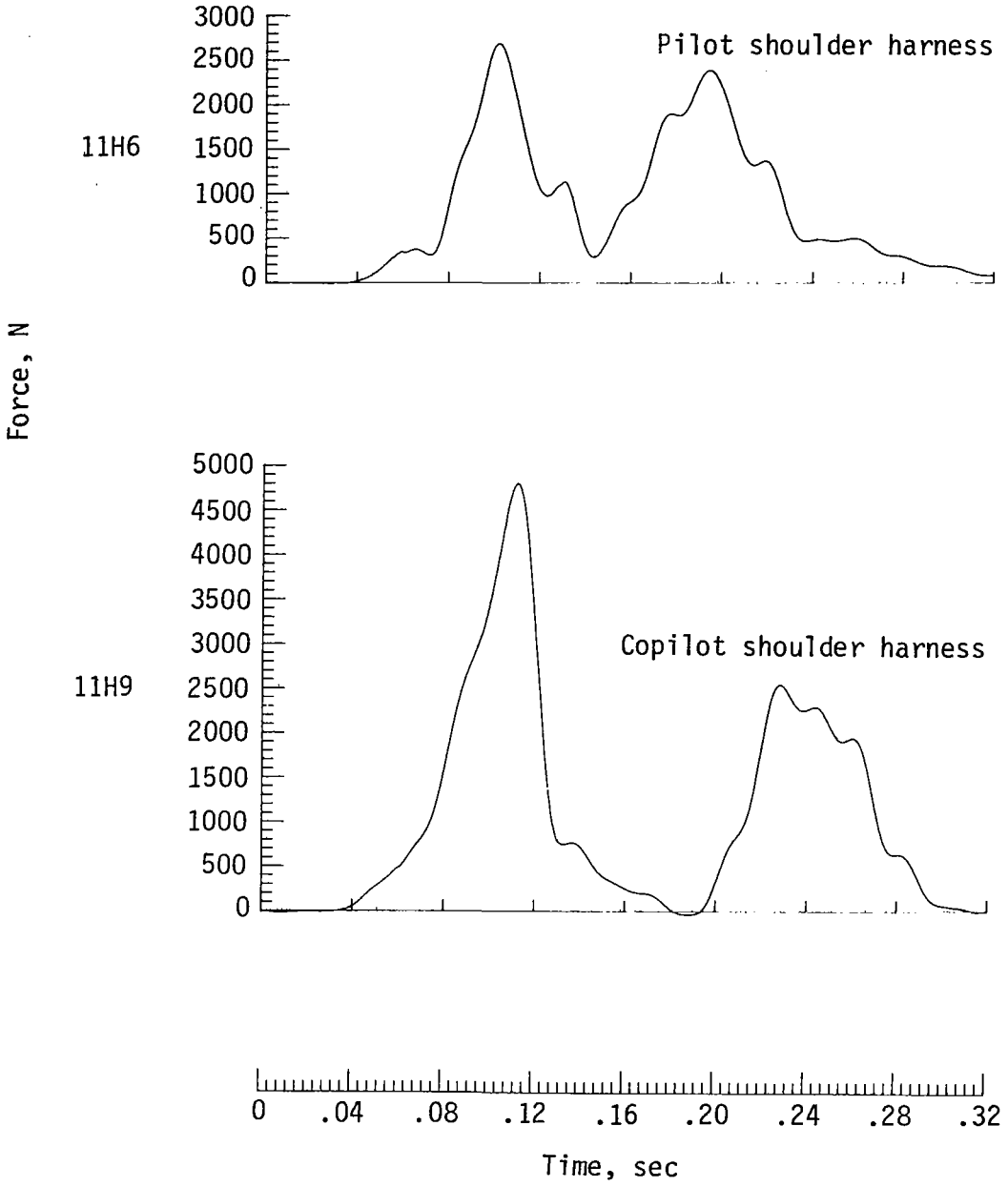

(f) Restraint loads for first 30° nose-down test.

Figure C4.- Continued.

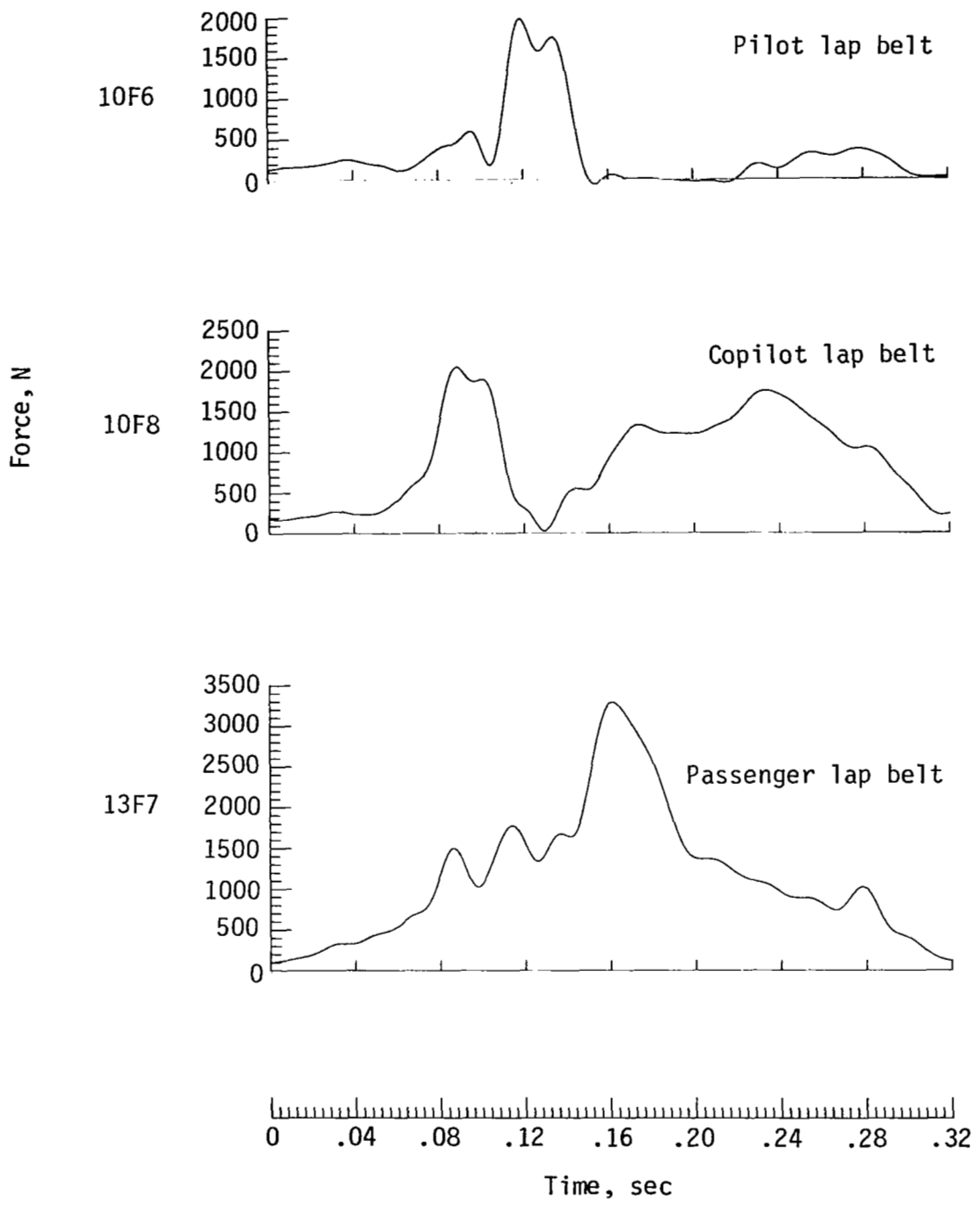

(g) Lap-belt loads for first 30° nose-down test.

Figure C4.- Continued.

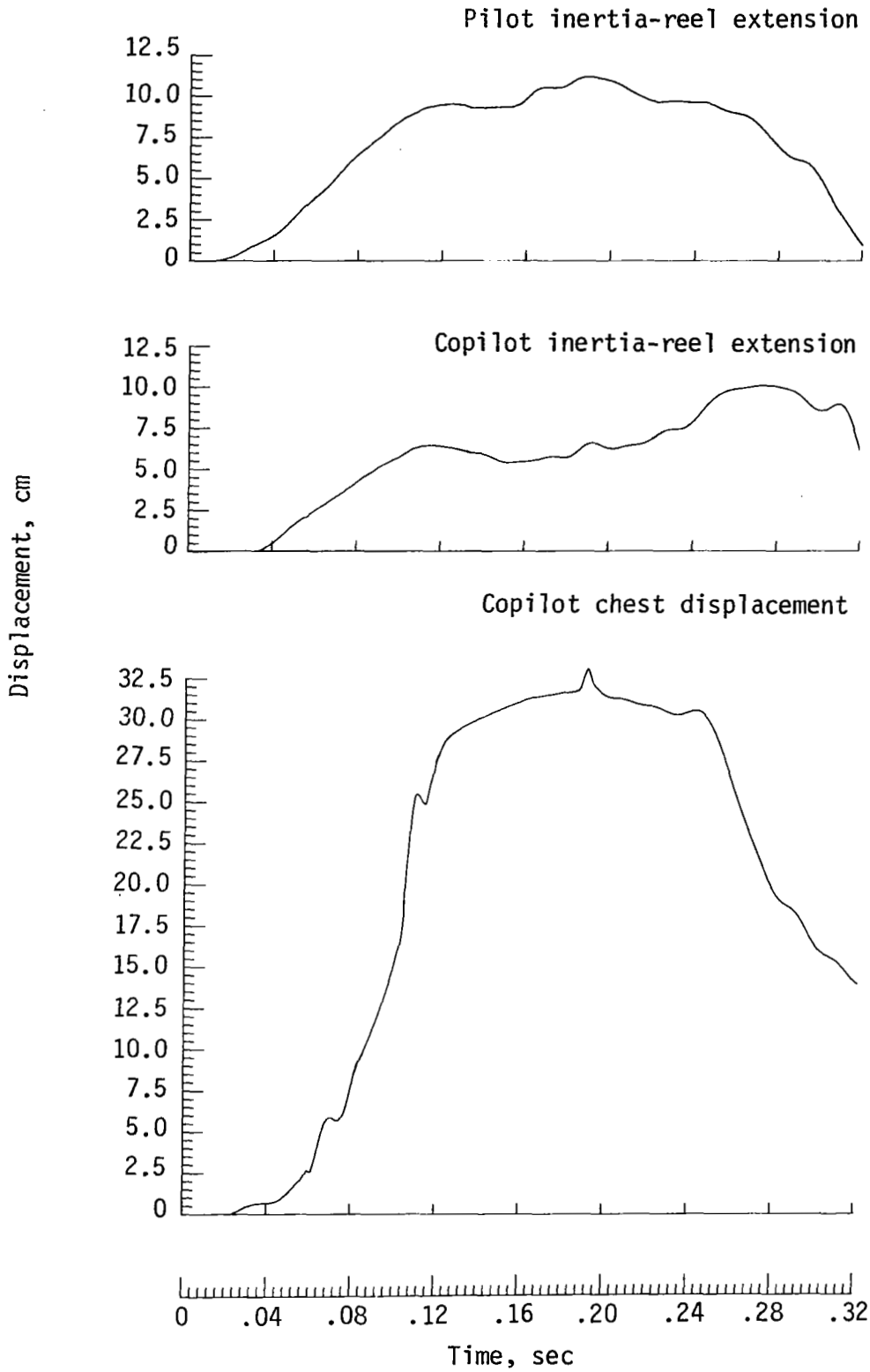

(h) Inertia-reel and chest displacement data for first 30° nose-down test.

Figure C4.- Continued.

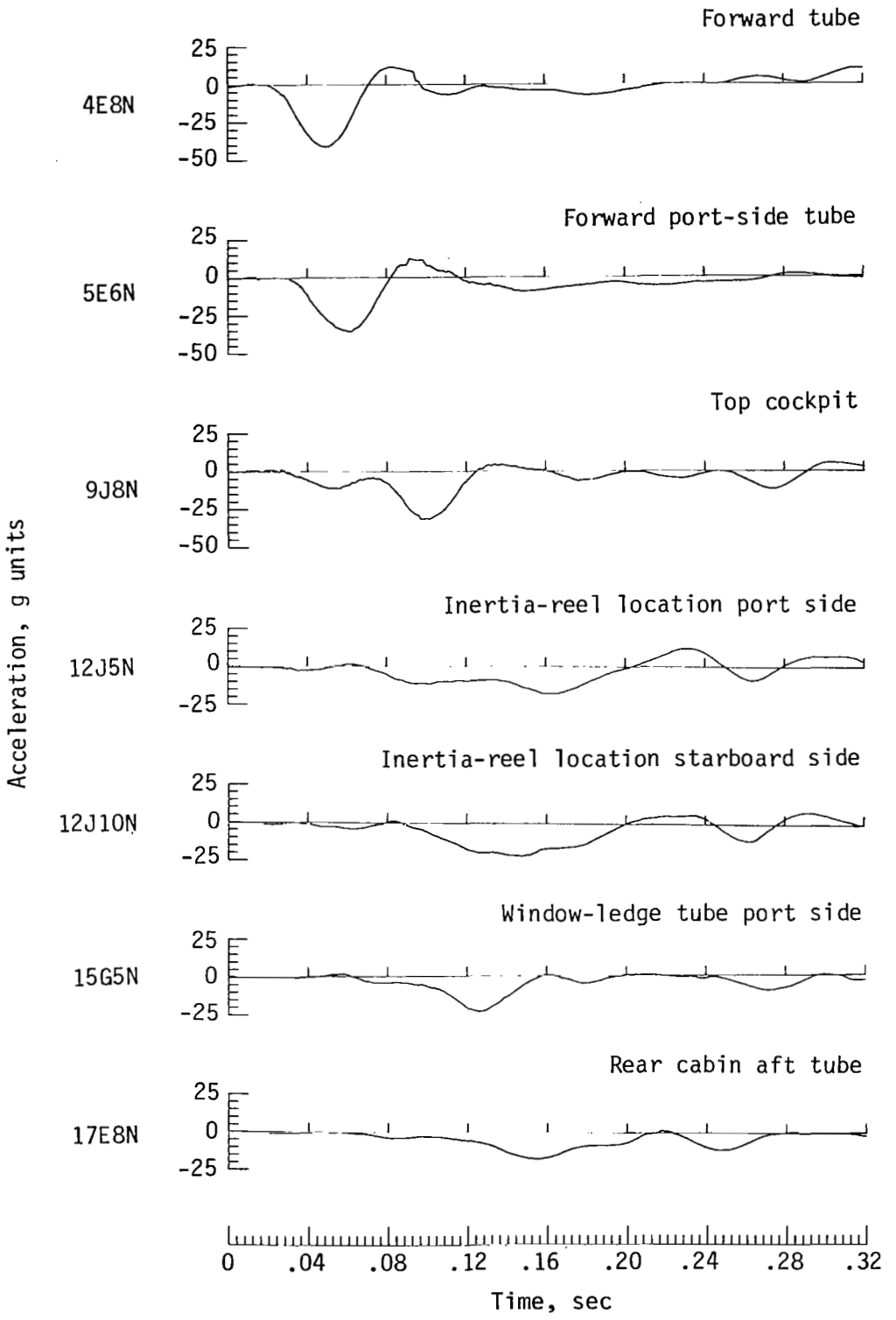

(i) Aircraft structure normal accelerations for first 30° nose-down test.

Figure C4.- Continued.

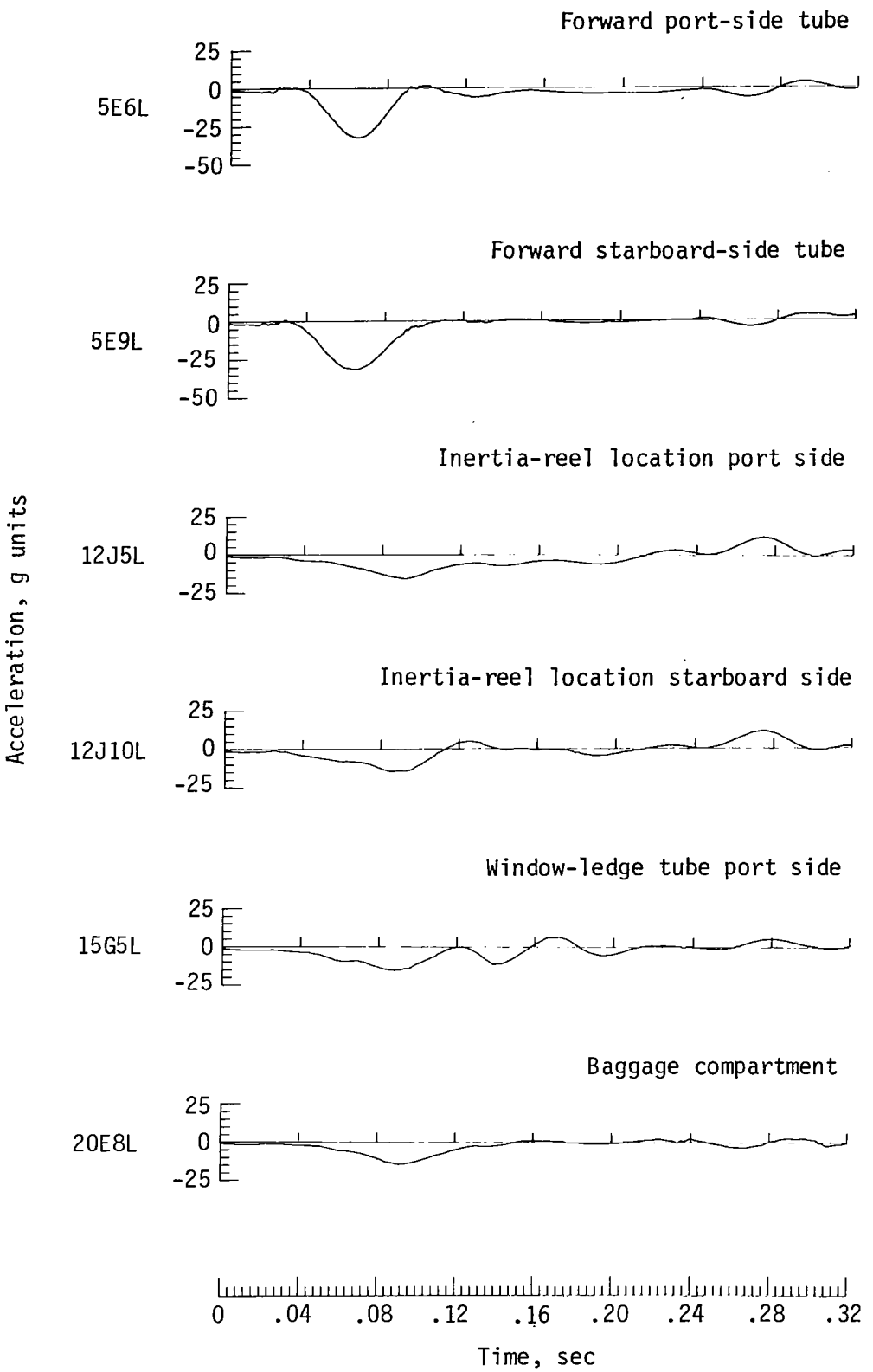

(j) Aircraft structure longitudinal accelerations for first 30° nose-down test.

Figure C4.- Continued.

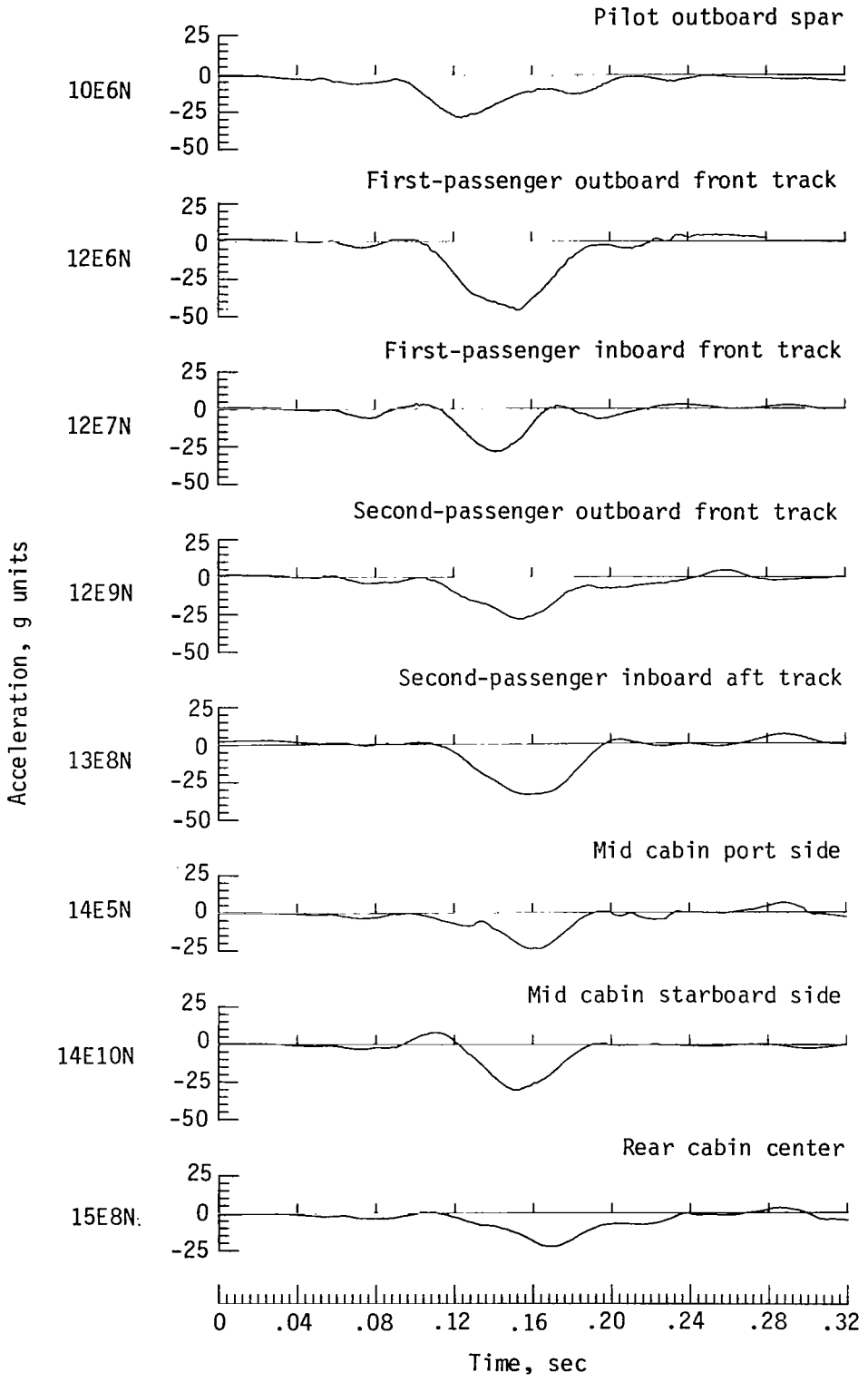

(k) Normal floor accelerations for second 30° nose-down test.

Figure C4.- Continued.

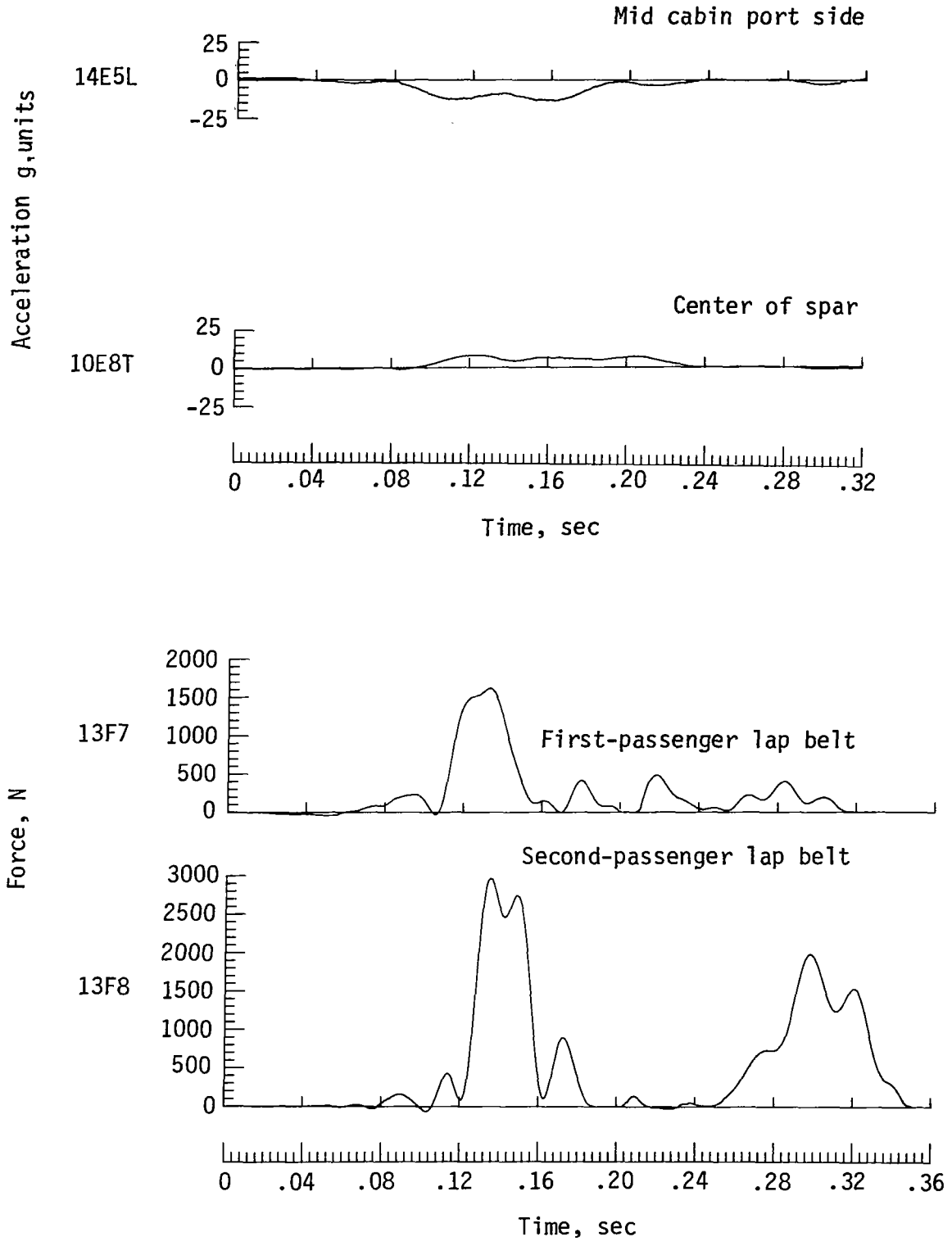

(1) Longitudinal and transverse floor accelerations and restraint loads for second 30° nose-down test.

Figure C4.- Continued.

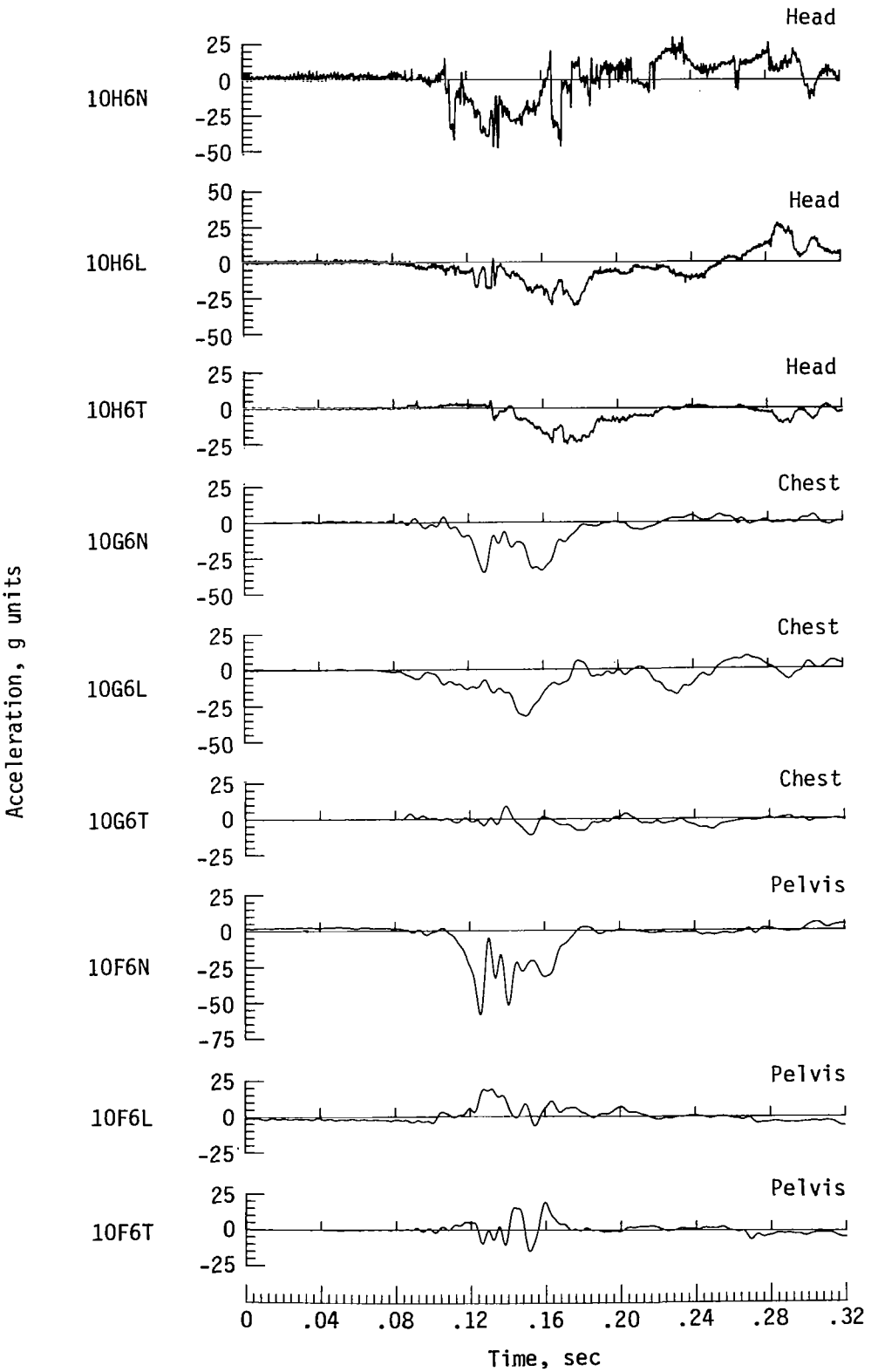

(m) Pilot accelerations for second 30° nose-down test.

Figure C4.- Continued.

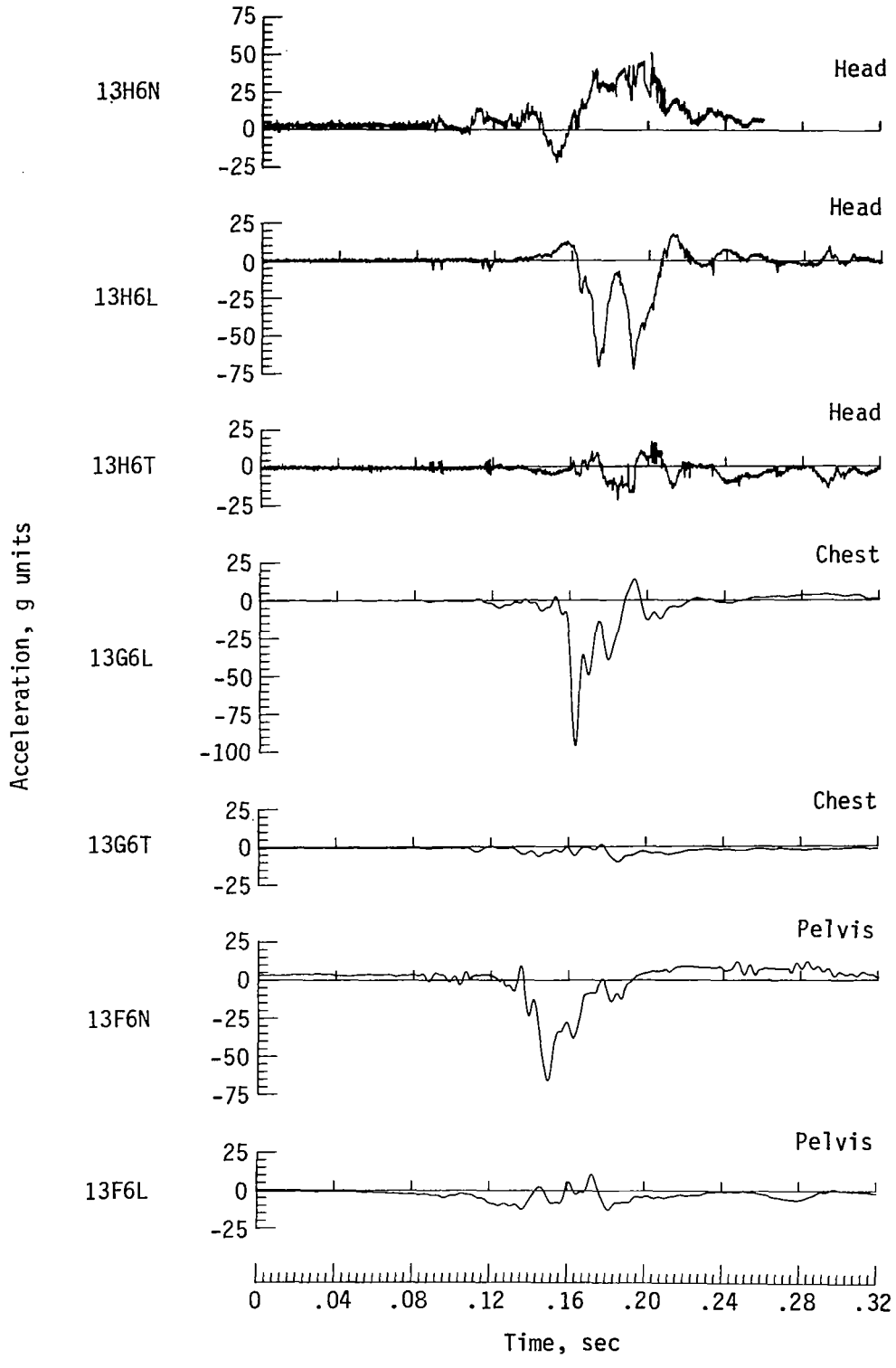

(n) First-passenger accelerations for second 30° nose-down test.

Figure C4.- Continued.

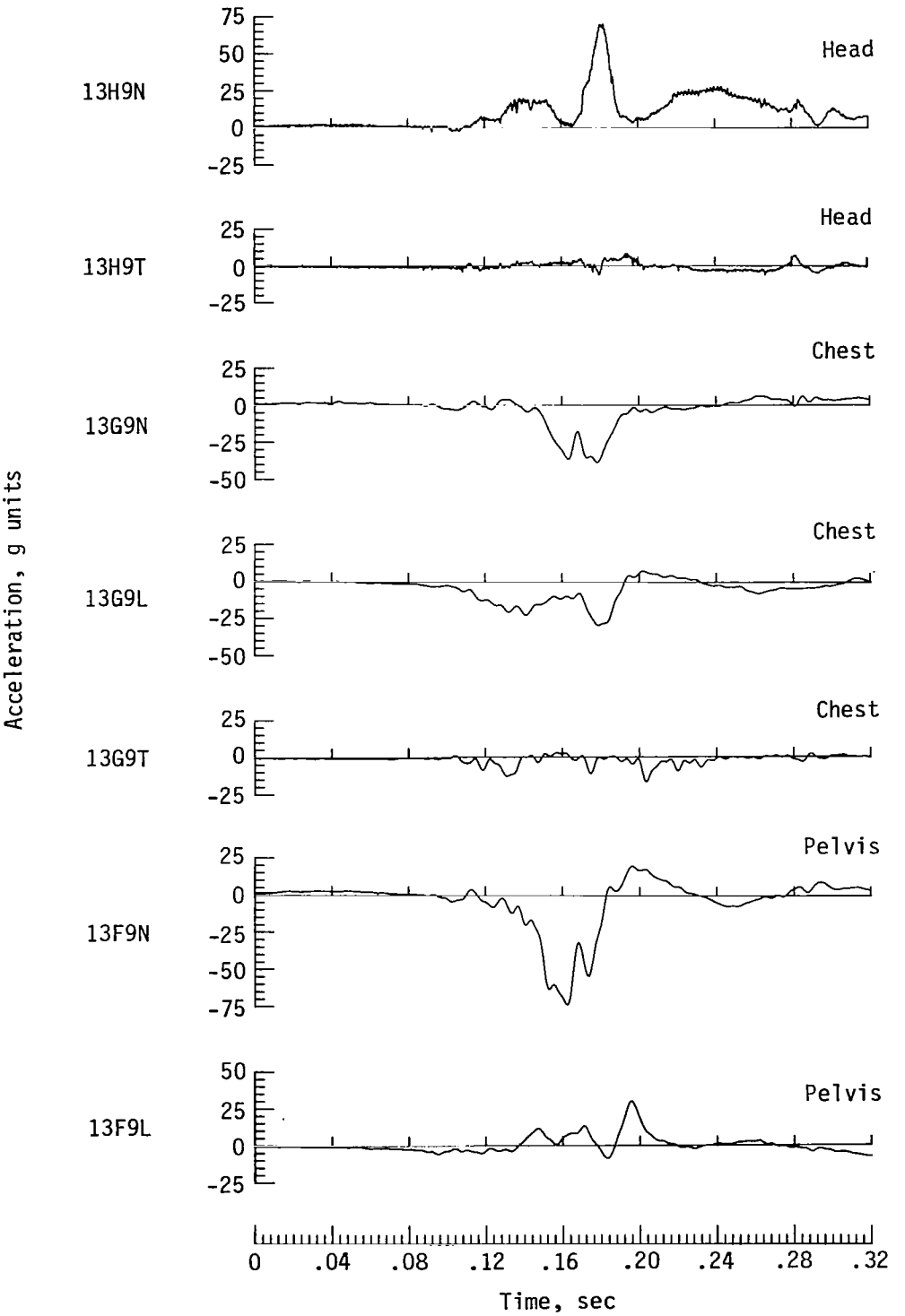

(o) Second-passenger accelerations for second 30° nose-down test.

Figure C4.- Continued.

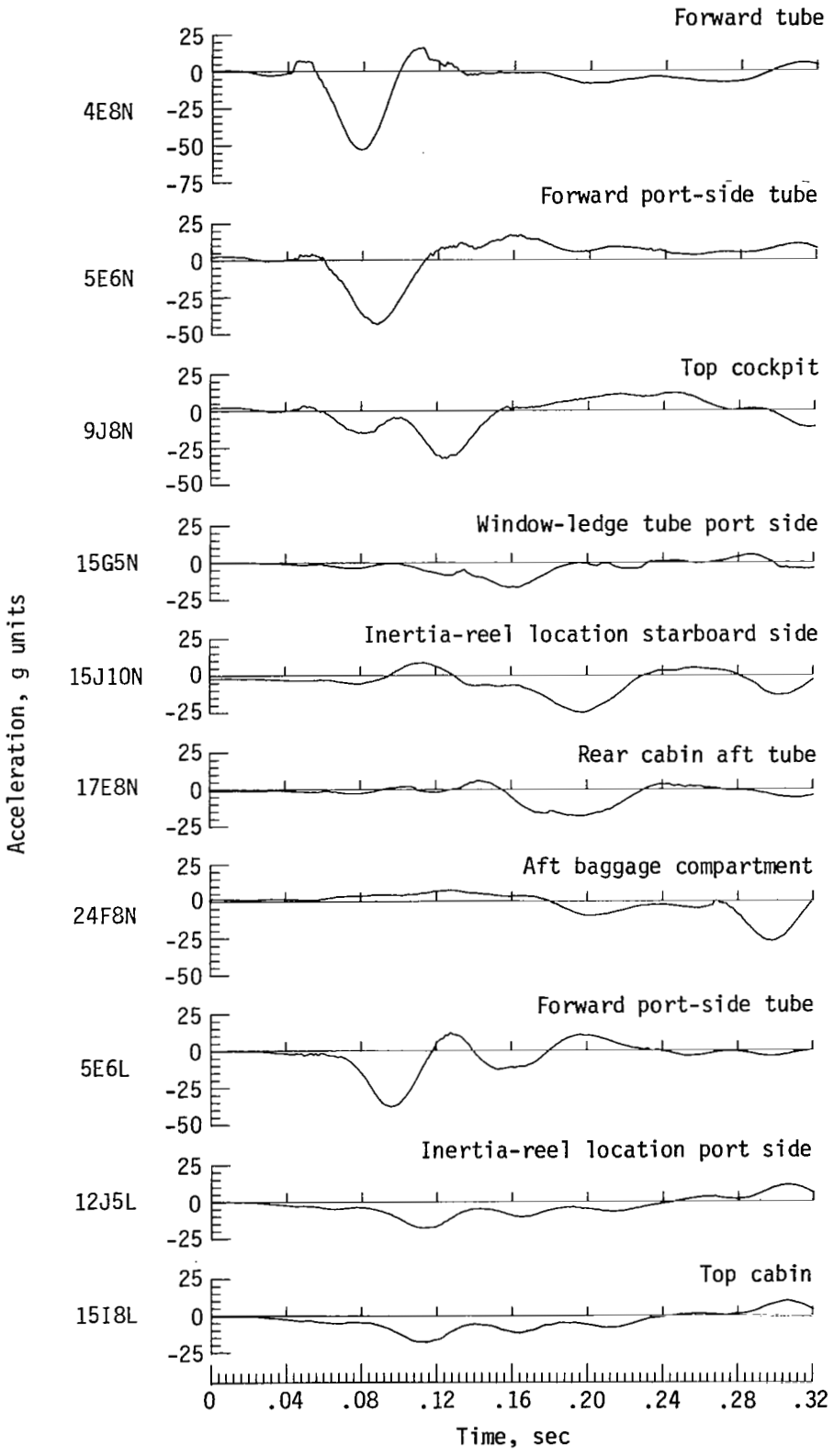

(p) Aircraft structure normal and longitudinal accelerations for second 30° nose-down test.

Figure C4.- Concluded.

REFERENCES

1. Preston, G. Merritt; and Moser, Jacob C.: Crash Loads. NACA Conference on Airplane Crash-Impact Loads, Crash Injuries and Principles of Seat Design for Crash Worthiness. Apr. 1956, pp. 2-1 - 2-47.

2. Eiband, A. Martin; Simpkinson, Scott H.; and Black, Dugald O.: Accelerations and Passenger Harness Loads Measured in Full-Scale Light-Airplane Crashes. NACA TN 2991, 1953.

3. Pinkel, I. Irving; and Rosenberg, Edmund G.: Seat Design for Crash Worthiness. NACA Rept. 1332, 1957. (Supersedes NACA TN 3777.)

4. Hayduk, Robert J.; Thomson, Robert G.; and Carden, Huey D.: NASA/FAA General Aviation Crash Dynamics Program - An Update. Forum, vol. 12, no. 3, Winter 1979, pp. 147-156.

5. Alfaro-Bou, Emilio; and Vaughan, Victor L., Jr.: Light Airplane Crash Tests at Impact Velocities of 13 and 27 m/sec. NASA TP-1042, 1977.

6. Castle, Claude B.; and Alfaro-Bou, Emilio: Light Airplane Crash Tests at Three Flight-Path Angles. NASA TP-1210, 1978.

7. Castle, Claude B.; and Alfaro-Bou, Emilio: Light Airplane Crash Tests at Three Roll Angles. NASA TP-1477, 1979.

8. Vaughan, Victor L., Jr.; and Alfaro-Bou, Emilio: Light Airplane Crash Tests at Three Pitch Angles. NASA TP-1481, 1979.

9. Vaughan, Victor L., Jr.; and Hayduk, Robert J.: Crash Tests of Four Identical High-Wing Single-Engine Airplanes. NASA TP-1699, 1980.

10. Gadd, Charles W.: Use of a Weighted-Impulse Criterion for Estimating Injury Hazard. Proceedings of Tenth Stapp Car Crash Conference, Soc. Automot. Eng., Nov. 1966, pp. 164-174. (Available as SAE Preprint 660793.)

11. Payne, Peter R.; and Stech, Ernest L.: Dynamic Models of the Human Body. AMRL-TR-66-157, U.S. Air Force, Nov. 1969. (Available from DTIC as AD 701 383 and also available as NASA TM X-67038.)

12. Vaughan, Victor L., Jr.; and Alfaro-Bou, Emilio: Impact Dynamics Research Facility for Full-Scale Aircraft Crash Testing. NASA TN D-8179, 1976.

13. Anthropomorphic Test Dummies. Transportation, Code of Federal Regulations, Title 49, Chapter VI, Part 572, U.S. Govt. Printing Off., Oct. 1, 1981, pp. 421-443.

14. Alfaro-Bou, Emilio; Williams, M. Susan; and Fasanella, Edwin L.: Determination of Crash Test Pulses and Their Application to Aircraft Seat Analysis. SAE Tech. Paper 810611, Apr. 1981.

15. Brinkley, James W.; and Shaffer, John T.: Dynamic Simulation Techniques for the Design of Escape Systems: Current Applications and Future Air Force Requirements. AMRL-TR-71-29, Paper No. 2, U.S. Air Force, Dec. 1971. (Available from DTIC as AD 740 439.)

16. Snyder, Richard G.: Occupant Impact Injury Tolerances for Aircraft Crashworthiness Design. SAE Tech. Paper 710406, Mar. 1971.

17. Eiband, A. Martin: Human Tolerance to Rapidly Applied Accelerations. NASA MEMO 5-19-59E, 1959.

1. Report No.	2. Government Accession No.	3. Recipient's Catalog No.
NASA TP-2070		

4. Title and Subtitle	5. Report Date
CRASH TESTS OF FOUR LOW-WING TWIN-ENGINE AIRPLANES WITH TRUSS-REINFORCED FUSELAGE STRUCTURE	September 1982
	6. Performing Organization Code: 505-41-33-01
7. Author(s): M. Susan Williams and Edwin L. Fasanella	8. Performing Organization Report No.: L-15379
	10. Work Unit No.
9. Performing Organization Name and Address: NASA Langley Research Center, Hampton, VA 23665	11. Contract or Grant No.
	13. Type of Report and Period Covered: Technical Paper
12. Sponsoring Agency Name and Address: National Aeronautics and Space Administration, Washington, DC 20546	14. Sponsoring Agency Code

15. Supplementary Notes

M. Susan Williams: Langley Research Center.
Edwin L. Fasanella: Kentron International, Inc., Hampton, Virginia.

16. Abstract

Four six-place, low-wing, twin-engine, general-aviation airplane test specimens were crash tested at the Langley Impact Dynamics Research Facility under controlled free-flight conditions. All airplanes were impacted on a concrete test surface at a nominal flight-path velocity of 27 m/sec. Two tests were conducted at a -15° flight-path angle (0° pitch angle and 15° pitch angle), and two were conducted at a -30° flight-path angle (-30° pitch angle). The average acceleration time histories (crash pulses) in the cabin area for each principal direction were calculated for each crash test. In addition, the peak floor accelerations were calculated for each test as a function of aircraft fuselage longitudinal station number. Anthropomorphic-dummy accelerations were analyzed using the dynamic response index (DRI) and severity index (SI) models. Parameters affecting the dummy restraint system were studied; these parameters included the effect of no upper-torso restraint, measurement of the amount of inertia-reel strap pullout before locking, measurement of dummy chest forward motion, and loads in the restraints. With the SI model, the dummies with no shoulder harness received head impacts above the concussive threshold.

17. Key Words (Suggested by Author(s))	18. Distribution Statement
Airplane crash tests Crash damage Crash worthiness General aviation Impact tests Crash dynamics Anthropomorphic dummy	Unclassified - Unlimited Subject Category 39

19. Security Classif. (of this report)	20. Security Classif. (of this page)	21. No. of Pages	22. Price
Unclassified	Unclassified	119	A06

For sale by the National Technical Information Service, Springfield, Virginia 22161 NASA-Langley, 1982

National Aeronautics and Space Administration

Washington, D.C.
20546

Official Business
Penalty for Private Use, $300

THIRD-CLASS BULK RATE

Postage and Fees Paid
National Aeronautics and
Space Administration
NASA-451

U.S.MAIL

4 1 1U,D, 820923 S00903DS
DEPT OF THE AIR FORCE
AF WEAPONS LABORATORY
ATTN: TECHNICAL LIBRARY (SUL)
KIRTLAND AFB NM 87117

NASA

POSTMASTER: If Undeliverable (Section 158 Postal Manual) Do Not Return